ABSTRACT

ZHU, XIANGQI. DSM-Based Methodology Development for Addressing Problems of High PV Penetrated Distribution System. (Under the direction of Dr. Ning Lu).

Rooftop photovoltaic (PV) systems supply customer loads without the need of transporting electricity through long distance, making them an efficient distributed generation resource for supplying residential and small commercial loads. With the declination of the PV panel price and the installation cost, many areas such as Hawaii and California start to see large-scale deployment of residential and commercial roof-top PV systems [1].

However, because solar is a variable generation resource with intermittency and uncertainty in its power outputs, both the end users and the utilities would suffer some problems with the implementation of the PV panel. For end users, because there is a high possibility that the user consumption profile is not consistent with the PV power profile, the generated solar power cannot be efficiently utilized if no further measures such as installing appropriate energy storage (ES) or applying energy management programs could be implemented. For utilities, the intermittence of PV outputs may cause no or little operational issues as long as the solar penetration level is lower than 10% because power distribution systems are designed to handle large load variations. However, in areas where solar resources are abundant, policies support investment made towards PV installations, and environmental consciousness of residents are high, solar penetration levels are quickly reaching 20% or higher on some residential feeders. As a result, distribution grid operators start to observe overvoltage and reverse power flow at the point of connection and neighboring distribution networks [2-5].

In this dissertation, proper methodologies and approaches have been derived to solve or mitigate the problems and fulfil the requirements and expectations of both the end users and

utilities from various aspects. In the first part of the dissertation, I focused my effort on developing residential PV and energy storage sizing methods considering demand-side management (DSM). Then, I studied the aggregated impact of high penetration of residential PV systems on distribution feeders operations. In the second part of the dissertation, I focused my effort on solving the voltage problems caused by PV integration. I developed a two-stage hierarchical control strategy for deploying demand response on distribution system, with the control objective of implementing demand response requirement from transmission system while regulating the voltage profiles at distribution system. This control strategy enables the co-optimization of demand response operation between the transmission and distribution systems. The Voltage-Load Sensitivity Matrix (VLSM) and the price functions for different demand response resources we developed have enabled us to consider the coordination among different demand response resources including both customer-owned and utility-owned devices.

DSM-Based Methodology Development for Addressing Problems of High PV Penetrated Distribution System

by
Xiangqi Zhu

A Dissertation submitted to the Graduate Faculty of
North Carolina State University
in partial fulfillment of the
requirements for the degree of
Ph.D.

Electrical Engineering

Raleigh, North Carolina

2017

APPROVED BY:

_____	_____
Dr. Ning Lu Committee Chair	Dr. David Lubkeman
_____	_____
Dr. Mo-Yuen Chow	Dr. Yunan Liu

DEDICATION

To my mother Shilan Yan, my father Lianfu Zhu

BIOGRAPHY

Xiangqi Zhu was born in Shandong, China. She received her B.S. degree in electrical engineering from Shandong University, Jinan, China in 2013. She is currently pursuing the Ph.D. degree in electrical engineering at North Carolina State University, Raleigh, NC. Her current research interests include home energy management system, energy storage sizing and voltage control for renewable energy integrated microgrid.

ACKNOWLEDGMENTS

My foremost and deepest gratitude goes to my advisor, Prof. Ning Lu, for her continual support, encouragement, and guidance. Prof. Lu is my role model, not only in academic study, but also in career and life. She showed me the way to be a good researcher and educator, and she always inspired me to pursue my dream. The invaluable advice she provided me on research, career development, presentation, technical writing, and many other aspects is a priceless fortune to me.

My great appreciation and thankfulness also goes to my committee members: Prof. David Lubkeman, Prof. Mo-Yuen Chow, and Prof. Yunan Liu, for their precious time and help. Their passion on research always motivated me to devote myself to my research and the exploration to the new areas.

I am also grateful for having many great lab mates in my life, I would like to express my sincere thanks to them: Jiahong Yan, Jiyu Wang, Xinda Ke， Jian Lu, Gonzague Henri, David Mulcahy, Weifeng Li, Fuhong Xie, and Ming Liang. All of the great memories with them are indispensable parts of my life.

At last, I would like to thank my parents for their love and support since my birth. They always encourage me to chase my dream and provide me the opportunity to be the person I want to be.

TABLE OF CONTENTS

LIST OF TABLES vii
LIST OF FIGURES viii
CHAPTER 1 INTRODUCTION 1
1.1 HEMS Algorithm Development 4
1.2 PV and ES Sizing Methodology and Tool Development 6
1.3 Cost-Benefit Study for Sizing PV and ES Systems 8
1.4 Voltage-Load Sensitivity Matrix (VLSM) Based Voltage Control 10
CHAPTER 2 DSM-BASED ENERGY STORAGE SIZING METHODOLOGY DEVELOPMENT 14
2.1 HEMS Algorithm Development 14
2.1.1 Design Considerations of the HEMS Algorithm Development Toolbox 14
2.1.2 GUI Design and Modeling Approach 20
2.1.3 Case Studies 24
2.2 PV and ES Sizing Methodology and Tool Development 27
2.2.1 Data Preparation 27
2.2.2 ESD Sizing Method 31
2.2.3 Simulation Results 41
2.2.4 Tool Interface Development 53
2.3 Cost-Benefit Study for Sizing PV and ES Systems 54
2.3.1 Modeling Methods 55
2.3.2 Setup of the Cost-Benefit Study 56
2.3.3 Cost-Benefit Study Results 60
CHAPTER 3 DSM-BASED VOLTAGE REGULATION METHODOLOGY DEVELOPMENT 67
3.1 A Hierarchical VLSM-Based DSM Strategy for Coordinative Voltage Control between T&D Systems 67
Nomenclature 67
3.1.1 VLSM and Price Functions 71
3.1.2 Optimization Control Strategy Modeling 75
3.1.3 Feeder Setup 82
3.1.4 Feeder Analysis 88
3.1.5 Test Cases 91

CHAPTER 4 SUMMARY 97
REFERENCES 101

LIST OF TABLES

Table 2. 1 Season Categorization for ESD Sizing Studies 31
Table 2. 2 TOU Price of Duke Energy 58
Table 2. 3 Price of PV Panel and ES 59
Table 2. 4 NPV of House1 63
Table 2. 5 CA Rate Structure 66

Table 3. 1 Parameters for Price Functions 74
Table 3. 2 Main Steps of Load Disaggregation Process 86
Table 3. 3 VR Move Analysis 91
Table 3. 4 Error Percentage for First Stage Control Case 92
Table 3. 5 Error Percentage for First Stage Control Case 94
Table 3. 6 Error Percentage for Second Stage Control Case 96
Table 3. 7 Error Percentage for Time Series Study 96

LIST OF FIGURES

Fig 1. 1 Dissertation Outline 3
Fig 1. 2 T&D interaction structure 13

Fig. 2.1 The architecture of the FREEDM HEMS 16
Fig. 2.2 The modeling of a virtual house 17
Fig. 2. 3 Modeling coupled load consumptions 18
Fig. 2. 4 Sample baseload profiles 19
Fig. 2. 5 The main interface of the HEM GUI 21
Fig. 2. 6 Parameter setting interfaces for controllable loads 23
Fig. 2. 7 Calculation of probability of use 24
Fig. 2. 8 Total consumption of a house 24
Fig. 2. 9 Algorithm development flow 25
Fig. 2. 10 Result of price-cap control HEM algorithm 26
Fig. 2. 11 Result of solar-driven HEM algorithm 26
Fig. 2. 12 Examples of the load profile 27
Fig. 2. 13 Sample solar power output for PV panel of 6kW capacity 29
Fig. 2. 14 Sample appliance profiles generated using load models 30
Fig. 2. 15 Daily load duration curves for cold and warm months 31
Fig. 2. 16 Setup of the tri-level simulation 32
Fig. 2. 17 An ensemble of a summer day net loads for a house with a 4 kW rooftop PV 33
Fig. 2. 18 Control logic of the ESD for minimizing backfeeding energy 36
Fig. 2. 19 Daily operation sample of ESD 37
Fig. 2. 20 CDF of the daily backfeeding energy 38
Fig. 2. 21 E_{neg} for a range of P_{ESD} or E_{ESD} 40
Fig. 2. 22 Q_{ES} and P_{ES} of different solar capacity 42
Fig. 2. 23 Sizing ESDs for different seasons 42
Fig. 2.24 Sizing ESDs for different homes 44
Fig. 2. 25 Sizing ESDs for aggregated homes 45
Fig. 2. 26 Sizing ESDs for 80% PV penetration level 46
Fig. 2. 27 Sizing ESDs for 100% PV penetration level 47
Fig. 2. 28 Size ESD for different PV penetration levels (80~100%) 47
Fig. 2. 29 Flow chart of controlling cooling loads for self-consumption of solar power 48
Fig. 2. 30 DSM impact on sizing ESDs at home-, transformer-, and community- levels 50
Fig. 2. 31 Backfeeding energy among different sizing methods 51
Fig. 2. 32 Results comparison of multiple years 52
Fig. 2. 33 Net present value of various ES sizes 53
Fig. 2. 34 Toolbox interface 54
Fig. 2. 35 Sample output of the load and PV models 56
Fig. 2. 36 On-Peak and Off-Peak period hours 59
Fig. 2. 37 Sample monthly savings 61
Fig. 2. 38 Sample yearly savings 61
Fig. 2. 39 Saving from PV (20 years) 62
Fig. 2. 40 Saving from PV (25 years) 62
Fig. 2. 41 YR of various houses 64

Fig. 2. 42 Time schedule of CA rate 65
Fig. 2. 43 Bill saving comparison 66

Fig.3. 1 Price curves of controllable load (a) and PV (b) 75
Fig.3. 2 Probability density function for f_j^{down} 80
Fig.3. 3 Feeder topology of the IEEE 123-bus system 83
Fig.3. 4 Sample house load profiles 85
Fig.3. 5 Load disaggregation method 86
Fig.3. 6 Load profiles at the load bus on a distribution feeder 87
Fig.3. 7 Sample PV profiles 88
Fig.3. 8 Voltage profile comparison: with and without PV 89
Fig.3. 9 Profile boxplot comparison between without VR (a) and with VR (b) 90
Fig.3. 10 Voltage deviation comparison between without VR (a) and with VR (b) 90
Fig.3. 11 DR response at each node 91
Fig.3. 12 Voltage magnitude at each node 92
Fig.3. 13 DR response at each node 93
Fig.3. 14 Voltage magnitude at each node 93
Fig.3. 15 Required response amount of P and Q from transmission system 95
Fig.3. 16 Voltage profiles at bus 11 phase A 95
Fig.3. 17 Voltage profiles at bus 65 phase C 95

CHAPTER 1 INTRODUCTION

Rooftop photovoltaic (PV) systems supply customer loads without the need of transporting electricity through long distance, making them an efficient distributed generation resource for supplying residential and small commercial loads. With the declination of the PV panel price and the installation cost, many areas such as Hawaii and California start to see large-scale deployment of residential and commercial roof-top PV systems [1].

However, because solar is a variable generation resource with intermittency and uncertainty in its power outputs, both the end users and the utilities would suffer some problems with the implementation of the PV panel. For end users, because there is a high possibility that the user consumption profile is not consistent with the PV power profile, the generated solar power cannot be efficiently utilized if no further measures such as installing appropriate energy storage (ES) or applying energy management programs could be implemented. For utilities, the intermittence of PV outputs may cause no or little operational issues as long as the solar penetration level is lower than 10% because power distribution systems are designed to handle large load variations. However, in areas where solar resources are abundant, policies support investment made towards PV installations, and environmental consciousness of residents are high, solar penetration levels are quickly reaching 20% or higher on some residential feeders. As a result, distribution grid operators start to observe overvoltage and reverse power flow at the point of connection and neighboring distribution networks [2-5].

In this dissertation, proper methodologies and approaches have been derived to solve or mitigate the problems and fulfil the requirements and expectations of both the end users and

utilities from various aspects. In the first part of the dissertation, I focused my effort on developing residential PV and energy storage sizing methods considering demand-side management (DSM). Then, I studied the aggregated impact of high penetration of residential PV systems on distribution feeders operations. In the second part of the dissertation, I focused my effort on solving the voltage problems caused by PV integration. I developed a two-stage hierarchical control strategy for deploying demand response on distribution system, with the control objective of implementing demand response requirement from transmission system while regulating the voltage profiles at distribution system. This control strategy enables the co-optimization of demand response operation between the transmission and distribution systems. The Voltage-Load Sensitivity Matrix (VLSM) and the price functions for different demand response resources we developed have enabled us to consider the coordination among different demand response resources including both customer-owned and utility-owned devices. An outline for the research works I developed and will develop are shown in Fig.1.1.

To size the residential PV and energy storage (ES) systems, the main consideration is to consume solar power for utility bill reduction. Therefore, the utility rates and the load characteristics including the controllability of loads are the predominant factors under consideration. My research focused on two aspects: design and develop home energy management algorithms to increase the controllability of home appliances and integrate cost-benefit analysis to help end users select PV and ES not only from the technical perspective but also from the economic perspective.

When homes and buildings have PV installed and when energy management algorithms are applied, the feeder load profiles are undergoing significant changes. To address the impact of

those changes, in the second part of my thesis I will conduct an aggregation study for thousands of homes on a few realistic feeder network model. To resolve the overvoltage and reverse power flow issues, I plan to develop two algorithms. The first algorithm is to use voltage-load sensitivity matrix (VLSM) based voltage control to select the right resources for regulating the voltage profile. The second algorithm will be a price-incentive coordination scheme for coordinating the demand response through price signals.

The state of art for each work will be introduced in the following part respectively, demonstrating what methodologies are in the literature and what approaches proposed in my dissertation.

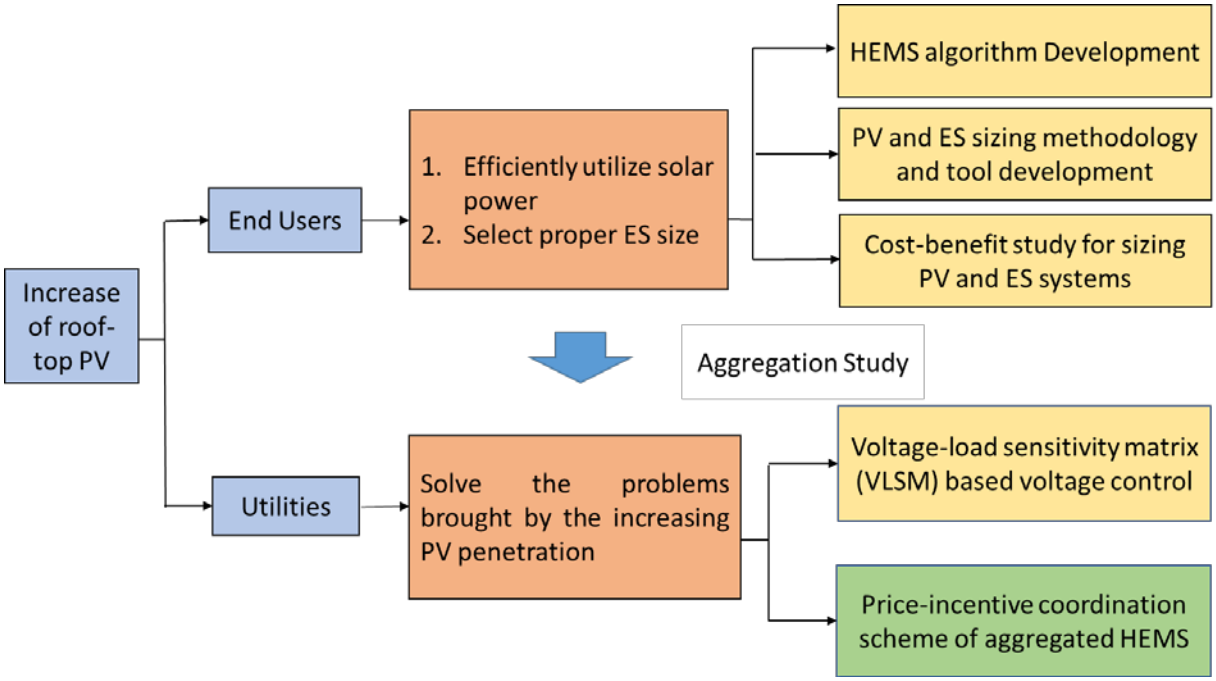

Fig 1. 1 Dissertation Outline

1.1 HEMS Algorithm Development

DSM programs are important resources for future power grid operation. DSM applications include improving energy efficiency, peak shaving and load shifting, load following and regulation, smoothing renewable generation outputs, and hedging high electricity prices [6-8]. In addition, DSM programs can greatly improve the flexibility, economics, and reliability of grid operation by coordinating distributed energy resources (DERs) such as electric vehicles, energy storage, distributed generations, and controllable load resources.

In the past, DSM resources are mainly large commercial and industrial loads [9]. The advancements in information technology, advanced sensor networks, data storage and processing capability, and communication make it possible to manage electricity consumption at end user level. Therefore, a major shift in DSM in recent years is focus on developing residential HEMS that allow residential customers to participate in energy efficiency and energy saving programs, as well as provide grid energy and ancillary services.

The majority of the ongoing research efforts have been focused on the development of HEMS algorithms for controlling appliances, electric vehicles (EVs), behind-meter rooftop photovoltaics (PVs), and energy storage devices (ESDs) for providing DR services such as peak shaving and ancillary service [10-16]. A wide range of models have been developed by different research groups. For example, major home appliances are divided into thermostatically-controlled appliances (e.g. refrigerators, water heaters, spacing heaters, air conditioners) and non-thermostatically-controlled appliances (e.g. pool pumps, washers, dryers, dishwashers). Dynamic and steady state models for PV, ESD, and EV are also developed by research institutes, vendors, and university teams.

However, although the modeling of individual appliance can be relatively accurate, modeling residential household energy consumption remains a challenge. For example, how to accurately model the overall electricity consumption of a household under a wide range of consumption patterns and weather conditions? How to tune the devices and appliance models in the house model so that the modeled load profile matches the actual measurements?

There are three main technical challenges. The first one is to represent the correlation between different end use consumptions. For example, the modeling of electric water heater loads needs to be associated with the modeling of washers and dish washers. Otherwise the large amount of hot water when washing clothes or dishes cannot be reflected in the modeling process. The washer load needs to be connected with the dryer load because most of the dryer normally starts working minutes after the washer finishes its task. The second challenge is the modeling of non-controllable loads, which is highly random and has very little patterns to follow. The third challenge is to reproduce an actual load profile given a set of field measurements. Other considerations include the occupants' behavioral patterns that dominate the energy consumptions of a household load. In general, a large amount of data is needed to quantify the resident's behavioral patterns in a specific period of time as the behavior may change over time. As a result, unsupervised modeling normally can't yield accurate results.

To tackle the above challenges, we've developed a matlab-based modeling platform to serve as a virtual household that allows the researchers to develop HEMS algorithms and test the performance. The architecture of the software modeling platform is built in our work. We also developed the data-driven modeling approach, the supervised modeling process for algorithm development, and the performance evaluation mechanism for comparing different approaches.

1.2 PV and ES Sizing Methodology and Tool Development

Rapid power and voltage fluctuations along distribution feeders caused by behind-meter PVs have created serious operational issues such as overvoltage, reverse power flow, flickers, and equipment overloading [17-18]. ES can store energy for future use, smooth out large power fluctuations, and provide reactive power support to stabilize system voltage, making them one of the most effective technical solutions for the aforementioned operational issues. However, ESs are expensive. Comprehensive cost-benefit studies [19-22] have shown that the following strategies will make using ES more cost-effective: 1) providing multiple services to increase the utilization rate and revenue streams, 2) using DSM to reduce the size of ESDs, and 3) sharing ES among a group of users to reduce the amount of ES needed at the aggregated level.

Previous studies on sizing ES based on technical requirements focused mainly on smoothing power outputs of large solar or wind farms [23-25]. In this work, we focus on sizing ES for residential households, communities, and feeders. At this level, sizing considerations may vary according to the ownership, location, and service requirements of an energy storage system. For example, an ES on a residential feeder can be owned by: 1) a homeowner for supporting the rooftop PV system, 2) a utility for power quality and reliability considerations, or 3) a third-party aggregator for providing grid services. A home-owned ES is behind-the-meter for balancing the home's own consumption needs. A utility-owned ES may be placed close to a transformer or provides feeder-level services that impact all users on the feeder. Third party-owned ES may be placed on separate sites or even on mobile trucks for providing services to whoever needs them. Therefore, to optimally size the ES, one will need to account for its ownership, placement, and service requirements.

Another technical challenge for the residential ES sizing study is the modeling of residential load consumptions. A typically approach is to use hourly average- or worst- case load profile derived from historical data for sizing ES. A major disadvantage of the approach is that it cannot account for the load pattern shift caused by behavioral changes of residential customers after the PV is installed. In addition, because both the PV generation and residential load consumptions are highly intermittent, considering a wider range of operation conditions is needed to size an energy storage system so that the performance of the ES will meet the requirements within a given risk margin.

In this study, a bottom up approach is used. The ES sizing problem is first formulated for each individual household. By summing up house-level loads, the energy storage needs at the distribution-transformer level for supplying 1-5 houses is considered. Next, a community consisting of 50 houses is studied. Based on historical solar radiation data, residential load profiles, and load models, an ensemble of net load profiles is created for a given solar installed capacity. Then, the cumulative distribution function (CDF) curve of a selected performance criterion for a given ES size at a given solar penetration is generated. By combining such CDF curves for different ES sizes and solar penetrations on a compressed, compact CDF (CC-CDF) plot, a user can graphically select the ES power and energy capacity based on expectation of meeting the performance criterion. A novel graphical capacity selection method using equal probability lines (EPLs) on CC-CDF curves is developed for sizing the energy storage needs at the house, distribution transformer, and community levels. This graphical method can compress the performance of ES sizing options in one plot. The method is generic and can be used to solve many other sizing problems. So far, we haven't seen any similar method for

power system applications published in literature. Therefore, we consider it is the main contribution of the work.

1.3 Cost-Benefit Study for Sizing PV and ES Systems

If the capacity and the size of the storage component equipped for PV system are not well selected, the voltage variation and the back-feeding power may cause deterioration in grid operation. In addition, different utilities have different retail rate structures, it is critical to estimate whether or not for a specific residential or commercial load, installing PV system will be economic. Therefore, in this work, we present a series of cost-benefit study on residential PV and energy storage (ES) system installation options.

To mitigate the intermittence of the PV power output as well as increase the reliability of the power supply, installing a PV system with an energy storage system that coordinates with load management through HEMS is the best option for fully utilizing the potential of the residential roof-top PV systems [26-27]. Therefore, in this study we focus on sizing the capacity of the PV, PV-ES, and PV-ES-DR systems to satisfy the power supply requirements and study whether or not installing such PV systems is an economically viable decision.

Various sizing criterions of PV and ES systems have been proposed by researchers. In [28], the authors sized ES for grid-connected PV systems for peak shaving and power arbitrage. In [29], the authors used the energy storage system to smooth the PV power outputs. However, unlike the grid-level PV and ES, the sizing of residential PV and energy storage is heavily influenced by the residential load consumptions. For example, if the electricity consumption of a house is in line with the PV generation profiles, there is little needs for installing an energy storage system. For the houses with smart appliances or home energy management systems,

the controllable loads can be shifted to periods when PV power is available. In addition, the rate structure also has a profound influence on the sizing of the PV and ES systems. If back-feeding power to the grid is not allowed (e.g. in Hawaii), it is then necessary to consider installing an energy storage system or invest on controllable loads so that PV power can be fully utilized. In both cases, detailed residential energy consumption needs to be used for sizing the needs for the PV and ES systems.

To facilitate the selection of PV and ES systems, we developed a method that can use a few customer inputs on their life styles to synthesize residential load profiles based on major appliance consumptions [30]. In this work, we present a cost-benefit study based on this method so that the synthesized residential loads can be used to simulate the impact of installing PV and energy storage systems of different capacity. The tariff we used in this study is the time-of-use (TOU) rate. Duke Energy time-of-use rate is used in major case studies, and PG&E time-of-use rate is added for comparison of bill saving brought by the PV-ES system under different rate structures. Four cases are designed and analyzed. Case 1 models residential loads with no PV and ES system installed and serves as the base case. Case 2 models the cases with only PV panels installed. Case 3 models the impact of installing an energy storage system together with the PV panels. In Case 4, we manage controllable loads to reduce the size of the storage system.

The money savings of each case is compared and analyzed. The marginal value of increasing one unit of PV and ES is investigated to help the home owners choose the optimal PV and ESD size based on their expectations of comfort and years of return. The net present value (NPV) and years of return (YR) are used to quantify the cost and benefit of installing a residential PV-

ES system, comparing which option will be economically viable and has the best outcome in terms of money savings and performance.

1.4 Voltage-Load Sensitivity Matrix (VLSM) Based Voltage Control

As mentioned before, advancements in solar power generation technologies significantly reduce the cost of roof-top PV systems in recent years [31]. The increasing environmental awareness among people together with subsidies and credits from the government and utilities are incentivizing more customers to install roof-top PV panels and consume greener power. Consequently, the installation capacities of roof-top PV systems are growing rapidly in recent years.

Ongoing studies have shown that high PV penetration causes voltage problems, such as rapid voltage variations and larger voltage ramps, in electric power distribution systems [17-18,32]. Those solar generation resources feed excess electricity from the distribution to the transmission systems, propagating the voltage problems to the transmission systems. More frequent and larger voltage fluctuations reduce the reliability and power quality of the power supply and require the voltage control devices to act more frequently to compensate for such fluctuations. Studies have shown that more voltage regulation devices are required in the distribution systems or the existing devices will need to act more often, causing significantly reduction of the lifetimes of those devices [33].

Existing studies focus on resolving those voltage issues through revising settings for voltage regulation devices in the distribution system including voltage regulators and capacitor banks, or relying on shunt devices in the transmission system[34-35]. However, only a few voltage regulation devices are installed on a distribution system and their operation is limited by their

locations. Devices such as capacitor banks and mechanically switched shunt devices do not have many levels of control. Also, the frequent switching of those devices will significantly reduce their lifespan.

An alternative approach to resolve the voltage problems caused by high PV generation is to vary loads. When PV generation is high, we can increase electricity consumption; when clouds passing by, we can reduce the consumption. In recent years, although demand response (DR) programs have been extensively investigated for providing grid services for peak shaving, load shifting, and providing ancillary services[36-39], employing DR for voltage control has not yet been fully studied.

In [40], Zakariazadeh et al. proposed a demand response approach applied in automated distribution system for voltage control, but it only focuses on emergency event such as outages of generators and lines. In [41], Christakou et al. proposed a method of aggregating small electric appliances to provide voltage regulation. However, only load was used as DR resource, coordination among different resources such as load, PV, and capacitors were not considered. The concept of sensitivity coefficient of voltage was used in [41]. However, they assumed that the coefficient could be calculated by the information obtained by state estimation and they calculated the coefficient every time step. But state estimation is difficult in distribution system because of the lack of measure units, and calculating the coefficient at every time step will increase computation load. Moreover, both papers focus only on distribution system without considering the interaction between transmission and distribution (T&D) systems. So far, coordination in voltage control between transmission and distribution grids has not yet been investigated in the literature. But the T&D interaction becomes very important as the

variability of PV has increasing influence on both T&D systems with high PV penetration.

Therefore, in this work, we propose a hierarchical two-stage VLSM-based DR strategy for regulating the voltage at distribution feeders while fulfilling the transmission system DR requests. The setup is shown in Fig.1.2. To coordinate the voltage control between the transmission and distribution systems, at the beginning of each operation interval, controller at the transmission level will first perform optimal power flow to determine the optimal increase and decrease of the real and reactive power at each load node so that at the transmission level, the optimization objectives such as minimizing losses, cost, and voltage deviation could be satisfied. Then, the transmission system controller will issue to the distribution system controllers DR commands for them to determine how they will employ resources in their systems to provide the real and reactive power increase or decrease.

The control strategy for distribution system is composed of two stages. In the first stage, the distribution system controller uses a VLSM-based dispatch algorithm to dispatch the available DR resources on the distribution feeder with an objective to minimize voltage deviations and DR cost. Then voltage violations will be checked after implementing first-stage DR results. A second stage VLSM-based DR dispatch will be performed to remove the violations if there are any detected. After that, the DR capacity for the next operation interval is sent back to the transmission system controller as constraints of the transmission optimization algorithm for making subsequent operation decisions. In this paper, we focus on elaborating the 2-stage DR strategy for distribution system.

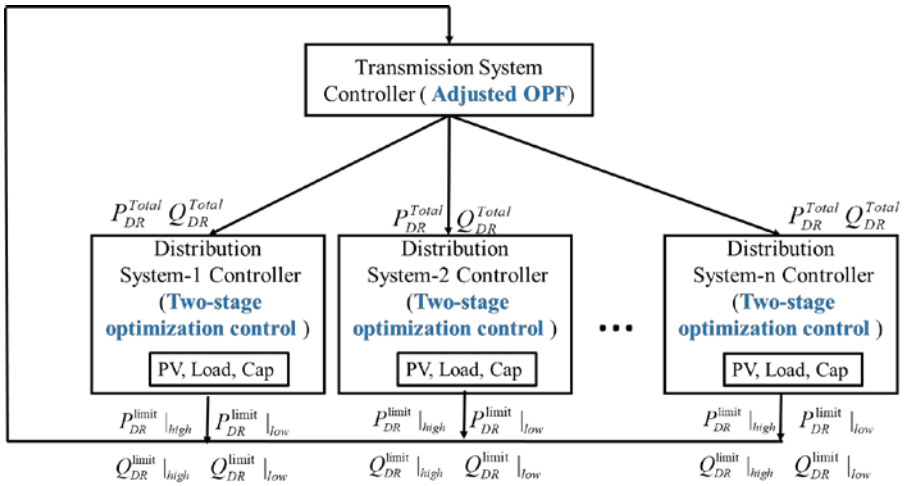

Fig 1. 2 T&D interaction structure.

The contributions of this paper are three-fold. First, the problem formulation enables the co-optimization of DR operation between the transmission and distribution systems. Second, we developed a VLSM-based resource dispatch strategy. The VLSM and the price functions for different DR resources have also been developed. Third, coordination among different DR resources including both customer-owned and utility-owned devices is accounted.

CHAPTER 2 DSM-BASED ENERGY STORAGE SIZING METHODOLOGY DEVELOPMENT

This chapter introduces the methodologies developed for addressing the issues of end users in high PV penetration residential feeders. The work constructed on HEMS algorithm development, PV and ES sizing, and cost-benefit study for sizing PV and ES systems will be demonstrated correspondingly.

2.1 HEMS Algorithm Development

This section is organized as follows. Sub-section 2.1.1 introduces the design considerations of the HEMS algorithm development toolbox. Sub-section 2.1.2 presents the GUI interface design and the modeling of the toolbox. Case studies are presented in sub-section 2.1.3. Conclusions and future research directions in this research area are summarized in sub-section 2.1.4.

2.1.1 Design Considerations of the HEMS Algorithm Development Toolbox

The goal for software architecture design for the FREEDM HEMS is to offer a common simulation platform for HEMS algorithm developers to implement and test their control algorithms more conveniently. As shown in Fig. 2.1, the information received from the utility (e.g. electricity prices, demand response commands), the weather service provider (e.g. temperature, humidity, wind speed, solar radiation), and the consumer's input settings (e.g. the appliance settings) will be selected through a graphical user interface (GUI) and stored into the HEM database. A house module contains appliance models, Distributed Energy Resource (DER) models and the simulation engine. The parameters of the appliance and DER models can be exchanged through the GUI and sent back to the HEM database. Algorithms are the

engines of the HEM system and algorithm selections can also be made through the GUI. Once an algorithm is selected, the user can call the appliance model parameters from the data base, run the algorithm, and generate simulation results, which are saved and sent back to the data base. Next, the GUI will display the results by reading data from the data base. This process allows the algorithm developers to develop and implement their algorithm independently while using the same model and operation conditions to compare the results generated through monitoring the results displayed by the GUI.

The standard setting of the smart house is a single-family home powered by a solar panel. The DERs include an energy storage device and electric vehicles. Each operation period is 24-hours and the simulation time step is 1-minute. There are three preloaded rate structures: flat rate, time-of-use, and critical-peak-price. Users also can define customized rate schemes through GUI inputs.

A. Design Consideration for the Graphical Interface

The considerations of the HEM GUI design are as follows [69]:

1) Provide a parameter setting interface for HEM controllable appliances and DERs.
2) Provide an input module that models the communication links with the other entities. For example, the prices signal from the utilities, the weather information (e.g. outdoor temperatures and humidity) from the weather forecast providers, and utility control signals (peak-shaving, etc.) from the grid services aggregators.
3) Provide output displays that summarize performances for cost-benefit comparisons and status reports for monitoring device conditions.
4) Provide side-by-side comparisons for different scenarios.

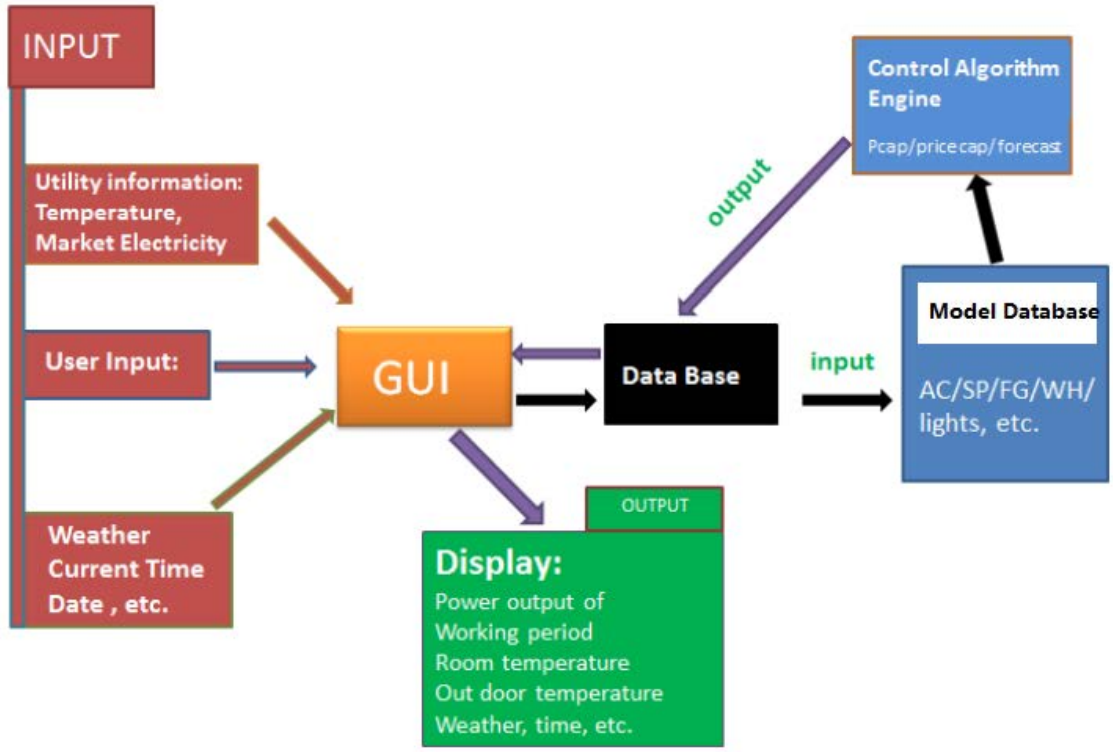

Fig. 2.1 The architecture of the FREEDM HEMS

B. Design Consideration of the Models

The HEM model data base includes four main components: appliance models, energy storage (ES) models (include electrical vehicles), distributed generation models, and baseload models.

As shown in Fig. 2.2, the appliance model database are divided into controllable and non-controllable appliance databases. Controllable database is further categorized into temperature sensitive loads (TSLs) [11][16,42]and behavior sensitive loads (BSLs) [16]. The group of TSLs include the loads whose consumption patterns are closely related to the temperature variation, such as air conditioner (AC) and electric water heater (EWH). The group of BSLs include the ones whose consumption patterns are directly associated with the behavior of the users, like dryer, washer and dish washer. The operation status of correlated consumptions are

coupled so that the change of status of one appliance will trigger the change of status of all the other coupled devices. As shown in Fig. 2.3, all the appliances that use hot water are coupled. In addition, washer loads are also coupled with dryer loads. Dishwasher loads are coupled with cooking loads.

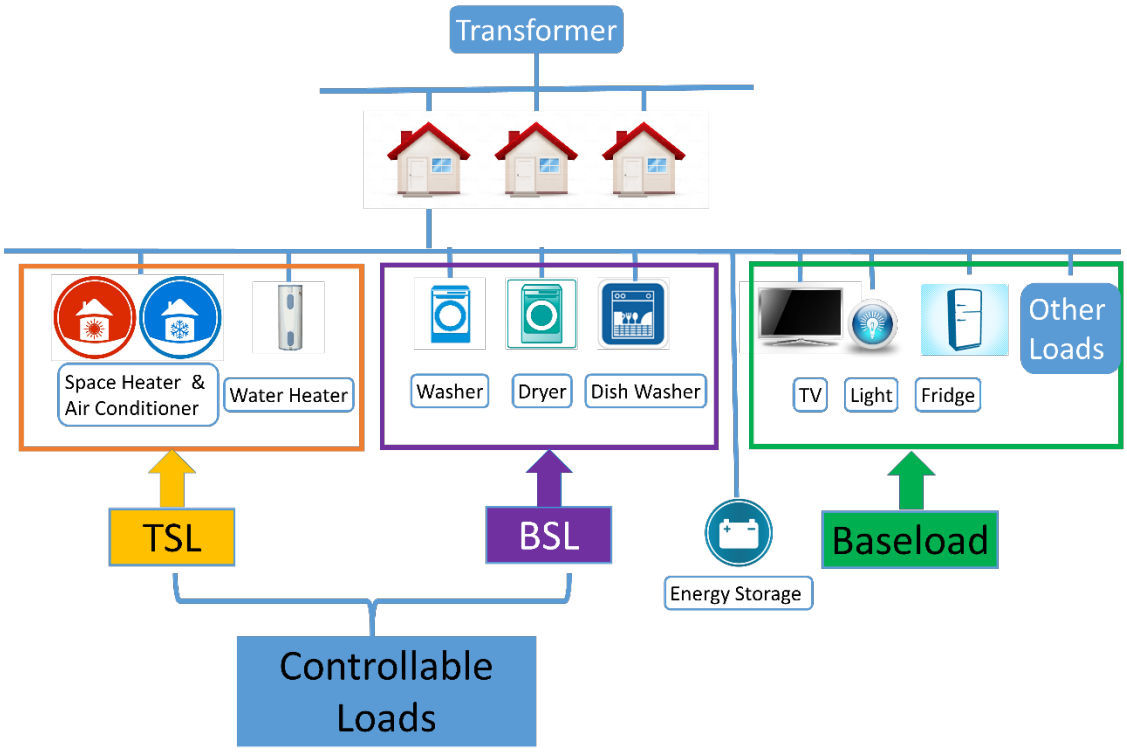

Fig. 2.2 The modeling of a virtual house

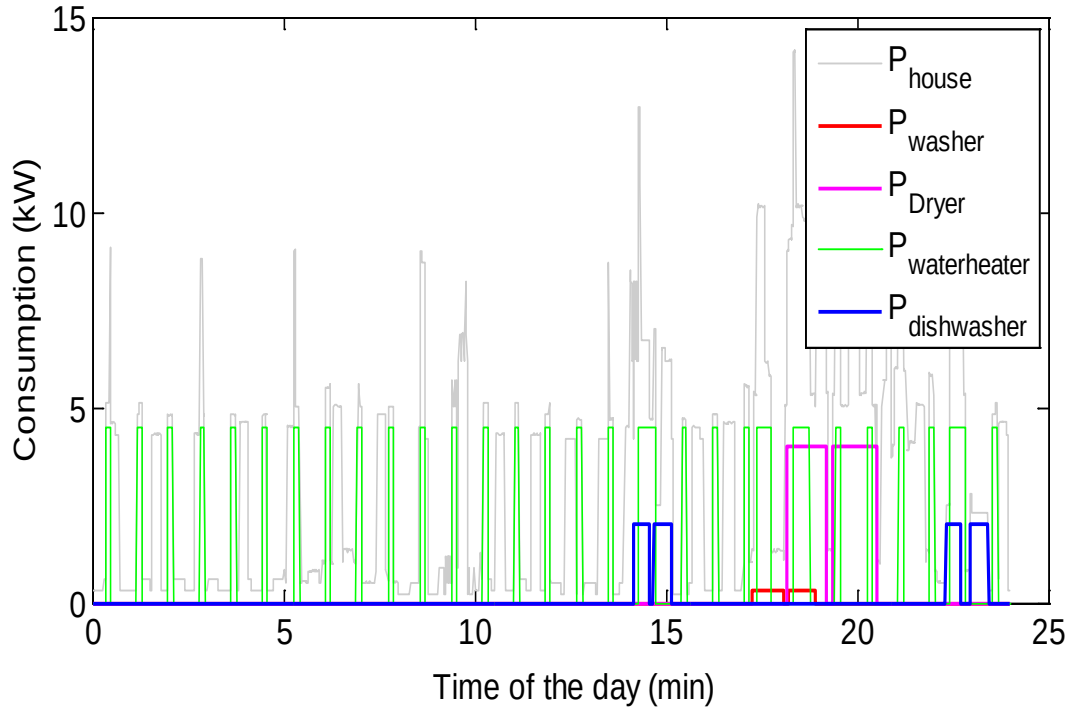

Fig. 2. 3 Modeling coupled load consumption*S*

The battery model developed in [43] is used in the toolbox. A salient feature of the battery model is that it includes a simplified lifetime estimation algorithm that allows the users to quantify the expected lifetime depreciation under different operation conditions.

As the modeling of distribution generation at the house level is mainly the modeling of rooftop PVs, we only included a PV model in the database. Because energy management is our main purpose, a simplified model that transforms the solar radiation data to the solar power outputs is used. However, we analyzed a few sets of PV data in North Carolina and developed a PV output database to represent different day types based on its probability of occurrence. This will allow the what-if scenarios to reflect the performance from a probabilistic-based approach.

The main technical challenge in developing a base-load database is the separation of major controllable appliance consumptions from the must-run house appliance loads. Load desegregation methods are applied on measurement data of 50 houses collected in 2006-2007. Then, the normalized realistic load profiles of the 50 houses are used to establish the base load pool by a number of clustering methods (e.g. baseline power and energy consumptions and different occupancy patterns). Fig. 2.4 shows an examples of the baseload profiles. There are two types of baseloads. Baseload 1 (BL1) is the baseload without TSLs and Baseload 2 (BL2) is the baseload without both BSLs and TSLs. This allows the algorithm developers to superimpose the controllable loads on the baseload to form different type of end use patterns. The baseloads are different for each season and covers high, medium, and light electricity consumption patterns.

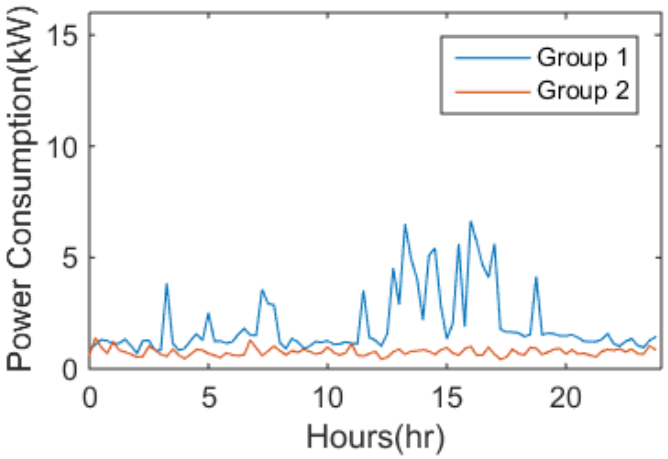

Fig. 2. 4 Sample baseload profiles

2.1.2 GUI Design and Modeling Approach

In this section, we briefly describe how to seamlessly integrate the models into a flexible modeling platform for algorithm development by meeting the modeling considerations presented in Section II.

A.Graphical Interface Design

When developing different HEM algorithms, based on different control objectives, different sets of controllable appliances and DERs may be selected to construct a house model representing the residential electricity energy consumption in different seasons. As shown in Fig. 2.5, a GUI is developed to accommodate this selection process. By accessing the main GUI interface, the algorithm developer can quickly change the settings of the physical models used for modeling the TSLs and BSLs as shown in Fig. 2.6 (a)-(c). This interface is also used to collect the customer comfort settings and responses when testing the algorithms during the algorithm development phase so that the human reaction can be recorded and analyzed [64].

Fig. 2. 5 The main interface of the HEM GUI

B.Modeling Behavior Sensitive Loads

BSLs are modeled using randomized arrivals and consumer designated time slots. Two approaches are used to model BSLs: consumer designated time slots and randomized arrivals. The modeling principles of the two methods are described as

$$P_i(t) = P_i^{rated} \bullet S(t) \tag{2.1}$$

$$P_i(t) = P_i^{rated} \bullet p_i(t) \tag{2.2}$$

where $P_i(t)$ is the power consumption of load i at time t; $S(t)$ is the on (1)/off (0) status of the load; P_i^{rated} is the rated power of load i, and $p_i(t)$ is the probability of use of load i at time t.

For method of consumer designated time slots, as shown in (1), the power consumption of load i at designated time t (see Fig.2.6) when this load is on, is defined as its rated power. For method of randomized arrivals, the power consumption of load i at time t is calculated by multiplying its rated power by the probability it will be on at this time slot. The method of randomized arrivals is usually used in large scale simulation which involves lots of homes. The probability of use is calculated from the data base which is composed of field measured data of the appliances in the houses.

The probability of use of load i at time t is calculated by

$$p_i(t) = \frac{P_i^{1/N}(t)}{P_i^{rated}} \tag{2.3}$$

$$P_i^{1/N}(t) = \frac{P_i^N(t)}{N} \tag{2.4}$$

where $P_i^{1/N}(t)$ is the average consumption of load i at time t in one house and $P_i^N(t)$ is the total consumption of all the load i at time t of a community with N houses. Fig. 7 demonstrates the calculation of the probability of use of BSLs. Fig. 2.7 (a) shows the $P_i^{1/N}(t)$ of a sample day, and Fig. 7 (b) shows the corresponding probability of use calculated from Fig. 2.7 (a).

The method of consumer designated time slots is normally used for small scale simulation which include one or several homes. The status of the BSLs are exactly on or off at each time slot. Fig. 2.8 shows the sample load profile of a house load composed of TSLs, BSLs, and baseload.

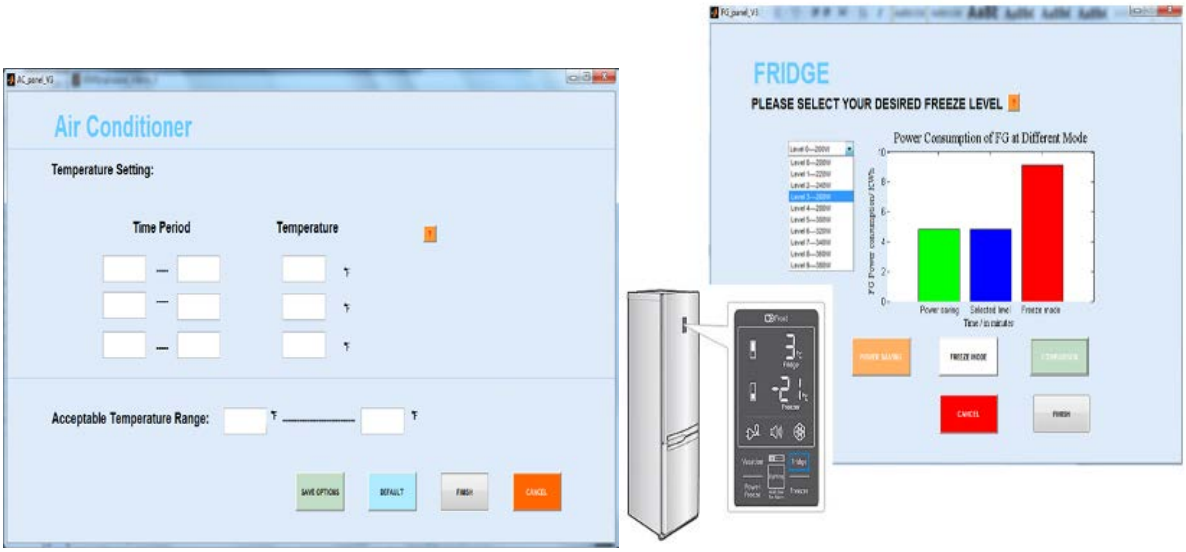

(a) Air conditioning loads and refrigerator Loads

(b) BSLs

(c) Electric vehicles

Fig. 2. 6 Parameter setting interfaces for controllable loads

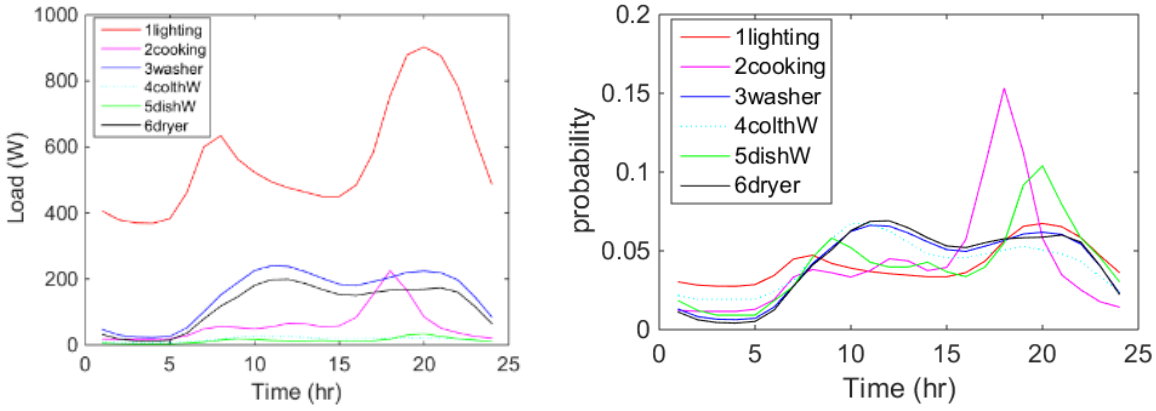

(a) (b)

Fig. 2. 7 Calculation of probability of use

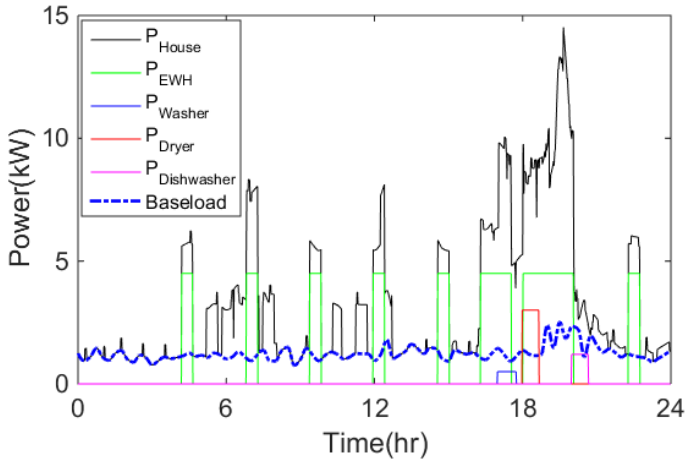

Fig. 2. 8 Total consumption of a house

2.1.3 Case Studies

As shown in Fig. 9, this toolbox allows algorithm developers to import weather data, electricity prices, and user input information to construct the customized house load model. Thus, the modeling is a supervised process. Based on different modeling considerations, the modelers can model standard household behaviors and also adjust the model parameters so that the consumption of the virtual house matches an actual set of field measurements. After

incorporating the ES and PV model, the house can be operated off-grid and simulate the HEM in Microgrid operation modes.

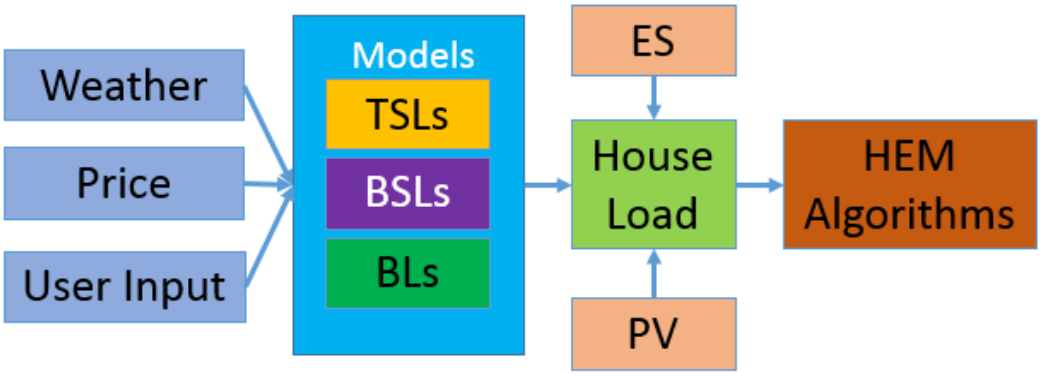

Fig. 2. 9 Algorithm development flow

Several HEM algorithms have been developed on this modeling platform. Two examples are shown in Fig. 10 and 11 to demonstrate the effectiveness of the toolbox. As shown in Fig. 10, a price-cap control HEM algorithm for reducing the electricity payment is modeled and compared with the no-HEM-control case. The TSLs and BSLs will be deployed to reduce the electricity consumption according to the priority list determined by the customer. The red circled areas represent decreased consumption during high price intervals.

The second algorithm is a solar powered household. The HEM algorithm aims at decreasing the daily back feeding energy. Consumers will first set a temperature range representing their comfort levels. Then, within the comfort constraints, the AC is used to precool the room if there is excess solar power. Examples of the testing results are shown in Fig. 11. The bottom bar charts represent the back feeding energy of with and without using HEM.

Because the same set of appliance models are used, the performance of different algorithms can be compared on a fair basis. In addition, students are invited as guests for testing the performance of the algorithms. The data are stored in the database so that the customer behaviors can be analyzed.

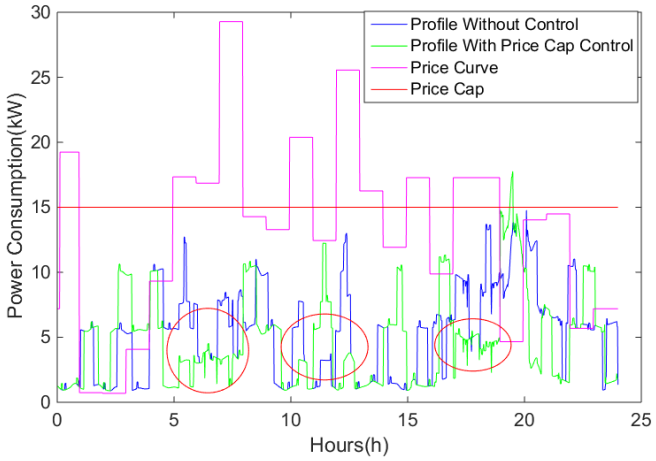

Fig. 2. 10 Result of price-cap control HEM algorithm

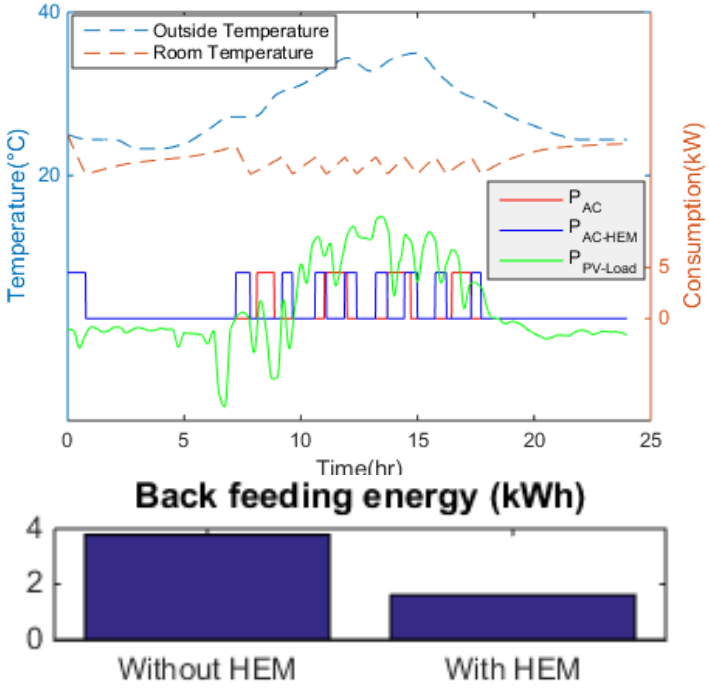

Fig. 2. 11 Result of solar-driven HEM algorithm

2.2 PV and ES Sizing Methodology and Tool Development

This section is organized as follows. Sub-section 2.2.1 describes the data used in the study. Sub-section 2.2.2 introduces the energy storage sizing considerations and methods. The simulation results are discussed in sub-section 2.2.3. Sub-section 2.2.4 summarizes the conclusion.

2.2.1 Data Preparation

A. Load Data Preparation

The residential load data used in the work is collected by Pacific Northwest National Laboratory at Olympia Peninsula (the Olypen data), WA in the GridWise demonstration project [44]. Energy consumptions of 50 residential homes were measured at 15-minute resolution for a year (April, 2006 - March, 2007), so there are 96 data points for a 24-hour period. At Olympia Peninsula, air conditioners are operated only occasionally in summer because of the mild weather in the area, thus the cooling loads can be filtered out by clustering load profiles into “a/c on” and “a/c off” days. Then, disaggregation methods [45-46] can be used to obtain the *Baseload 1* (BL1) profiles that contains temperature-insensitive loads, as shown in Fig. 1(a).

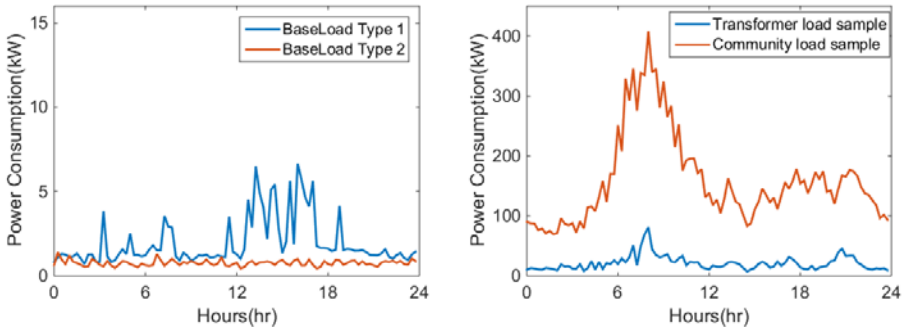

(a) (b)

Fig. 2. 12 Examples of the load profile

Similar clustering methods also allow us to obtain *Baseload 2* (BL2) profiles that exclude infrequently-used, controllable residential loads (e.g. washers, dryers, and dishwashers), as shown in Fig. 2. 12(a) [47]. The BL2 loads are mainly uncontrollable loads such as cooking, lighting, and refrigerating loads. Thus, baseload profiles randomly selected from the BL1 and BL2 databases, together with the controllable load profiles created by load models, can be used to model residential household loads. This hybrid load profile synthesis process allows us to preserve the correlation between the outdoor temperature and the cooling and heating load consumptions. In addition, the method makes it possible for us to model the control of load-side resources for reducing the size of the ESD. This process is a critical step for producing residential load profiles to generate the net load ensembles and is one of the main contributions of this study.

In this study, we assume that a distribution transformer supplies up to 5 residential homes and a community supplies up to 50 homes. Examples of the aggregated load profiles at the transformer- and community- levels are shown in Fig.2.12 (b).

B. Solar Data Preparation

Two sets of solar data are used in this study. When studying the seasonal differences, the hourly solar data collected in Olympia Airport [48] and Olypen load data are used. In the rest of the studies, we used the 5-minute solar radiation data collected from April 2006 to March 2007 in Raleigh, NC. To model the temperature impact on loads, temperature sensitive loads are modeled using the temperature data collected in Raleigh in the same time period. The baseloads are extracted from the BL1 database.

The solar radiation data is converted to PV generation profiles with the consideration of conversion efficiency as 20% [49]. A solar output database including four basic solar profiles (sunny, partially cloudy, cloudy, and rainy) was created, as shown in Fig. 2.13.

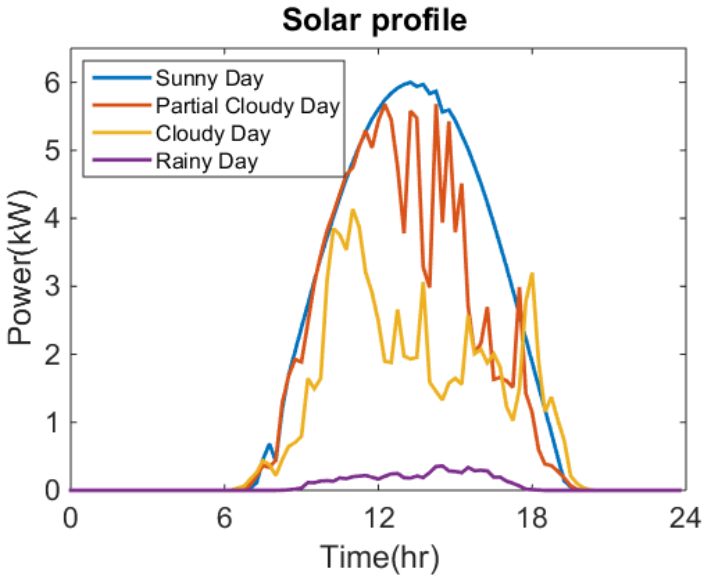

Fig. 2. 13 Sample solar power output for PV panel of 6kW capacity

C. Controllable Appliances Modeling

To quantify the benefit of managing controllable load resources for reducing the energy storage needs, six controllable appliances are modeled: air-conditioning units (used in summer), space heating units (used in winter), water heaters, dryers, washers, and dishwashers. The load profiles of a few controllable appliances are shown in Fig. 2.14. Controllable appliances are divided into thermostatically-controlled appliances (TCAs) and non-thermostatically controlled appliances (non-TCAs). Air conditioners, space heaters, and water heaters are TCAs. Washers, dryers, and dishwashers are non-TCAs. The residential controllable load models are introduced in details in [50].

D. Seasonal Impact on Energy Storage Size Selection

Fig. 2.15 shows daily average load duration curves for a residential home and the average daily high and low temperatures of each month. The Olypen load is winter-peaking because electric space heaters are used. In summer months, the average daily high temperature is about 25°C, so the cooling load is low. Because load consumption patterns are very different in the summer and winter seasons, we divided the yearly data into two seasons: cold and warm, as shown in Table 2.1. This allows us to address the difference in energy storage size selection caused by seasonal load variations [66].

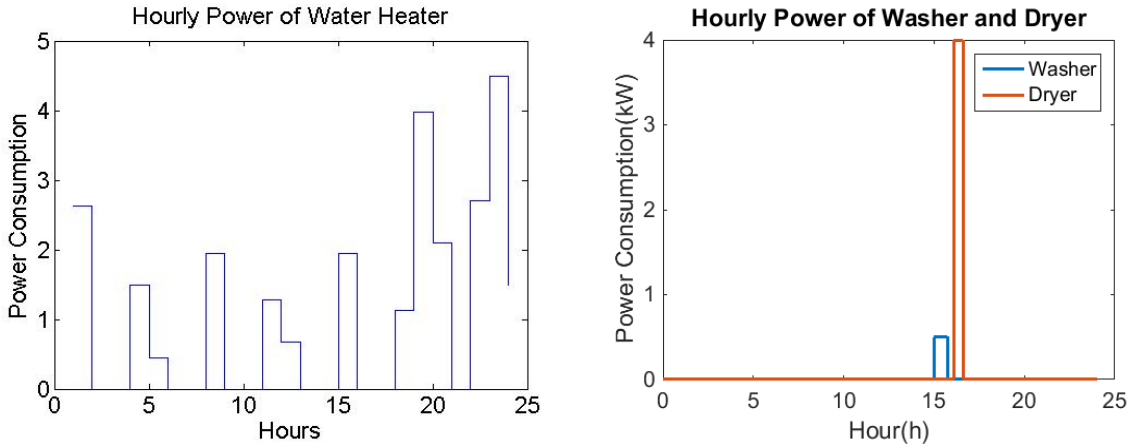

(a) (b)

Fig. 2. 14 Sample appliance profiles generated using load models

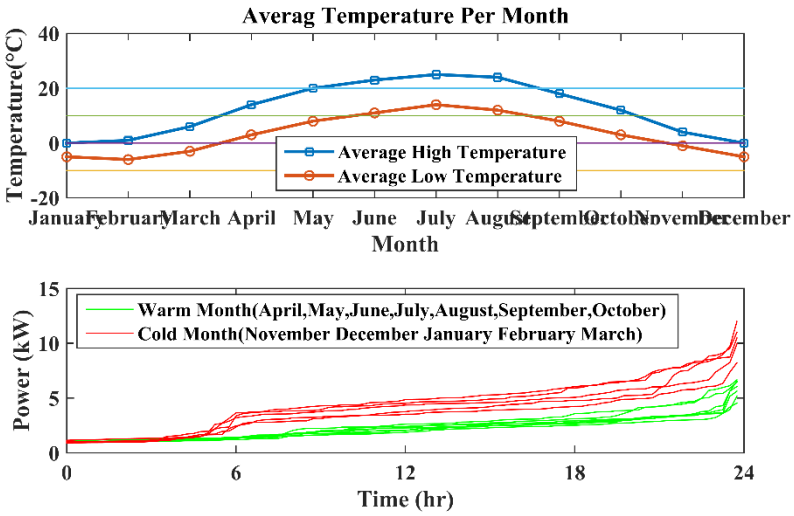

Fig. 2. 15 Daily load duration curves for cold and warm months

Table 2. 1 Season Categorization for ESD Sizing Studies

Cold season	November, December, January, February, March
Warm season	April, May, June, July, August, September, October

2.2.2 ESD Sizing Method

The ESD sizing procedure and methodologies are presented in the following subsections.

A. Setup of the Tri-level Simulation

As shown in Fig. 2.16, the setup of the simulation includes three levels: home-level, transformer-level, and community-level. Three home types are modeled: home without controllable loads, with TCAs as controllable loads, and with both TCAs and non-TCAs as controllable loads. For homes using TCAs as controllable loads, baseload profiles from the BL1 database are used for baseload and outdoor temperature profiles are used as inputs to the

TCA models. For homes using both TCAs and non-TCAs as controllable loads, baseload profiles from the BL2 database are used.

At home-level, the PV installed capacity ranges from 1kW to 6kW. ESDs within a community can be shared for storing excess solar generation to decrease reverse power flow and smooth power variations

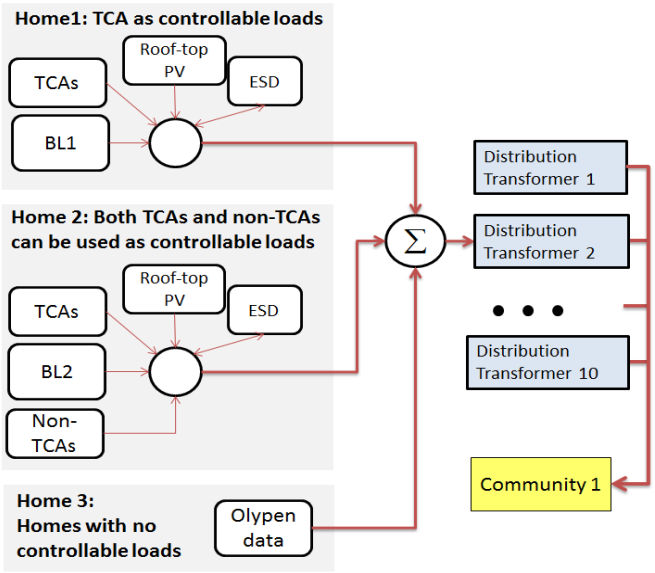

Fig. 2. 16 Setup of the tri-level simulation

B. Energy Storage Sizing Method

There are three key steps in the energy storage sizing method as illustrated below.

Step 1. Generate the ensemble of the net load profiles

The first step of the sizing process is the calculation of the ensemble of the home net load profiles using a shuffling algorithm. Let P_{Solar} be the power output of the rooftop PV and P_{Load} be the total household load consumption, the net load P_{net}, can be calculated as

$$\begin{aligned} &P_{net}(i,j) = P_{Load}(i,j) - P_{Solar}(i,j) \\ &i = 1,2,\ldots,N_{days} \qquad N_{days}^{Cold} = 152 \quad N_{days}^{Warm} = 213 \\ &j = 1,2,\ldots,N_{data} \qquad N_{data} = 96 \end{aligned} \tag{2.5}$$

where i is the i^{th} day, and j is the j^{th} data point. In our residential load database, there are 152 days in the cold season and 213 days in the warm season. Hence, N_{days}^{Cold} =152 and N_{days}^{Warm} =213. N_{data} represents the data number in a day. The consumption is metered every 15-minute, hence N_{data} is equal to 96.

The shuffling algorithm works as follows. Take warm season as an example, for the i^{th} day load profile, replace the solar radiation data of the i^{th} day with that of the other 212 days to obtain an ensemble of net load profiles for the i^{th} day. This process can be represented by

$$\begin{vmatrix} P_{net}(i,1:j,1) \\ P_{net}(i,1:j,2) \\ \vdots \\ P_{net}(i,1:j,k) \\ \vdots \\ P_{net}(i,1:j,N_{days}) \end{vmatrix} = \begin{vmatrix} P_{\text{Load}}(i,1:j) \\ P_{\text{Load}}(i,1:j) \\ \vdots \\ P_{\text{Load}}(i,1:j) \\ \vdots \\ P_{\text{Load}}(i,1:j) \end{vmatrix} - \begin{vmatrix} P_{Solar}(1,1:j) \\ P_{Solar}(2,1:j) \\ \vdots \\ P_{Solar}(k,1:j) \\ \vdots \\ P_{Solar}(N_{days},1:j) \end{vmatrix} \tag{2.6}$$

$$k = 1,2,...,N_{days}$$

The ensemble of a summer day net loads is shown in Fig. 2.17.

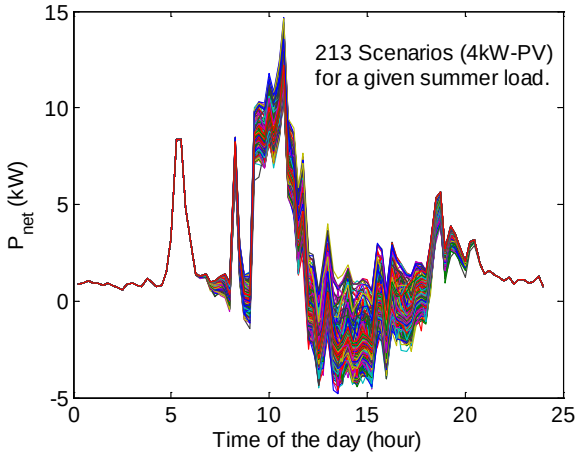

Fig. 2. 17 An ensemble of a summer day net loads for a house with a 4 kW rooftop PV

To obtain the ensemble *M* of the net load profiles for the whole season, repeat this process for all load profiles in the seasonal database (e.g. $N_{days}^{Cold} = 152, N_{days}^{Warm} = 213$):

$$M = \begin{bmatrix} P_{net}(1,1:j,1) \\ \dots \\ P_{net}(1,1:j,N_{days}) \\ \vdots \\ P_{net}(i,1:j,1) \\ \dots \\ P_{net}(i,1:j,N_{days}) \\ \vdots \\ P_{net}(N_{days},1:j,1) \\ \dots \\ P_{net}(N_{days},1:j,N_{days}) \end{bmatrix}_{N_{days}^2 \times 96} = \begin{bmatrix} M(1,1) & \dots & M(1,96) \\ M(2,1) & & M(2,96) \\ \vdots & \cdots & \vdots \\ M(N_{days} \times N_{days},1) & \dots & M(N_{days} \times N_{days},96) \end{bmatrix} \quad (2.7)$$

For instance, the ensemble matrix M for the warm season will include 213×213 net load profiles. This process is highly scalable. When more load and solar radiation data becomes available, N_{days} can be increased to obtain more solar-load combinations. Shuffling the solar radiation data of the entire season against a load profile might result in unrealistic cases. However, the more measurements we have in the database, the closer the obtained net load profiles reflect the actual statistics because the unrealistic cases will become outliers that have little impact on the final result.

Step 2. Perform capacity-iteration

Although home-owned ESDs can be used for a variety of purposes, one of the main reasons for the consumer to own an ESD is to self-consume the solar power. Therefore, in this study, the ESD is controlled to minimize the backfeeding energy. Let $P_{ESD}(t)$ represent the power output of the ESD at time t and $E_{ESD}(t)$ represent the energy level of the ESD at time *t*. $P_{ESD}(t)$ is

negative when charging and positive when discharging. Then, the power difference at time t, $\Delta P(t)$ can be calculated as

$$\Delta P(t) = P_{load}(t) - P_{solar}(t) - P_{ESD}(t) \tag{2.8}$$

Define $P_{neg}(t)$ as the power backfed to the main grid and calculate $P_{neg}(t)$ as

$$\begin{aligned} &if \quad \Delta P(t) \geq 0, \quad P_{neg}(t) = 0 \\ &else \quad P_{neg}(t) = -\Delta P(t) \end{aligned} \tag{2.9}$$

Then, the objective of sizing home-owned ESD is to minimize the total backfeeding energy E_{neg}:

$$\min \quad E_{neg} = \sum_{t=1}^{T} P_{neg}(t) \tag{2.10}$$

where E_{neg} is the total backfeeding energy and T is the total time. Let E_{ESD}^{Max} and E_{ESD}^{Min} be the upper and lower charging limits of the ESD and E_{ESD}^{t} be the energy level of ESD at time *t*. The above optimization problem can be solved by a straight forward control strategy shown in Fig. 7. The ESD will be charged whenever $P_{net}^{t} < 0 \,\&\, E_{ESD}^{t} < E_{ESD}^{Max}$, and discharged whenever $P_{net}^{t} > 0 \,\&\, E_{ESD}^{t} > E_{ESD}^{Min}$. Note that in our study, P_{net}^{Ref} is equal to zero and the charging and discharging efficiency are both set as 90% [65].

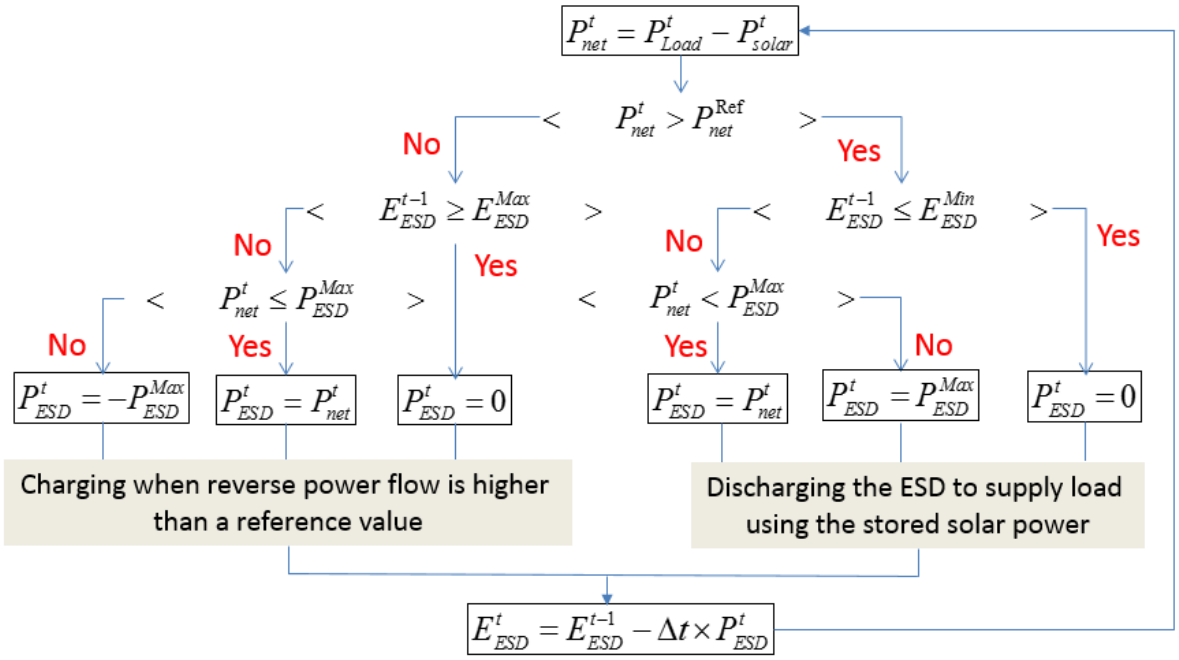

Fig. 2. 18 Control logic of the ESD for minimizing backfeeding energy

An example of the daily operation of an ESD is shown in Fig. 2.19. For a given combination of P_{ESD} and E_{ESD}, we run the algorithm to calculate E_{neg} for all the net load profiles in *M*. This will result in 213×213 and 152×152 sets of E_{neg} values in the warm and cold seasons, respectively. Those values will then be used to generate the cumulative distribution function (CDF) curve for the given energy storage size.

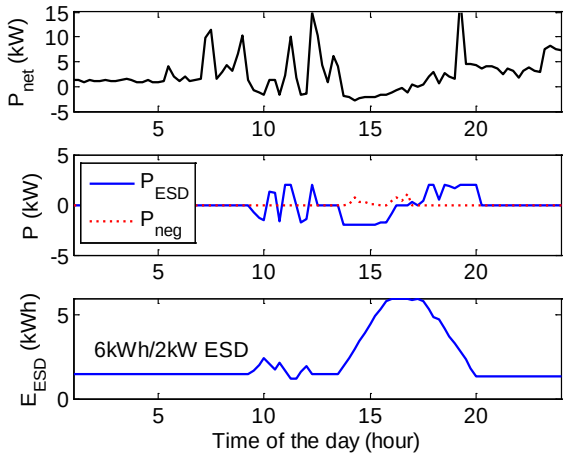

Fig. 2. 19 Daily operation sample of ESD

The CDF curve of the backfeeding energy in the cold season for a 3kW/3kWh ESD is shown in Fig. 2.20(a) and is compared with the CDF curve of the No-ESD case. Let E_{ESD} equal to 1kWh and P_{ESD} increase from 1kW to 5kW. We calculate the CDFs of the five cases and plot them in Fig. 2.20(b). The zoom-in plot in Fig. 2.20(c) at the 80% quantile shows that increasing the power rating from 1kW to 5kW while maintaining the energy capacity at 1kWh can only reduce E_{neg} by 0.4 kWh. This shows that the energy capacity of the ESD is the key limiting factor.

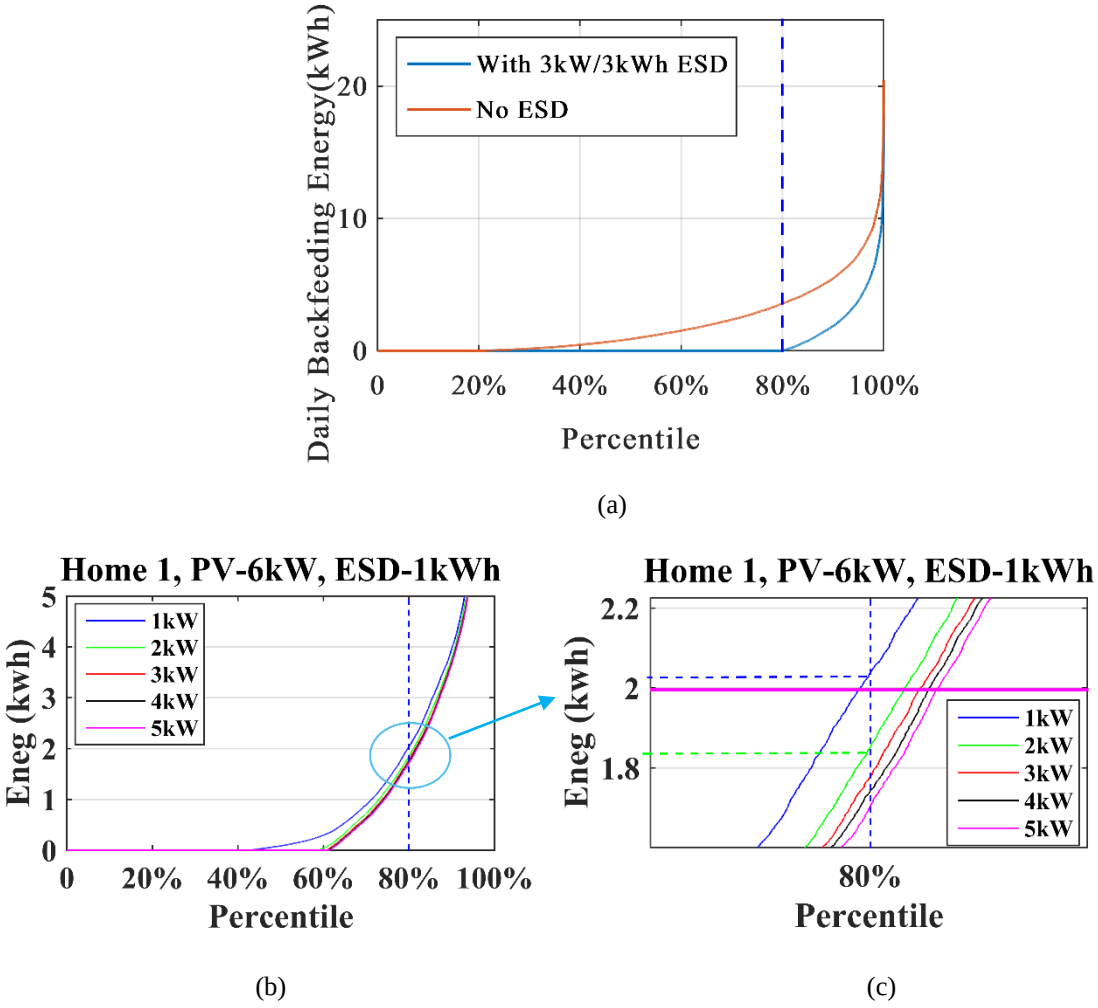

Fig. 2. 20 CDF of the daily backfeeding energy

Let $E_{\text{neg}}^{\text{Target}}$ represents the user defined backfeeding energy constraints. To find the smallest P_{ESD} and E_{ESD} that can meet the constraints, if E_{neg} meets the targeted values of $E_{\text{neg}}^{\text{Target}}$, we will reduce the P_{ESD} or E_{ESD} by ΔP_{ESD}^{Band} or ΔE_{ESD}^{Band}, respectively, until the $P_{\text{neg}}^{\text{Target}}$ and $E_{\text{neg}}^{\text{Target}}$ cannot be met; if E_{neg} cannot meet the targeted values of $E_{\text{neg}}^{\text{Target}}$, we will increase the P_{ESD} or E_{ESD} until the $P_{\text{neg}}^{\text{Target}}$ and $E_{\text{neg}}^{\text{Target}}$ can be met.

The cost difference, ΔC, between self-consuming $E_{\text{neg}}^{\text{Target}}$ and selling $E_{\text{neg}}^{\text{Target}}$ to the grid, can be calculated as

$$\Delta C = E_{\text{neg}}^{\text{Target}} \times (p_{buying} - p_{selling}) \tag{2.11}$$

where p_{buying} is the price at which utilities buy extra solar power from the homeowners, and $p_{selling}$ is the price for selling grid power to users. This allows the home-owner to determine $E_{\text{neg}}^{\text{Target}}$ based on electricity prices. Another way of determining $E_{\text{neg}}^{\text{Target}}$ is the utility requirement at the point of coupling. In this study, our focus is to develop the sizing procedure and methodologies for comparing different sizing options based on the net load ensembles. Therefore, we assume that the value of a desired $E_{\text{neg}}^{\text{Target}}$ has been computed and is a known input of the sizing problem.

Step 3: Generate the compressed, composite CDF curve and use the Equal Probability Line method to select the optimal ESD size

By compressing the x-axis of Fig. 2.20 into a 0-1 block, we can put the CDF plots of different battery size options side-by-side in one figure to create a compressed, composite CDF (CC-CDF) plot for comparing the different options. As shown in Fig. 2.21, one CC-CDF plot consists of 25 CDFs that represent five E_{ESD} size options (1, 2, 3, 4, and 5kWh) and five P_{ESD} options (1, 2, 3, 4, and 5kW). If we connect the points bearing the same cumulated probability of occurrence on the 25 CDF plots together, we receive a line called the equal probability line (EPL). For example, if we connect all the points representing 80% cumulated probability of occurrence together, we obtain the 80% EPL (the blue solid line in Fig. 2.21). By checking the

y-axis of the intersection between the EPL and the CDF curves, the user can quickly find an ESD size for his home to meet a the daily backfeeding energy limit 80% of time. Assume that a customer wants to install a battery for a 6-kW PV system and he wants the backfeeding power to the grid below 1.5 kWh 80% of time. As shown in Fig. 2.21, as long as the battery energy capacity is above 2kWh, the customer's requirement can be satisfied. Once the battery energy rating is above 3kWh and power rating is above 2kW, the marginal reduction of backfeeding energy by increasing the battery energy and power sizes are diminishing, so the customer may want to choose at most a 3 kWh/2kW battery. If the battery cost is also known, how much it costs to reduce backfeeding energy for any given PV capacity could also be calculated.

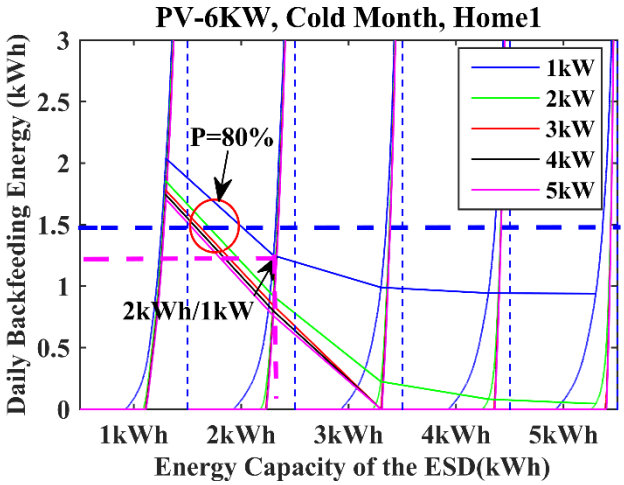

Fig. 2. 21 E_{neg} for a range of P_{ESD} or E_{ESD}.

Because the CC-CDF curves and the EPLs offer a straightforward way to select the ESD size based on probability of meeting the operational constraints and the gradients of the EPLs reflect the marginal benefit of increasing the ESD power and energy capacities, we will use this graphical method to analyze our results throughout the rest of the study. The CC-CDF and EPL methods developed in this work can be used for many other probabilistic-based

evaluations with multiple optimization variables associated with monotonically increase or decrease continuous or discontinuous functions. Therefore, the development of this graphical method is considered to be one of the main contributions of this work.

2.2.3 Simulation Results

In this section, simulation results for sizing home-owned ESDs, transformer-ESDs, and community-owned ESDs are presented. Five E_{ESD} options (1, 2, 3, 4, and 5kWh) and five rated power options (1, 2, 3, 4, and 5kW) are considered for six installed PV capacities (1, 2, 3, 4, 5, and 6kW). Two different load patterns (winter and summer) are compared to assess the necessity of sizing ESDs for different seasons. The capabilities of using DSM to reduce the size of the ESD are also assessed. For all the cases, results are produced using the capacity-iteration method and analyzed by projecting the 80% EPLs on the CC-CDF curves as introduced in Section III.

A. Size the ESD Considering the Seasonal Load Pattern Shifts

The CC-CDF curves for the cold month loads are shown in Fig. 2.22. The 80% EPLs for installing a 4, 5, and 6-kW PV system are plotted for selecting the power and energy capacities of the energy storage system based on the daily backfeeding energy limit, $E_{\text{neg}}^{\text{Target}}$. The figure shows that if the PV capacity is less than 5kW and $E_{\text{neg}}^{\text{Target}}$ is 1.5 kWh, there is no need for using an ESD. If the PV capacity is 6 kW, a 1kW/2kWh ESD may meet the $E_{\text{neg}}^{\text{Target}}$ 80% of the time. Another observation is that the power rating of the ESD is not as critical as the energy rating because increasing the power rating will not significantly reduce the backfeeding energy.

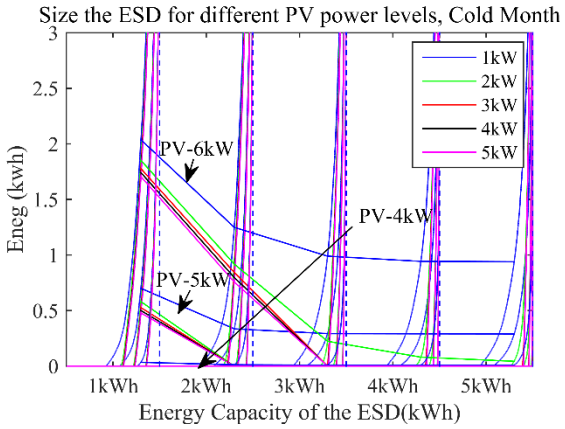

Fig. 2. 22 Q_{ES} and P_{ES} of different solar capacity

The CC-CDF curves of the summer months are shown in Fig. 2.23 by repeating the above analysis for the summer months. To better demonstrate the seasonal difference, as mentioned in Section 2.2.1, a set of solar radiation data collected in the same area where the load data was collected is used to do the same analysis.

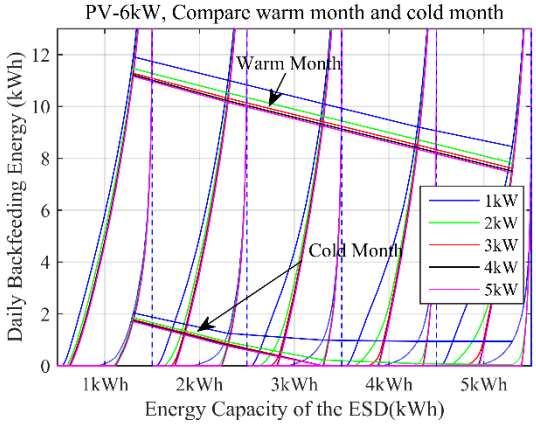

Fig. 2. 23 Sizing ESDs for different seasons

Note that most houses in Olympic Peninsula have very low air conditioning loads because of the mild weather in that area. Therefore, in the summer months, the self-consumption capability of a household is very limited. As a result, there is a greater need for storing energy to meet the same $E_{\text{neg}}^{\text{Target}}$ in summer months than in the winter months. The result reveals that

seasonal needs of energy storage can be very different. For example, in Southern cities, winter loads are low and summer loads are high, so the capability of self-consumption are higher in summer. Thus, ESD renting programs for meeting the different seasonal needs between summer and winter peaking regions may become an economic solution.

B. Size the ESD for Aggregated Residential Loads at the Transformer- and Community-Levels

The ESD sizing curves for 4 homes with 6-kW PV systems in the cold months are shown in Fig. 2.24. The CDF of the daily backfeeding energy of each home can be very different because each home has its unique consumption pattern and load characteristics. For example, a gas-heating residence has significantly lower energy consumptions than an electric-heating one. When multiple homes share an ESD, the load diversity tends to increase the self-consumption capacity and reduce the ESD size.

Fig. 2.25 shows the results of sizing ESD for 2~3 homes. As expected, backfeeding energy decreases significantly for the same total ESD capacity. For instance, if home 2 and home 3 each has a 1kWh/1kW ESD, E_{neg} can reach approximately 14kWh. However, if these two homes share a 1kWh/1kW ESD, E_{neg} can be reduced to approximately 9kWh.

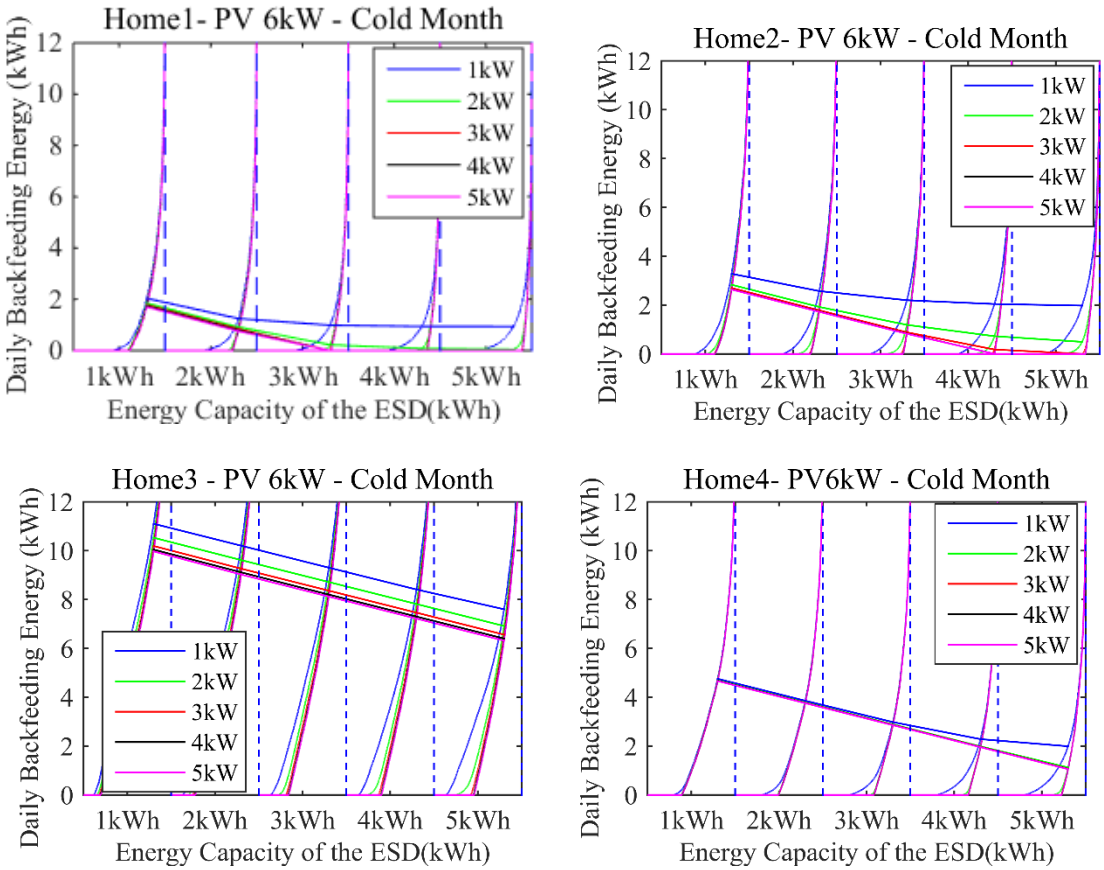

Fig. 2.24 Sizing ESDs for different homes

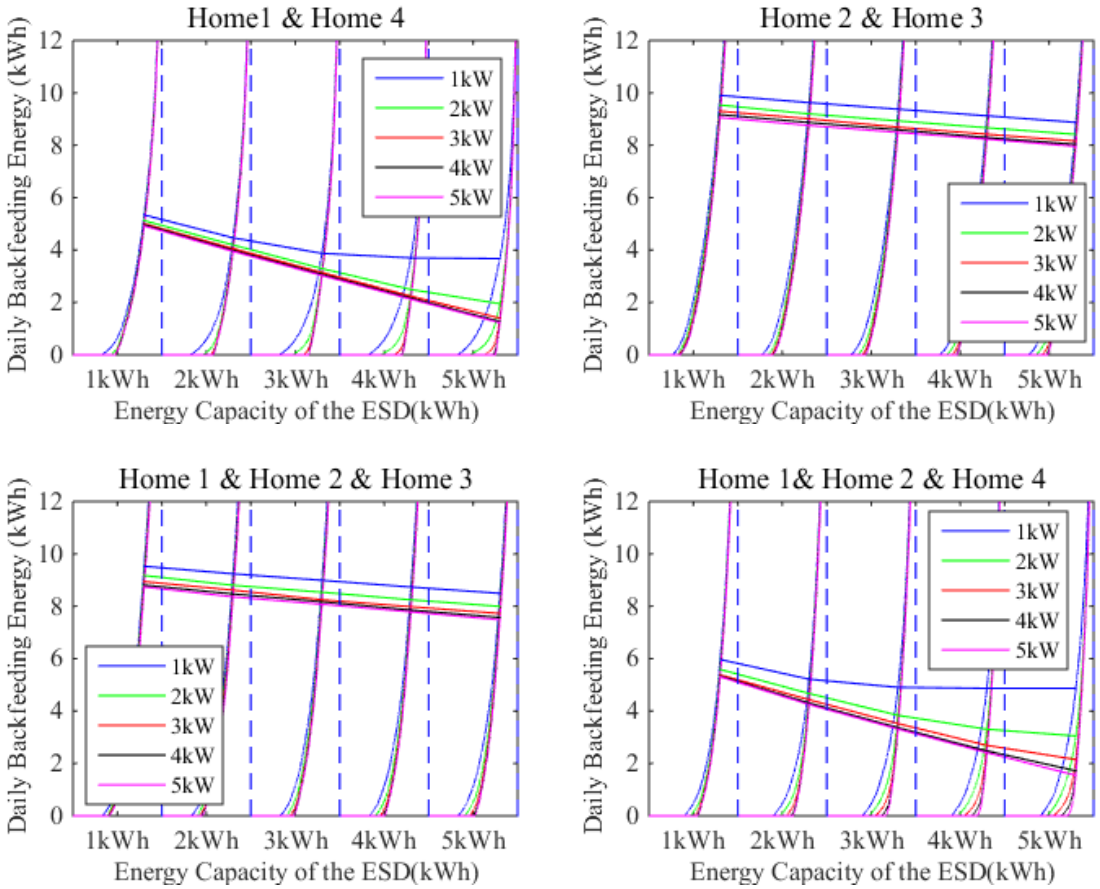

Fig. 2. 25 Sizing ESDs for aggregated homes

Define the PV penetration level of the community as the percentage of the homes in the community that have PV installed. The CC-CDF of a community with 33 homes using their winter net load ensembles is calculated. For each home with PV installed, the installed capacity is assumed to be 6kW. As shown in Fig. 2.26, if the penetration level is less than 80%, there is no need to install an ESD using the following criteria: "E_{neg}^{Target} *is less than 1kWh 80% of the time*".

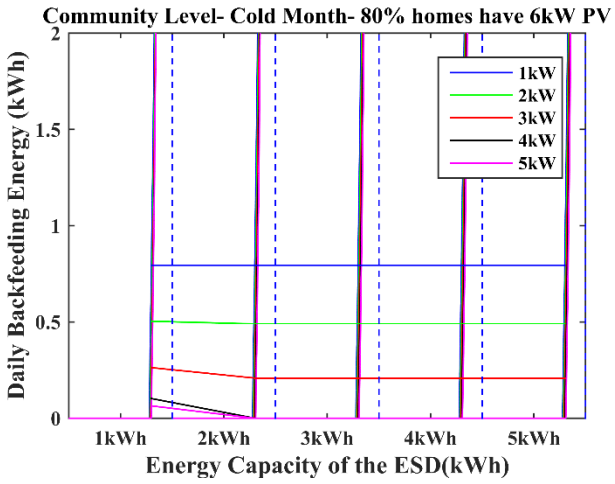

Fig. 2. 26 Sizing ESDs for 80% PV penetration level

However, if the penetration reaches 100% (see Fig. 2.27) as all the 33 homes have a 6-kW PV system installed, E_{neg} can increase significantly. If the capacity of the community ESD is still 1kWh/1kW, E_{neg} can be controlled to be less than 15kWh 80% of time. Fig. 2.28 (a) shows the performances of different ESD capacity options when the PV penetration level increases from 80% to 100%. The plot also shows the expected improvement per capacity increase.

Set $E_{\text{neg}}^{\text{Target}}$ of a community at 8kWh. Assume each house in the community has a 6kW PV system installed such that the PV penetration level in the community is 100%. The optimal ESD sizes for a community with 10, 15, 20, 25, 30, or 33 houses are plotted in Fig. 2.28 (b). At first, the size of the ESD increases when there are more houses in the community. However, after the number of houses increase to 30 houses, we start to see decreasing needs for energy storage. This is because the loads are more diversified when more houses are integrated in the community. As a result, more solar power can be self-consumed within the community.

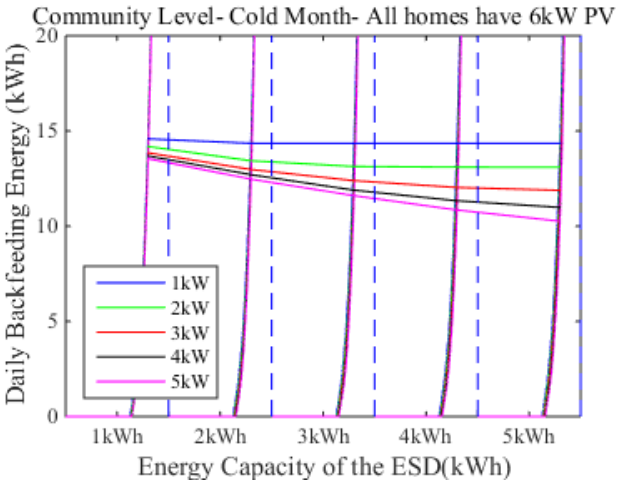

Fig. 2. 27 Sizing ESDs for 100% PV penetration level

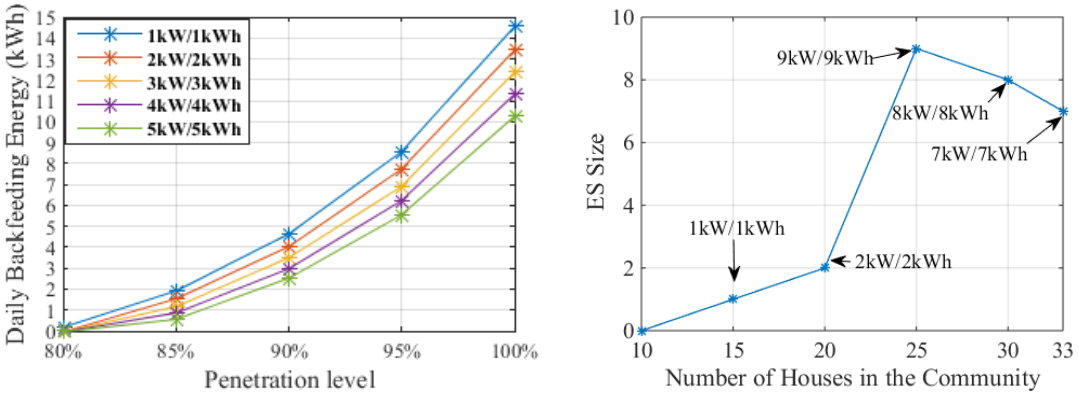

(a) (b)

Fig. 2. 28 Size ESD for different PV penetration levels (80~100%)

C. Sizing ESDs Considering Demand-side Management

The ESD size is expected to be further decreased if DSM could be used for self-consumption of solar power. Because the development of advanced DSM algorithms for self-consumption of the PV outputs is not the focus of this work, a simple DSM algorithm is used to illustrate how to size an ESD when considering DSM. As illustrated in Fig. 2.29, the air conditioning

(AC) unit is controlled to assist the self-consumption of the PV power. The AC will operate within a temperature band $[T_{low}, T_{high}]$. The middle of the band is the AC set point T_{set}. At every time step, $P_{solar}(t)$ and $P_{load}(t)$ will be checked, if $P_{solar}(t) > P_{load}(t)$, then the AC status and room temperature will be checked successively. If AC is "off" and room temperature is higher than T_{set}, AC will be turned on to cool the room.

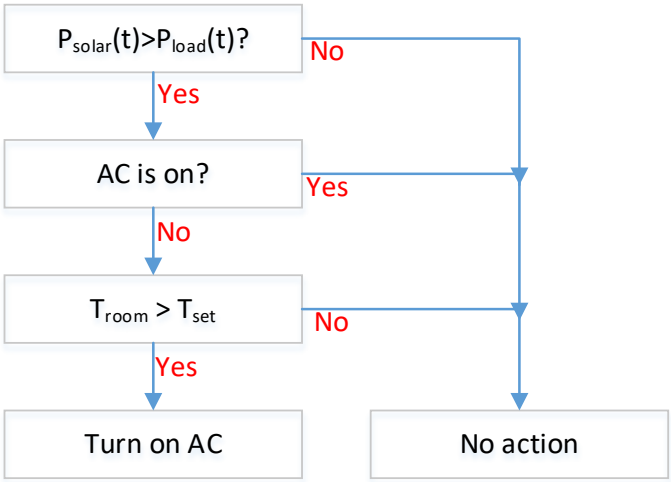

Fig. 2. 29 Flow chart of controlling cooling loads for self-consumption of solar power

The simulation results at the home-, transformer-, and community- levels are shown in Fig. 2.30.

1) Home-level study

Fig. 2.30(a) shows the results of sizing the ESD with- and without- DSM at the home level. Applying DSM will decrease the size of the ESD significantly. For instance, if the ESD is 1kW/5kWh, E_{neg} can be decreased by 64%.

2) Transformer-level study

The simulation results at the transformer level are shown in Fig. 2.30(b). The percentage of E_{neg} reduction is around 34% after using DSM. The size of the ESD is 3kW/1kWh to maintain the $E_{\text{neg}}^{\text{Target}}$ below 10kWh without DSM. With DSM, the size of the ESD is reduced to 1kW/1kWh, representing a 67% reduction.

3) Community-level study

To further investigate the aggregation impact of using DSM for helping reducing the size of community ESD, aggregated loads of 33 homes (each home has a 3kW roof PV system) are used. As shown in Fig. 2.30(c), the percentage of E_{neg} reduction by DSM is 27% at the community level. The above results show that applying DSM will reduce the size of ESD significantly. However, to make DSM program more efficient, more elaborated algorithms and coordination among different households are needed to further reduce the backfeeding power.

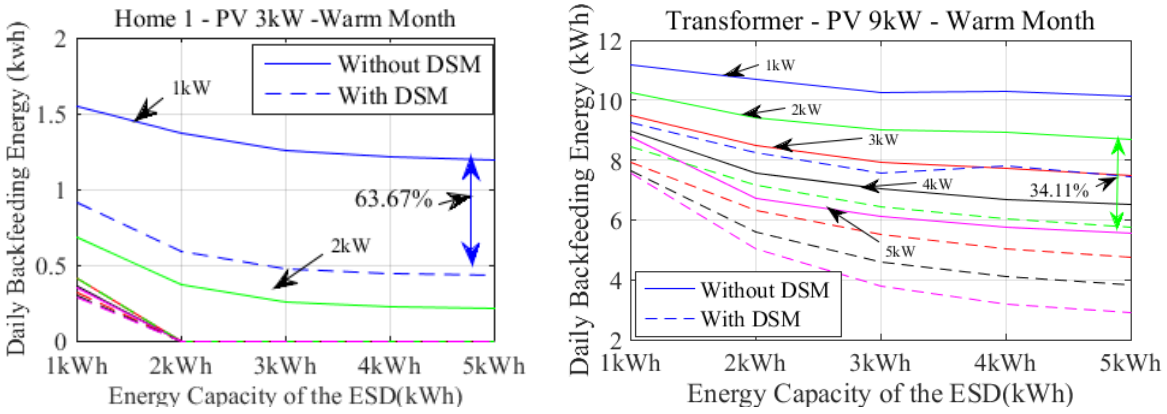

(a) (b)

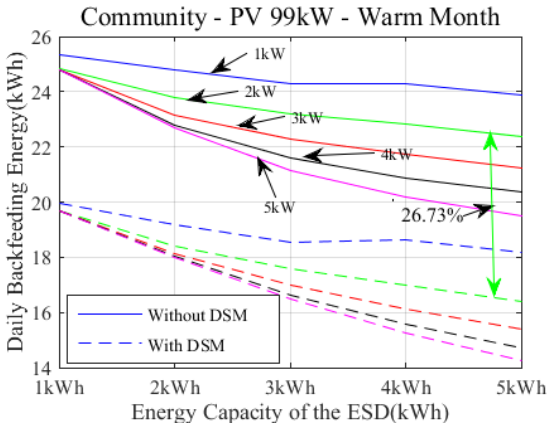

(c)

Fig. 2. 30 DSM impact on sizing ESDs at home-, transformer-, and community- levels

D. Comparison with Other Sizing Methods

In the literature, many sizing methods use the worst case scenarios or the average case scenarios for sizing ESDs. To compare with the results obtained by those sizing methods, E_{neg} calculated by different sizing methods are compared in Fig. 2.31. The worst case scenario is obtained by using the net load in a sunny, light load day. The average case is obtained using

the net load in a sunny, average load day. If a 5-kW PV and a 3-kW ESD are selected, we can compare the energy capacities of the ESD selected by different sizing methods.

Assume that $E_{\text{neg}}^{\text{Target}}$ is 6kWh, the proposed sizing methodology suggests that the user can use a 3kW/1kWh ESD for the warm months and no ESD is needed in the cold months. The average case method suggests that no ESD is needed and the worst case method indicates that a 3kW/3kWh ESD is needed for an entire year. The comparison shows that the average case tends to underestimate the ESD needs and the worst case tends to overestimate the ESD needs depending on how the worst case is constructed.

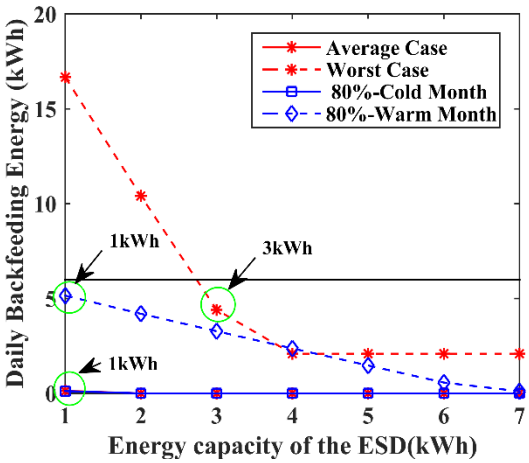

Fig. 2. 31 Backfeeding energy among different sizing methods

E. Comparison using Data from Multiple Years

Solar radiation data from ten years (2001-2010) are used to compare results among different years. A 6kW PV and 1kW ESD are used. The simulation is conducted for the cold months. Assume that the load consumption patterns are similar for the 10 years. As shown in Fig. 2.32, the results are consistent for all the years except for 2005. Although the EPL of the year of 2005 is away from the EPLs of the others, the majority is very close to each other. This

simulation results show that except for a few years, the results obtained using the proposed method are consistent. If more data are available, the upper and lower boundaries of the sizing curve can be obtained to further enhance the results.

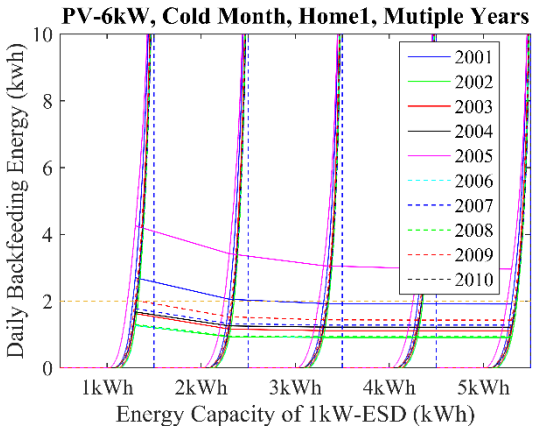

Fig. 2. 32 Results comparison of multiple years

F. Cost-benefit Analysis under TOU Tariff

An example of adding the cost-benefit element into the sizing considerations is given in this section to show how to combine the performance-based sizing approach with the cost-based analysis. The time-of-use tariff used in the cost benefit study is obtained from the Duke Energy Progress website [51]. The ESD price is $200/kWh and $175/kW [52]. The price of a 6kW residential PV panel is $1.5/W [53]. The project span is considered as 25 years and the replacement cost of an ESD is estimated to be $200/kWh every 5 years. The net present values (NPV) of installing an ESD of different rated power and storage capacity at House 1 are plotted in Fig. 2.33 (a). Fig. 2.33 (b) shows the NPV of installing an ESD from 2kW/2kWh to 6kW/6kWh at five different houses. The optimal ES size derived from the performance-based approach can then be compared with that of the cost-based approach to reach an optimal option that meets both budget constraints and performance expectations.

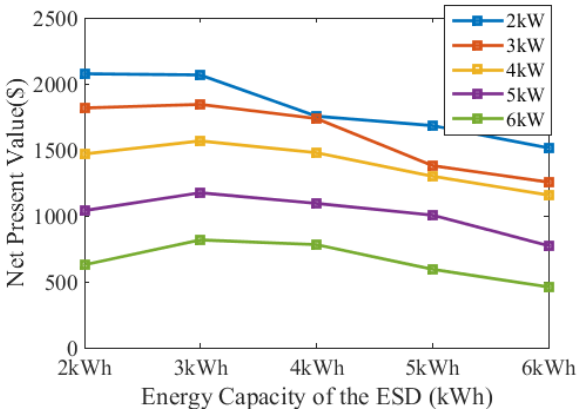

(a)

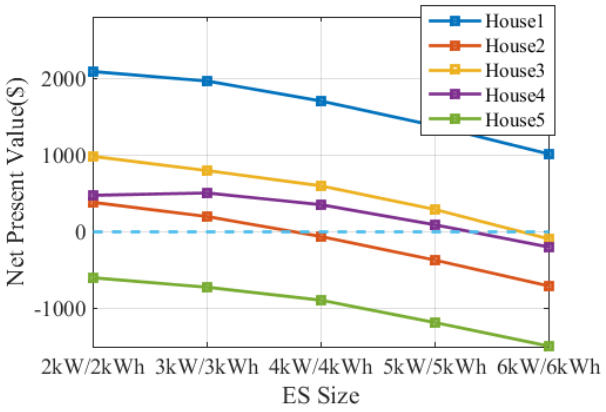

(b)

Fig. 2. 33 Net present value of various ES sizes

2.2.4 Tool Interface Development

The graphical interface of the tool is shown in Fig 2.34 [67]. The interface allows the users to select the size of the PV and ESD by running through all the possible loading conditions. The sizing tool will yield an operation statistic that shows the probability of occurrence of the reverse power. Comparison can be made for different PV and ESD combinations. If there is a price difference between buying the grid power and selling the self-generated solar power, a comparison of costs among different PV and ESD combinations can be provided. The users

can either optimally size ESD for a given PV capacity or select an optimal PV and ESD combination based on the characteristics of their non-controllable and controllable loads. Besides allowing the user to select solar and battery capacity for different load patterns, it also allows the user to consider DSM options. The users can evaluate the summary of the reverse power for all the available scenarios for making an informed decision.

Fig. 2. 34 Toolbox interface

2.3 Cost-Benefit Study for Sizing PV and ES Systems

This section is organized as follows: Sub-section 2.3.1 introduces the load models and PV database. Sub-section 2.3.2 discusses the formulation and tariff information of the cost-benefit study. Sub-section 2.3.3 analyzes the case studies. Sub-section 2.3.4 summarizes the conclusions and states the future work.

2.3.1 Modeling Methods

There are two main models used in the cost benefit study: residential load models and PV output models based on historical solar insolation data [65].

The modeling details of residential loads can be found in [16, 30, 37, 40, 44]. Major household electricity consumptions are categorized into temperature sensitive loads (TSLs), behavior sensitive loads (BSLs), and daily repetitive base loads. The TSLs such as air conditioner (AC), space heater (SPH), refrigerator, and electric water heater (EWH), are modeled by equivalent thermal circuit models using temperature profiles as inputs [16]. The BSL loads including washers, dishwashers, and dryers, are large loads but used infrequently. Those loads are modeled based on a probability-based approach presented in [30]. Daily repetitive base loads such as cooking, lighting, and entertainment loads can be extracted from actual historical load profiles for different types of households as introduced in [37]. Using load models as well as typical base load profiles, we can construct yearly load profiles for different types of residential homes with very limited customer inputs. This allows a customer without a power meter installed to estimate the yearly load profile when selecting a PV system.

Hourly solar insolation data for ten years are used to establish the PV database [48]. Power output profiles of the PV panels are converted from these insolation data considering a conversion efficiency of 20%. A few typical load profiles and PV outputs are shown in Fig. 2.35.

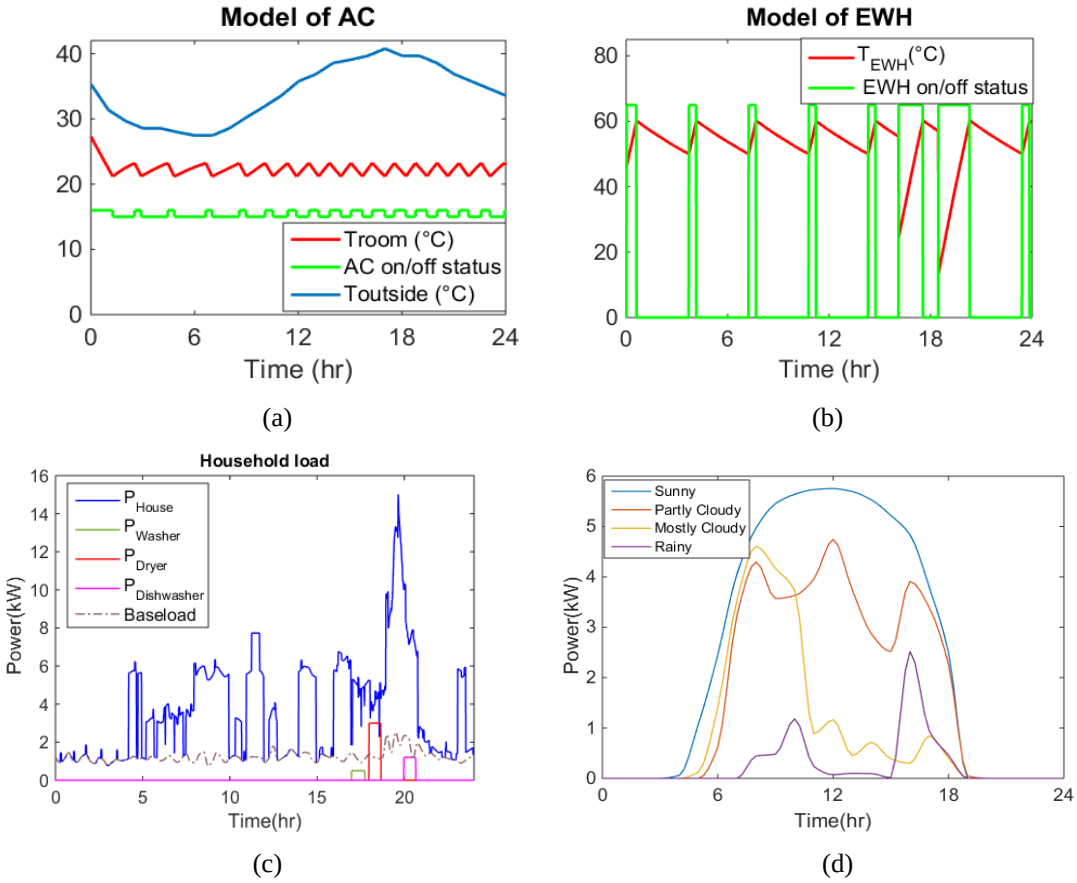

Fig. 2. 35 Sample output of the load and PV models

2.3.2 Setup of the Cost-Benefit Study

The cost-benefit study in this work is based on the TOU tariff of Duke Energy in North Carolina [51] as shown in Table 2.2 and Fig. 2.36. Note that backfeeding power to the grid is not paid in this rate structure. The price of PV panel we used is based on the pricing information provided in the NREL technical report [53] and the price of ES is from the technical report of Sandia National Lab [52], as shown in Table 2.3. Based on different sizes of the PV and ES selected for the modeled residential annual net load profile, NPV and YR are calculated for each option [54].

The present value of the total saving, S_{sum}, in n years is calculated as

$$S_{sum} = \sum_{i=1}^{n} S(i)\left(\frac{1+e}{1+d}\right)^{n} \tag{2.12}$$

where $S(i)$ is the saving in year i, e is the escalation rate, and d is the discount rate. Note that $S(i)$ is the saving in the electricity bill in year i compared to base case.

Similarly, the present value of the total cost is calculated as

$$C_{sum} = C_{PV} + C_{ES-init} + \sum_{i=1}^{n} R(i)C_{repl}\left(\frac{1}{1+d}\right)^{n} + C_{O\&M}\frac{(1+d)^{n}-1}{d(1+d)^{n}} \tag{2.13}$$

where C_{PV} is the total cost of PV panel installation, $C_{ES\text{-}init}$ is the initial installation cost of ES, C_{repl} is the replacement cost of the ES, and $R(i)$ (0/1= no/yes) represents the status of ES replacement need in the i^{th} year.

The net present value is calculated as

$$NPV = S_{sum} - C_{sum} \tag{2.14}$$

When $NPV(r)$ is equal to zero, we can calculate the year at which the saving and the cost will breakeven.

$$NPV(r) = S_{sum}(r) - C_{sum}(r) = 0 \tag{2.15}$$

In this work, we used the escalation rate as 2% and discount rate as 5%. More details regarding the rate selection can be found in [54].

Table 2. 2 TOU Price of Duke Energy

Time of Use Price		
Basic Facilities Charge per month		$13.38
Energy Charge	On-Peak per month, per kWh	$0.069283
	Off-Peak per month, per kWh	$0.056902
On-Peak Demand Charge per month, per kW	Summer Months	$7.77
	Winter Months	$3.88
On-Peak Period Hours	Summer Months	1:00 p.m. – 7:00 p.m. M-F
	Winter Months	7:00 a.m. – 12:00 noon M-F
Off-Peak Period Hours		All other weekday hours and all Saturday and Sunday hours
Summer Months		June 1-September 30
Winter Months		October 1- May 31

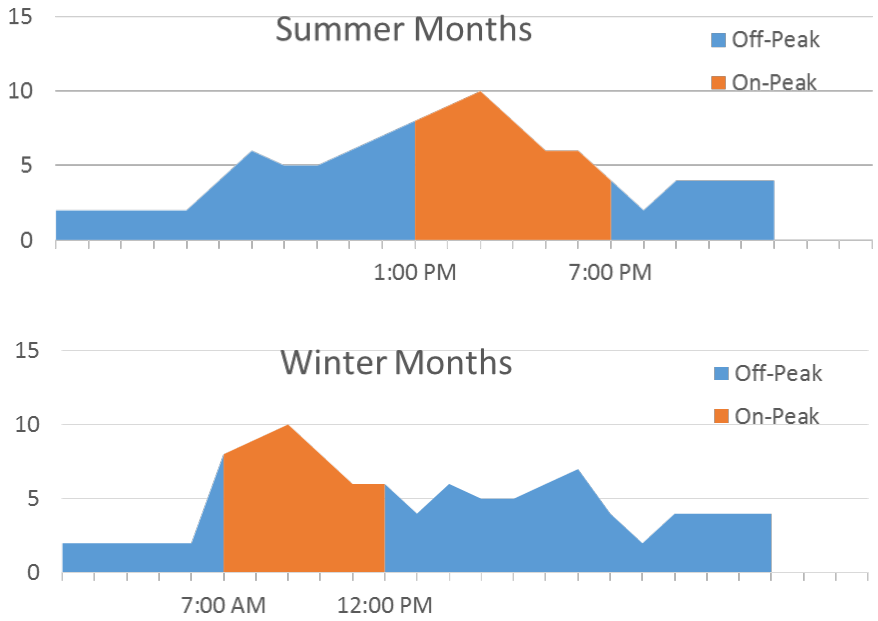

Fig. 2. 36 On-Peak and Off-Peak period hours

Table 2. 3 Price of PV Panel and ES

Price of PV panel and ES		
Residential PV panel		$1.5/W
Energy Storage Device	Energy-Related Cost	$200/kWh
	Power-Related Cost	$175/kW
	Replacement Cost	$200/kWh
	Replacement Frequency	5 years
	Fixed O&M	$5/kW-yr

Using the TOU tariff illustrated in Table 2.2, the cost-benefit study has been conducted for 5 different houses. We study four cases: a base case with no solar, no ESS, and no DSM (Case 1), base case with PV added (Case 2), base case with PV and ESD added (Case 3), and base

case with PV, ESD, and DSM added (Case 4). The study period is 10 to 25 years. We assume similar household loads with changing solar insolation.

In this study, the size of the roof PV panel is assumed to be 6kW, the size of the ESS for each home is 2kW/2kWh. The ESS will be charged if there is extra solar available and will be discharged otherwise. The load used for DMS is the spacing heating and cooling loads. They will be turned on to consume the excess solar power to minimize the backfeeding power.

2.3.3 Cost-Benefit Study Results

This section presents the results of the cost-benefit study of five residential homes for four system options.

A. Monthly and Yearly Savings

To evaluate the savings of each household in different seasons of a year, monthly savings of each case compared with the base case in 2001 are plotted out in Fig. 2.37. It can be observed that savings in summer months are significantly larger than those in the winter months, especially for case 3 (with PV, ESD, and DSM). In July, case 3 has a saving of $90, almost 60% of the original electricity bill. This is because in North Carolina area, summer loads peak at day-time coincide with the solar generation. Therefore, more solar is consumed instead of being backfed to the grid.

Yearly savings of the 5 houses in case 1 (only with PV) for 9 years are shown in Fig. 2.38. It can be observed that the savings of the 5 houses for the 9 years all have a steady trend. Therefore, for a household without significant changes in its electricity consumption patterns, the savings are fairly consistent in each year.

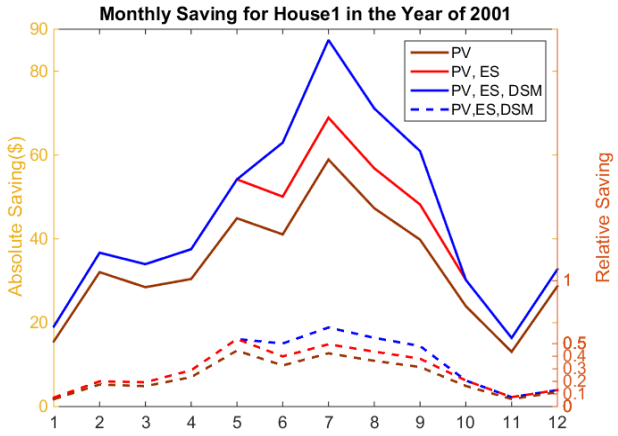

Fig. 2. 37 Sample monthly savings

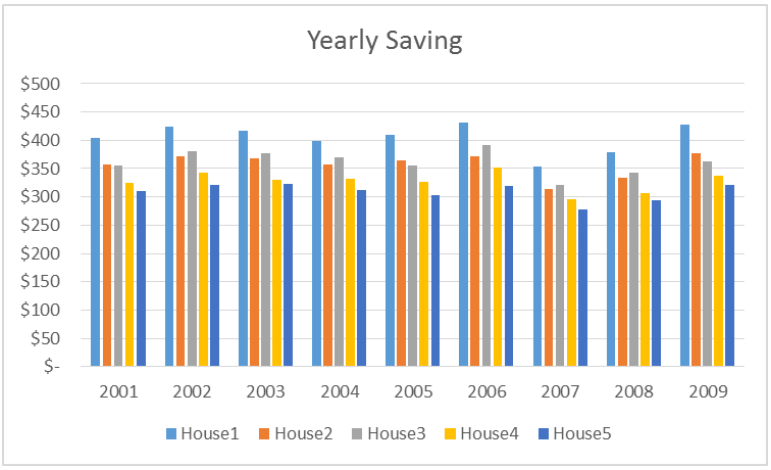

Fig. 2. 38 Sample yearly savings

B. Marginal Value of PV and ES

We vary the capacities of PV and ESD in case 2 (with only PV) and case 3(with PV and ES) to investigate the marginal saving of increasing the size of PV and ESD by one unit capacity. Assume that the life time of PV panel to be 20 years, the savings against cost in each case is plotted out in Fig. 2.39.

Under the TOU tariff, marginal saving of the PV panel will start to decrease once the PV capacity exceeds the load. For example, for household 1, installing a PV panel of 3-5kW is appropriate, but installing a 6-kW PV panel will no longer be profitable.

The household electricity consumption pattern is critical for PV capacity selection. For instance, for house 1 and house 3, installing a PV panel of 4-kW will be profitable but for house 2, 4, and 5, it is not. In fact, for house 5, installing a PV system is not profitable as the savings will never exceed the cost.

Assume that the life time of PV panel can be extended to 25 years, the savings in each case is shown in Fig. 2.40. From the results, we can see that the extension of the lifespan of PV panels significantly increase the profitability of the system, making installing PV (from 1 to 6-kW) profitable for all the five houses, as shown in Fig. 2.40.

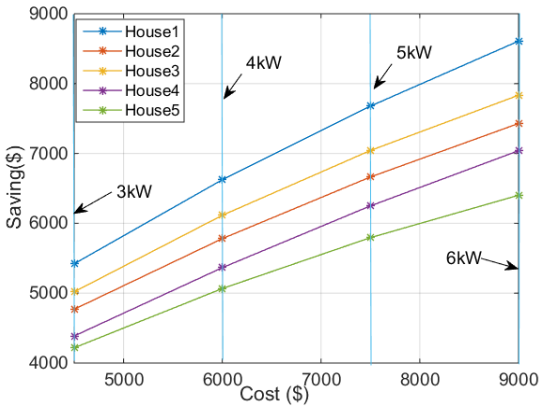

Fig. 2. 39 Saving from PV (20 years)

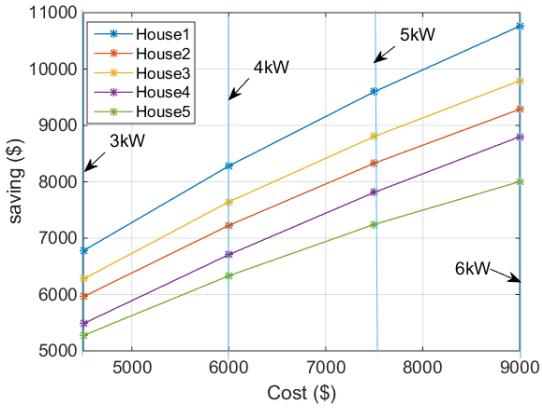

Fig. 2. 40 Saving from PV (25 years)

C. Net Present Value and Years of Return

For case 2 with PV of 6kW, case 3 with ES of 2kW/2kWh, case 4 with AC as a DSM resource, considering a length of 25 years, the NPV of house 1 has been shown in Table 2.4. It shows that installing ES has decreased the NPV but utilizing DSM could improve the NPV a lot. This demonstrates the value of implementing applicable DSM in residential houses installed with PV panel and ES.

Table 2. 4 NPV of House1

House1	Case 2	Case 3	Case 4
NPV($)	1761	1722	3137

Fig. 2.41 shows the years of return (YR) of house 2-5. Left side figures represent case 2, right side figures represent case 3. The intersection of the cumulative cashflow with zero axis is the year from which this project start gain profit. It can be observed that case 2 and case 3 for house 2 have similar TR, which shows that adding ES could not bring more profit to house2. For house 3 and house 5, Adding ES even cause money loss. So it's not wise for the households in these two houses to install ES for the PV panel. For house 4, installing ESD is a good choice to improve the profit because the YR of case 3 is much better than that of case 2.

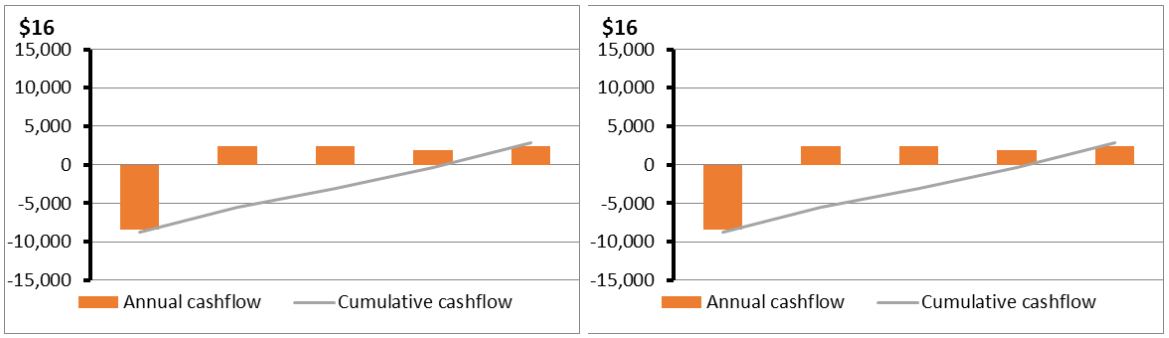

(a) House 2

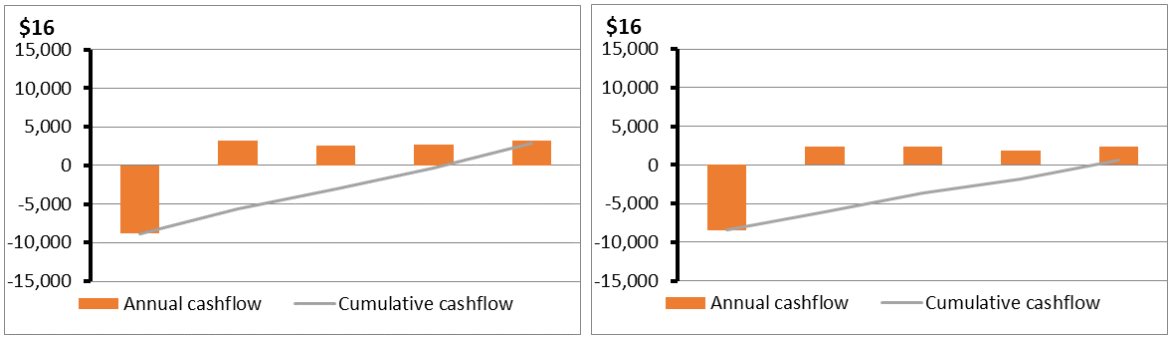

(b) House 3

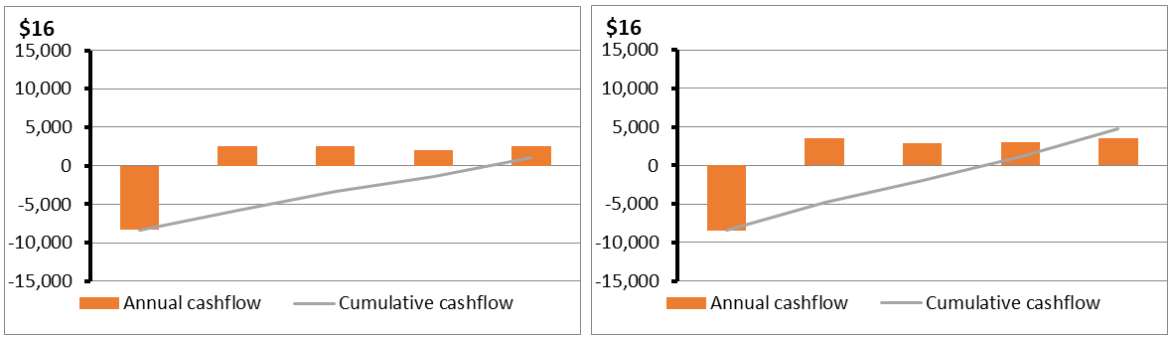

(c) House 4

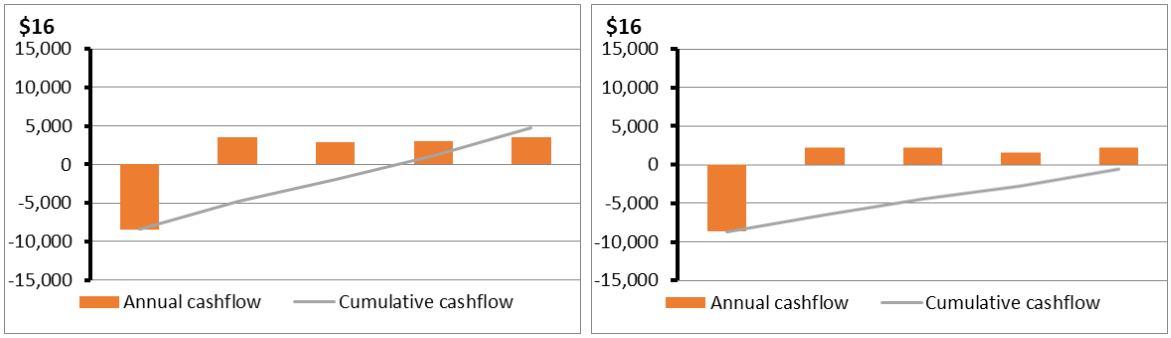

(d) House 5

Fig. 2. 41 YR of various houses

D. Results Comparison between Different Rate Structures

In order to investigate the impact of rate structure on choosing ES and PV from economic perspective, the same 5 five houses have been put under one of the California (CA) TOU rates [55] to explore the bill saving results.

As shown in Fig. 2.42, the TOU rate designed by PG&E in California have three different price intervals including peak time, partial peak time, and off-peak time. Also, different interval definitions are provided for summer time and winter time, weekday and weekend. Table 2.5 shows the rate structure of this CA rate, it can be observed that three energy tiers have been defined and the price will jump to a new level when the consumer's energy consumption reaches one tier.

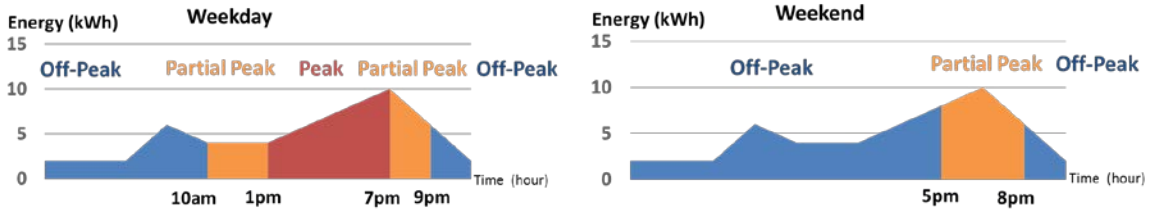

(a) Summer

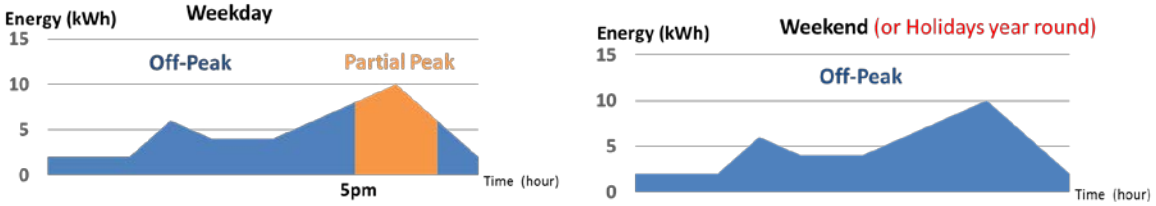

(b) Winter

Fig. 2. 42 Time schedule of CA rate

Table 2. 5 CA Rate Structure

Time of Use Price	Tier 1	Tier 2	Tier 3
MAY - OCTOBER			
High Demand	34.2¢	40.0¢	55.9¢
Medium Demand	22.6¢	28.5¢	44.3¢
Low Demand	15.0¢	20.8¢	36.7¢
NOVEMBER - APRIL			
Medium Demand	17.1¢	23.0¢	38.8¢
Low Demand	15.4¢	21.3¢	37.1¢

As shown in Fig. 2.43, the electricity bill saving brought by PV and PV-ES combination under two rate structures have been compared, for house 4 in the year of 2006. It can be drawn that PV and ES installation will bring more electricity bill saving under CA rate, the saving under CA rate is 11% higher than that under NC rate. The absolute dollar saving is even far more substantial than that under NC rate. It can be inferred that the houses which are not proper for PV and ES installations in NC would become suitable for the installations if they are located in CA. Therefore, the cost-benefit results for PV and ES installation not only depend on the home load pattern and local climate, but also rely on the utility rate plans.

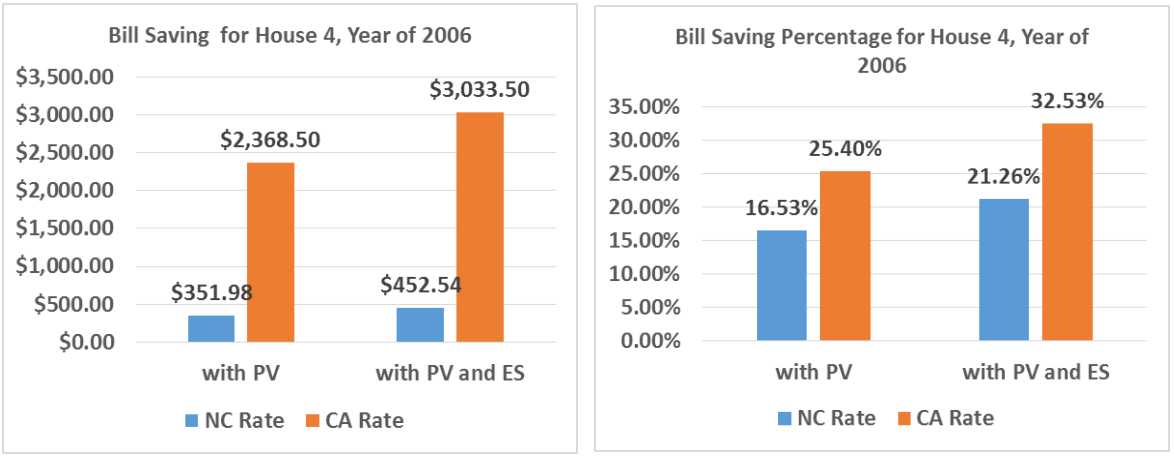

Fig. 2. 43 Bill saving comparison

CHAPTER 3 DSM-BASED VOLTAGE REGULATION METHODOLOGY DEVELOPMENT

3.1 A Hierarchical VLSM-Based DSM Strategy for Coordinative Voltage Control between T&D Systems

The two-stage control strategy will be modeled in this section [63]. The VLSM and price functions which play important roles in the control strategy will be introduced first. Then the optimization control scheme for the two stages will be formulated. The constraints generation will be formulated after that. Finally the simulation results will be discussed.

Nomenclature

C	Total cost of demand response ($).
C_2	Total cost of demand response for second stage ($).
C_{PV}	Cost of demand response using PV ($).
C_{Load}	Cost of demand response using controllable loads ($).
C_{Cap}	Cost of employing capacitors to do fulfil requirement ($).
f_j^{up}	Probability for appliance *j* to be turned on.
f_j^{down}	Probability for appliance *j* to be turned off.
i	Node number
j	Node number
k	Improved factor for reactive power constraint, 1.1 for a normal IGBT based PV inverter.

N	Number of nodes at this distribution system.
N_{APP}	Number of appliances participated in demand response in a house.
n	Number of nodes considered in VLSM
n_T	Number of time steps in one power flow case
$P_{PV}(i)$	Current PV power output at node *i* (kW).
$P_{DR}^{PV}(i)$	PV curtailment on node *i* (kW).
$P_{DR}^{PV}\|_{\max}(i)$	Maximum PV curtailment could be done at node *i* (kW).
$P_{DR}^{Load}(i)$	Demand response using controllable load at node *i* (kW).
$P_{DR}^{Load}\|_{\max}^{up}(i)$	Maximum load increase could be done at node *i* (kW).
$P_{DR}^{Load}\|_{\max}^{down}(i)$	Maximum load decrease could be done at node *i* (kW).
P_{DR}^{Total}	Total demand response requirement of real power (kW).
$P_{DR}^{PV}\|_2(i)$	PV curtailment on node *i* for second stage (kW).
$P_{DR}^{Load}\|_2(i)$	Demand response using controllable load at node *i* for this second layer control (kW).
$P_{DR}^{Total}\|_2$	Total demand response of real power implemented on second stage (kW).
$P_{DR}^{\lim it}\|_{high}$	Demand response high limit of real power (kW).
$P_{DR}^{\lim it}\|_{low}$	Demand response low limit of real power (kW).
$P_{App}^{Rate}(j)$	Rated power of appliance *j* (kW).
$\tilde{P}_{PV}^{Total}$	Forecasted total PV output at next time step (kW).

δP	Real power perturbation (kW)
p_{11}	Sensitivity factor for real power
$Q_{DR}^{PV}\|_{\max}(i)$	Maximum reactive power support could be provided by smart inverter at node *i* (kvar).
Q_{DR}^{Total}	Total demand response requirement of reactive power (kvar).
$Q_{Cap}(i)$	The capacity of the capacitor at node *i* (kvar).
$Q_{DR}^{PV}\|_{2}(i)$	Reactive power generation or absorption of smart inverter on node *i* second stage (kvar).
$Q_{DR}^{Total}\|_{2}$	Total demand response of reactive power implemented on second stage (kvar).
$Q_{DR}^{\lim}\|_{high}$	Demand response high limit of reactive power (kvar).
$Q_{DR}^{\lim}\|_{low}$	Demand response low limit of reactive power (kvar).
q_{ij}	Sensitivity factor for reactive power
r_{PV}^{P}	Ratio of PV real power available for curtailment.
r_{PV}^{Q}	Ratio of PV reactive power available for demand response.
$S_{PV}(i)$	Capacity of PV panels at node *i* (kW).
$s(i)$	Status of on or off (1/0) of the capacitor at node *i*.
T_{out}	Outdoor temperature (°F).
T_{set}	Air conditioner set point (°F).
t	Time step

$V_0(i)$	Voltage magnitude of each node at current time step (p.u.).
$V_1(i)$	Voltage magnitude of each node at current time step after first stage control (p.u.).
$V_2(i)$	Voltage magnitude of each node at current time step after second stage control (p.u.).
$V_{\lim it}^{low}$	Lower bound of voltage limit (p.u.).
$V_{\lim it}^{high}$	Higher bound of voltage limit (p.u.).
ΔV	Total squared voltage deviation (p.u.^{2}).
$\delta V(i)$	Voltage deviation at bus *i*.
$\lvert VLSM_P \rvert_{N\times N}$	VLSM of real power.
$\lvert VLSM_Q \rvert_{N\times N}$	VLSM of reactive power.
Z_1	Minimization Objective.
Z_2	Objective of minimization for second stage.
λ_{PV}^{Q}	Price of reactive power generation or absorption of smart inverter ($/kW).
λ_{Cap}	Price of turning on the capacitor at node *i*, $/kvar.
λ_{Load}	Price of demand response of controllable loads at node *i* ($/kW).
$\varpi_1 \cdots \varpi_5$	Weight coefficient.
ξ	Correction coefficient.

3.1.1 VLSM and Price Functions

The VLSM and price functions will be introduced in this subsection.

A. Voltage Load Sensitivity Matrix (VLSM)

$VLSM_P$ and $VLSM_Q$ are defined as the sensitivity matrix for real power and reactive power, respectively. The voltage change, δV_i, at node i can be estimated by the real power change, δP_j, and the reactive power change, δQ_j, at all nodes (i.e. j=1…n) using the voltage-load sensitivity matrix, *VLSM*, as follows.

$$|\delta V| = |VLSM_P||\delta P| + |VLSM_Q||\delta Q| \tag{3.1}$$

i.e.

$$\begin{vmatrix} \delta V(1) \\ \delta V(2) \\ \vdots \\ \delta V(\mathrm{n}) \end{vmatrix} = \begin{vmatrix} p_{11} & p_{12} & \cdots & p_{1n} \\ p_{21} & \ddots & & p_{2n} \\ \vdots & & \ddots & \\ p_{n1} & p_{n2} & & p_{nn} \end{vmatrix} \begin{vmatrix} \delta P_1 \\ \delta P_2 \\ \vdots \\ \delta P_n \end{vmatrix} + \begin{vmatrix} q_{11} & q_{12} & \cdots & q_{1n} \\ q_{21} & \ddots & & q_{2n} \\ \vdots & & \ddots & \\ q_{n1} & q_{n2} & & q_{nn} \end{vmatrix} \begin{vmatrix} \delta Q_1 \\ \delta Q_2 \\ \vdots \\ \delta Q_n \end{vmatrix} \tag{3.2}$$

From (3.2), we can derive

$$\delta V(i) = \sum_{j=1}^{n} p_{ij}\delta P_j + \sum_{j=1}^{n} q_{ij}\delta Q_j \tag{3.3}$$

where p_{ij} and q_{ij} represents the real and reactive power sensitivity factor at bus i with respect to bus j.

The sensitivity factors represent the voltage change expected at bus i when the real and reactive power at bus j is perturbed by one unit. Algorithm 1 describes the process of calculating $VLSM_P$. The calculation of $VLSM_Q$ is a similar process, where the perturbation is done to the reactive power instead of to the real power at each load node [59].

To enhance the effectiveness of the *VLSM*, we calculated the average voltage changes by conducting a time-series power flow study (i.e. t=1…n_T) and perturbing P_i and Q_i at each time step. Then, the process will be repeated for several δP and δQ. This process will allow us to obtain an average of *VLSMs* as the final *VLSM* so that the sensitivity matrix will reflect the voltage change at node i with respect to different δP and δQ at different P and Q.

The $VLSM_P$ Calculation is summarized in Algorithm 1:

Algorithm 1 $VLSM_P$ Calculation

1: Conduct a time-series power flow study using a typical load profile at each node, $P(i,t)$ and $Q(i,t)$, i=1…n, t=1…n_T.

2: Obtain the voltage at each bus at each time step: $V(i,t)$, i=1…n, t=1…n_T.

3: Conduct the time series power flow study again when $P(1,t)$ is perturbed as $\tilde{P}(1,t) = P(1,t) + \delta P_1$, t=1…n_T.

4: Calculate the new voltage at each bus at each time step : $\tilde{V}(i,t)$, i=1…n, t=1…n_T.

5: Calculate the sensitivity factor for each bus:
$$p_{i1} = \frac{\sum_{t=1}^{n_T} \tilde{V}(i,t) - \sum_{t=1}^{n_T} V(i,t)}{n_T \delta P_1}, \; i=1\ldots n,\; t=1\ldots n_T.$$

6: Repeat step1-5 for nodes 2~n.

7: Obtain $VLSM_P^1$.

8: Repeat step 1-7 for δP_2… δP_m, to calculate $VLSM_P^1$ … $VLSM_P^m$.

9: Calculate the final $VLSM_P$:
$$VLSM_p = \frac{\sum_{ii=1}^{m} VLSM_P^{ii}}{m}, \; ii=1\ldots m.$$

10: End the $VLSM_P$ calculation.

B. Price Functions

The general market assumption here is as follows: We assume that a load aggregator will be responsible for controlling the load-side resources for providing DR services and will receive the command from the transmission level controller the DR requirements. The load aggregator will also maintain the voltage at each nodes in the distribution system within

operation limits. By meeting the DR requirements, the aggregator will be paid. However, extra response (i.e. additional increase or decrease of load) will not be paid. No payment will be made if the DR requirement is not fulfilled.

To prioritize different resources, we propose price functions for them. We assume the price for capacitors will stay constant as they are one-time switched on or off with a constant amount of reactive power support. Also, they are manufactured with standardized capable switching times. We set the price of capacitor at a high level to avoid frequently switching. But the price of controllable load response and PV curtailment would not stay the same as the required response and curtailment amount and condition change.

For curtailing PV, the cost can be estimated by the cost of the same amount of power purchased from the grid. Because the efficiency of the inverter will decrease with larger curtailments at lower power output, the loss of energy caused by the efficiency reduction need to be considered as well. Therefore, generally the price of PV curtailment will be higher when the curtailment amount is larger and when the curtailment happens at lower power outputs. We assume the price of PV curtailment would be different at each node since each node has different conditions for the PV panel output.

For controllable load response, as the required response amount increases, the price of the response will generally decrease. Because as the response amount increase, the house number need for this response will be larger, the house recruited in the response will be more diversified. More houses with larger response capacity will be recruited and the price per kW response would be cheaper. The price of controllable load response would be the same for each node if we consider one aggregator for one feeder.

Based on the above analysis, the general price functions of PV and load are formulated in (3.4) and (3.5) accordingly. The parameters of the two price functions need to be determined based on specific market definition such as the price of the voltage control service and the utility rate.

$$\lambda_{PV}^{P}(i) = -A_{PV} \cdot \ln(1-x) + B_{PV} \ , x = 1 - \frac{P_{PV}(i) + P_{DR}^{PV}(i)}{S_{PV}(i)} \tag{3.4}$$

$$\lambda_{Load} = \frac{A_{Load}}{x + B_{Load}} + C_{Load} \ , \ x = \sum_{i=1}^{N} (P_{DR}^{Load}(i))^2 \tag{3.5}$$

The price of PV curtailment is a function of the curtailed percentage, which is defined as x in (3.4). Because PV can only be curtailed, we use plus between $P_{PV}(i)$ and $P_{DR}^{PV}(i)$ because $P_{DR}^{PV}(i)$ is negative. The price of the controllable load response is a function of the total load response amount on the feeder. Because load can either be reduced or increased, and we need to count the absolute response amount, we use squared value for convenience of solving optimization problem.

According to the simulation using our developed house models [61-62] under the assumed market mechanism, the parameters used in this study for in (3.4) and (3.5) are calculated as shown in Table 3.1. The corresponding price curves are plotted in Fig.3.1 (a) and (b) respectively.

Table 3. 1 Parameters for Price Functions

A_{PV}	B_{PV}	A_{Load}	B_{Load}	C_{Load}
0.3186	0.7664	11	9	1

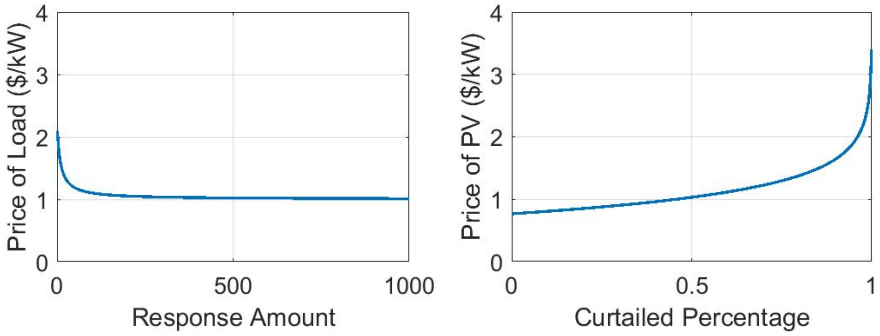

(a) (b)

Fig.3. 1 Price curves of controllable load (a) and PV (b)

3.1.2 Optimization Control Strategy Modeling

The two-stage control strategy will be modeled in this section. The optimization control scheme for the two stages will be first formulated. Then the constraints generation will be discussed. Finally the overall two-stage control algorithm will be introduced.

B. First-Stage Control Scheme

In the first stage, the demand response requirement from the transmission system controller is disaggregated to corresponding nodes such that the DR cost and the overall voltage deviation is minimized. We assume that 1) the real power requirement P_{DR}^{Total} will be fulfilled by curtailing PV or turn on/off the controllable loads; 2) the reactive power requirement Q_{DR}^{Total} will be fulfilled by smart inverter and capacitors; 3) the PV output can be curtailed but not increased and the controllable load cannot provide reactive power response.

With the assumptions, the problem is formulated as

$$\min \qquad Z_1 = \varpi_1 \xi C + \varpi_2 \Delta V \tag{3.6}$$

where

$$C = C_{PV} + C_{Load} + C_{Cap} \tag{3.7}$$

$$C_{PV} = \sum_{i=1}^{N}\left(\lambda_{PV}^{P}(i)\cdot\left(P_{DR}^{PV}(i)\right)^{2}\right)+\lambda_{PV}^{Q}\sum_{i=1}^{N}\left(\mathrm{Q}_{DR}^{PV}(i)\right)^{2} \tag{3.8}$$

$$C_{Load} = \lambda_{Load}\sum_{i=1}^{N}\left(P_{DR}^{Load}(i)\right)^{2} \tag{3.9}$$

$$C_{Cap} = \lambda_{Cap}\sum_{i=1}^{N}\left(s(i)\left(Q_{Cap}(i)\right)^{2}\right) \tag{3.10}$$

$$\lambda_{PV}^{P}(i) = -A_{PV}\cdot\ln\left(\frac{P_{PV}(i)+P_{DR}^{PV}(i)}{S_{PV}(i)}\right)+B_{PV} \tag{3.11}$$

$$\lambda_{Load} = \frac{A_{Load}}{\sum_{i=1}^{N}(P_{DR}^{Load}(i))^{2}+B_{Load}}+C_{Load} \tag{3.12}$$

$$\Delta V = \sum_{i=1}^{N}\left(V_{1}(i)-V_{obj}\right)^{2} \tag{3.13}$$

$$\begin{aligned} V_{1}(i) = V_{0}(i)&+\sum_{j=1}^{N}\left(VLSM_{P}(i,j)\cdot\left(P_{DR}^{Load}(j)-P_{DR}^{PV}(j)\right)\right)\\ &+\sum_{j=1}^{N}\left(VLSM_{Q}(i,j)\cdot\left(Q_{DR}^{PV}(j)+s(j)\cdot Q_{Cap}(j)\right)\right)\end{aligned} \tag{3.14}$$

Subject to:

$$0<\varpi_{1},\varpi_{2}<1 \tag{3.15}$$

$$\varpi_{1}+\varpi_{2}=1 \tag{3.16}$$

$$s(i)=0,1, s(j)=0,1 \tag{3.17}$$

$$-P_{DR}^{PV}|_{\max}(i) < P_{DR}^{PV}(i) < 0 \tag{3.18}$$

$$P_{DR}^{PV}|_{\max}^{down}(i) < P_{DR}^{Load}(i) < P_{DR}^{PV}|_{\max}^{up}(i) \tag{3.19}$$

$$-Q_{DR}^{PV}|_{\max}(i) < Q_{DR}^{PV}|_{2}(i) < Q_{DR}^{PV}|_{\max}(i) \tag{3.20}$$

$$-\sum_{i=1}^{N}P_{DR}^{PV}(i)+\sum_{i=1}^{N}P_{DR}^{Load}(i)=P_{DR}^{Total} \tag{3.21}$$

$$\sum_{i=1}^{N} Q_{DR}^{PV}(i) + \sum_{i=1}^{N} s(i) Q_{Cap}(i) = Q_{DR}^{Total} \tag{3.22}$$

Because C and ΔV are not at same order of magnitude, C is usually very large, but ΔV is usually very small, a correction coefficient ξ need to be applied to narrow the gap between C and ΔV so that the optimization could be emphasized equally for C and ΔV when the weight coefficients ϖ_1 and ϖ_2 are equal. Then, by adjusting ϖ_1 and ϖ_2, one can adjust the weights between minimizing the total cost and minimizing the total voltage deviation. Note that to make the MINLP problem solvable, square of the decision variables are used instead of using the absolute values, while calculating actual cost, the absolute values are used.

After solving (3.6-3.22), we will obtain the optimal P_{DR}^{PV}, P_{DR}^{Load}, and Q_{DR}^{PV}, for each node, as well as the "on" and "off" status of the capacitor bank, $s(i)$.

B. Second-Stage Control Scheme

The optimization objective for the second-stage control is to minimize the demand response cost and the total demand response amount while eliminating voltage violations in the distribution system. The second stage optimization is triggered only when voltage violations are detected in power flow results after the DR requirements have been executed. Only controllable loads and the smart inverters will be used for providing DR in the second-stage. Capacitors will not be used because turning on/off capacitors creates a large voltage change along the distribution feeder so they are not as flexible as the controllable loads and smart inverters.

The second-stage optimization problem is formulated as

$$\min \qquad Z_2 = \varpi_3 \xi C_2 + \varpi_4 P_{DR}^{Total}\,|_2 + \varpi_5 Q_{DR}^{Total}\,|_2 \tag{3.23}$$

$$C_2 = \lambda_{Load}\sum_{i=1}^{N}\left(P_{DR}^{Load}\mid_2(i)\right)^2 + \sum_{i=1}^{N}\lambda_{PV}^{P}(i)\cdot\left(P_{DR}^{PV}\mid_2(i)\right)^2 + \lambda_{PV}^{Q}\sum_{i=1}^{N}\left(Q_{DR}^{PV}\mid_2(i)\right)^2 \tag{3.24}$$

$$P_{DR}^{Total}\mid_2 = \sum_{i=1}^{N}\left(P_{DR}^{Load}\mid_2(i) - P_{DR}^{PV}\mid_2(i)\right)^2 \tag{3.25}$$

$$Q_{DR}^{Total}\mid_2 = \sum_{i=1}^{N}\left(Q_{DR}^{PV}\mid_2(i)\right)^2 \tag{3.26}$$

Subject to:

$$0 < \varpi_3, \varpi_4, \varpi_5 < 1 \tag{3.27}$$

$$\varpi_3 + \varpi_4 + \varpi_5 = 1 \tag{3.28}$$

$$-P_{DR}^{PV}\mid_{\max}(i) < P_{DR}^{PV}\mid_2(i) < 0 \tag{3.29}$$

$$P_{DR}^{Load}\mid_{\max}^{down}(i) < P_{DR}^{Load}\mid_2(i) < P_{DR}^{Load}\mid_{\max}^{up}(i) \tag{3.30}$$

$$-Q_{DR}^{PV}\mid_{\max}(i) < Q_{DR}^{PV}\mid_2(i) < Q_{DR}^{PV}\mid_{\max}(i) \tag{3.31}$$

$$V_2(i) = V_1(i) + \sum_{j=1}^{N}VLSM_P(i,j)\cdot\left(P_{DR}^{Load}(j) - P_{DR}^{PV}(j)\right) + \sum_{j=1}^{N}VLSM_Q(i,j)\cdot\left(Q_{DR}^{PV}(j) + s(j)\cdot Q_{Cap}(j)\right) \tag{3.32}$$

$$V_{\lim it}^{low} < V_2(i) < V_{\lim it}^{high} \tag{3.33}$$

Because we need to maintain the accomplish rate of transmission demand response requirement, we want to use the minimum amount of DR to eliminate the voltage violations. Therefore, ϖ_4 and ϖ_5 are set to be much larger than ϖ_3.

As shown in (3.32-3.33), the voltage after second stage control will be constrained in a

defined range. The low and high limit of the range can be adjusted as needed. Usually the range will be [0.95, 1.05].

C. Generating Operational Constraints

After the second-stage, electricity consumption and PV generation will be forecasted for the next operation interval. Then, the distribution system controller will calculate the real and reactive power increase and decrease limits, $P_{DR}^{\text{limit}}|_{high}$, $P_{DR}^{\text{limit}}|_{low}$, $Q_{DR}^{\text{limit}}|_{high}$, and $Q_{DR}^{\text{limit}}|_{low}$. Those limits will serve as operational constraints and be sent back to the transmission level controller for conducting transmission level optimization. Right now persistence method is used in our study. More forecasting methods could be used and tested in follow-up study.

The real power constraints are calculated based on the available controllable load resources and the PV curtailment capability as shown in (3.34) and (3.35).

$$P_{DR}^{\text{limit}}|_{high} = \sum_{j=1}^{N_{APP}} f_j^{up}(x_1, x_2, \ldots) \cdot N_{House} \cdot P_{APP}^{Rate}(j) + r_{PV}^{P} \cdot \tilde{P}_{PV}^{Total} \tag{3.34}$$

$$P_{DR}^{\text{limit}}|_{low} = \sum_{j=1}^{N_{APP}} f_j^{down}(x_1, x_2, \ldots) \cdot N_{House} \cdot P_{App}^{Rate}(j) \tag{3.35}$$

where r_{PV}^{P} is the ratio of the PV real power available for curtailment; $x_1, x_2, \ldots$ are the parameters of controllable appliances used for the appliance on/off probability estimation functions $f_j^{up}(x_1, x_2, \ldots)$ and $f_j^{down}(x_1, x_2, \ldots)$. For example, if the controllable appliances are air conditioners, $x_1, x_2, \ldots$ could be the outdoor temperature and the average air conditioner set point. When the outdoor temperature is high and the average set point is low, the air conditioners are more likely to be "on". Therefore, they are more likely to be available for

providing load reduction, i.e. $f_j^{down}(x_1, x_2, \ldots)$ is greater than $f_j^{up}(x_1, x_2, \ldots)$. In this paper, f_j^{down} for air conditioner is formulated as gamma distribution as shown in (3.36). The probability density function is plotted in Fig. 3.2. f_j^{up} is equal to 1 minus f_j^{down}, as shown in (3.37).

$$f_j^{down}(x) = \frac{1}{\beta^{\alpha}\Gamma(\alpha)} x^{\alpha-1} e^{\frac{-x}{\beta}} \tag{3.36}$$

where

$$x = 5 \big/ (T_{out} - T_{set}), \quad \alpha = 1, \quad \beta = 1$$

$$f_j^{up} = 1 - f_j^{down} \tag{3.37}$$

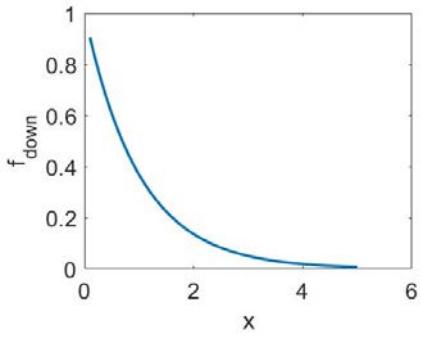

Fig.3. 2 Probability density function for f_j^{down}

If some air conditioners have moved their set points up to provide the load reduction service at current operational interval, the average T_{set} will increase so the x will be greater. Subsequently, f_j^{down} for next operational interval will be lower, as shown in Fig. 3.2.

The reactive power limits are calculated in (3.38) and (3.39). r_{PV}^{Q} is the ratio of the PV reactive power available for DR. The reactive power constraints are calculated based on smart inverter operation equation [60] and the available capacitors.

$$Q_{DR}^{\text{limit}}|_{high} = \sum_{i=1}^{N} r_{PV}^{Q} S_{PV}(i) \sqrt{\left(1 - \left(P_{PV}(i) \big/ S_{PV}(i)\right)^2\right) k^2} + \sum_{i=1}^{N} Q_{cap}(i) \qquad \text{if} \quad s(i) = 0 \tag{3.38}$$

$$Q_{DR}^{\text{limit}}|_{low} = \sum_{i=1}^{N} r_{PV}^{Q} S_{PV}(i) \sqrt{\left(1 - \left(P_{PV}(i) \big/ S_{PV}(i)\right)^2\right) k^2} + \sum_{i=1}^{N} Q_{cap}(i) \qquad \text{if} \quad s(i) = 1 \tag{3.39}$$

B. Two-Stage Control Algorithm

As shown in Algorithm 2, a control algorithm for the two-stage optimization scheme is developed. After receiving the DR requirement from the transmission system controller, the first stage optimization control will be performed and then the required response will be implemented at the feeder and power flow will be performed. At this point, the voltage at each node will be checked to examine if there is any node voltage violates the limitation.

If there is any violation detected, the second stage will be performed to eliminate the violations. Then the DR constraints for transmission system at next time step will be generated.

Algorithm 2 Two-Stage Control Algorithm

1: Receive demand response requirement from transmission system controller: P_{DR}^{Total} and Q_{DR}^{Total}
2: Perform first stage optimization control: solve problem formulated in (6-22), obtain $P_{DR}^{Load}(i)$, $P_{DR}^{PV}(i)$, $Q_{DR}^{PV}(i)$, and $s(i)$
3: Implement $P_{DR}^{Load}(i)$, $P_{DR}^{PV}(i)$, $Q_{DR}^{PV}(i)$, and $s(i)$ at the feeder
4: Run power flow simulation for the feeder
5: Voltage violation check
6: **if** any voltage violation detected **then**
7: Perform second stage optimization control, solve problem formulated in (23-33),

obtain $P_{DR}^{Load}|_2(i)$, $P_{DR}^{PV}|_2(i)$, and $Q_{DR}^{PV}|_2(i)$

8: Implement $P_{DR}^{Load}|_2(i)$, $P_{DR}^{PV}|_2(i)$, and $Q_{DR}^{PV}|_2(i)$ at the feeder

9: Run power flow simulation for the feeder

10 Voltage violation check

:

11 **if** no violation found **then**

:

12 End and exit the whole algorithm

:

13 **else**

:

14 Go to 6

:

15 **end if**

:

16 **else**

:

17 End and exit the whole algorithm

:

18 **end if**

:

19 Use (34-39) to generate constraints for transmission system for next time step: $P_{DR}^{\text{limit}}|_{high}$,

: $P_{DR}^{\text{limit}}|_{low}$, $Q_{DR}^{\text{limit}}|_{high}$, and $Q_{DR}^{\text{limit}}|_{low}$

3.1.3 Feeder Setup

IEEE standardized 123-bus feeder is used as test system in this study and the topology is shown in Fig. 3.3. There are 91 load nodes in the system, including both single-phase and 3-phase balanced and imbalanced loads. There are 4 capacitors on this feeder (installed at bus 83, 88, 90, and 92 respectively) [56].

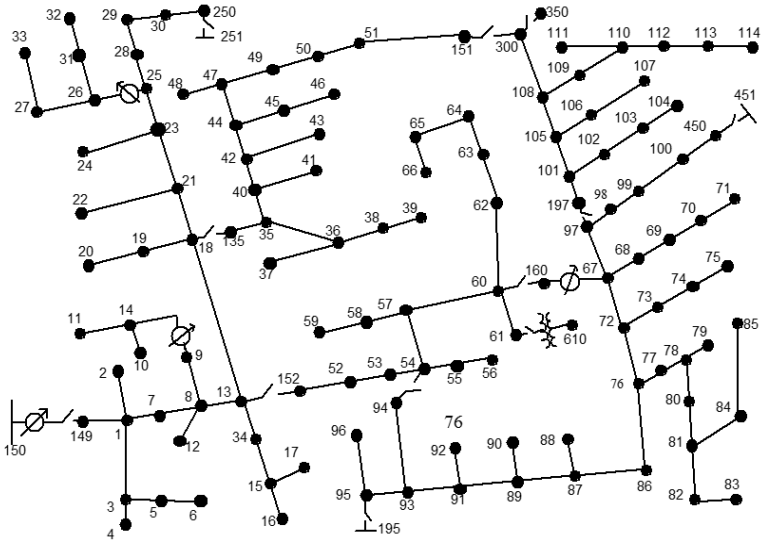

Fig.3. 3 Feeder topology of the IEEE 123-bus system

In past solar integration studies, researchers use one load shape for all load nodes in a distribution feeder. The magnitude of the load at each load node is scaled based on the distribution transformer capacity installed at that node. The assumption is that the load at each load node on the same feeder will vary similarly. This assumption ignores there are significant load diversity in loads at distribution transformer level. It also makes it impossible to study the influence of varying load consumption superposing the variation in PV generation outputs. Because loads are not modeled in detail, the approach also makes it impossible to develop demand response algorithms for alleviating the voltage problems caused by solar power variations.

To model the voltage changes along the feeder with respect to the net load variations as well as model the voltage-based demand response for conditioning the feeder voltage profiles, we need to model the load at each load node down to the residential home level with minute-by-minute resolution. Therefore, a load disaggregation method is developed to disaggregate the

feeder load profile to each load nodes using realistic home load profiles. Then, the minute-by-minute PV power outputs can be used to obtain the net load profile at each node. This method enables us to conduct time-series study instead of modeling only a few snap shots.

A. Load Data Preparation

The load profile at the feeder level can be obtained from utilities because those measurements are usually made available at the substation level. However, for most utilities, the load profiles at the sub-nodes are unknown. Therefore, the first step of this method is to establish a database that contains sufficiently large amount of residential home load profiles for different seasons at different locations.

The first data source we used is the load data collected in the Pecan Street project [57]. The second data source is the Olypen data collected by Pacific Northwest National Laboratory [44]. In total, we have access to actual load profiles for more than 800 residential houses. Because most of the measurements have a 1-min sampling resolution, detailed load variations can be modeled. To model the demand response, we extract the air conditioning and space heating loads from the measured load profiles and replace them by load models. A few load profiles used in our study are shown in Fig. 3.4.

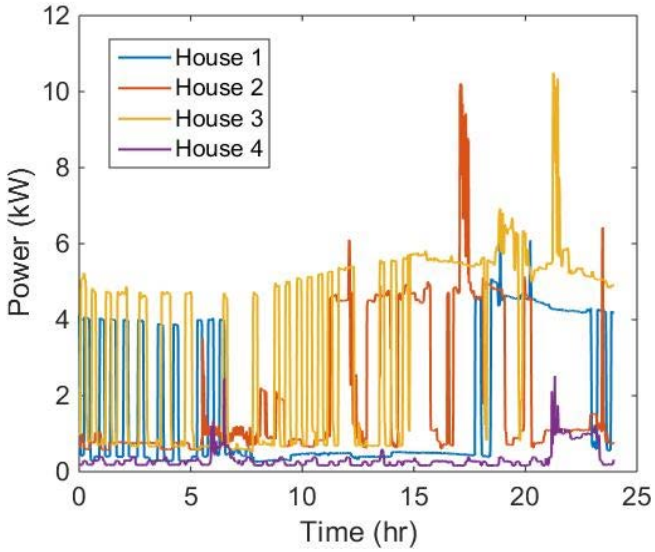

Fig.3. 4 Sample house load profiles

B. Load Disaggregation Method

A bottom-up approach has been used to construct load profiles at each load node so that the aggregated load profile matches the load profile at the feeder top. According to the load distribution ratio of the 123-bus system, the peak load at each node is calculated by allocating the total peak load to each bus. Then, the nodal peak loads are used to determine the number of houses at this node. Because the sum of the home-level peak demands is different from the total peak of the house group, a diversity factor, DF, is applied.

DF and the average peak load, Pave, for the house load pool can be calculated as

$$DF = \frac{\text{Maximum Noncoincident Demand}}{\text{Maximum Diversified Demand}} = \frac{\max(P_1) + \max(P_2) + \ldots \max(P_n)}{\max(P_1 + P_2 + \ldots + P_n)} \tag{3.40}$$

$$P_{ave} = \max\left(\frac{P_1 + P_2 + \cdots P_n}{n}\right) \tag{3.41}$$

where $P_1 \cdots P_n$ represents the load profiles in the database and n is the total number of house profiles. The flow chart of the disaggregation process is shown in Fig. 3.5 and the main steps are explained in Table 3.2.

Table 3. 2 Main Steps of Load Disaggregation Process

Step 1	Calculate the maximum non-coincident load by multiplying peak load with DF.
Step 2	Calculate the number of houses N through dividing the maximum non-coincident load by the average peak load.
Step 3	Select N house profiles from the load pool.
Step 4	Calculate the total load profile by summing up the selected profiles.
Step 5	Calculate the difference between the calculated peak total load and the given peak load and compare it with an error tolerance.
Step 6	If the error is greater than tolerance, repeat step 3–5. If the error is smaller than tolerance, STOP.

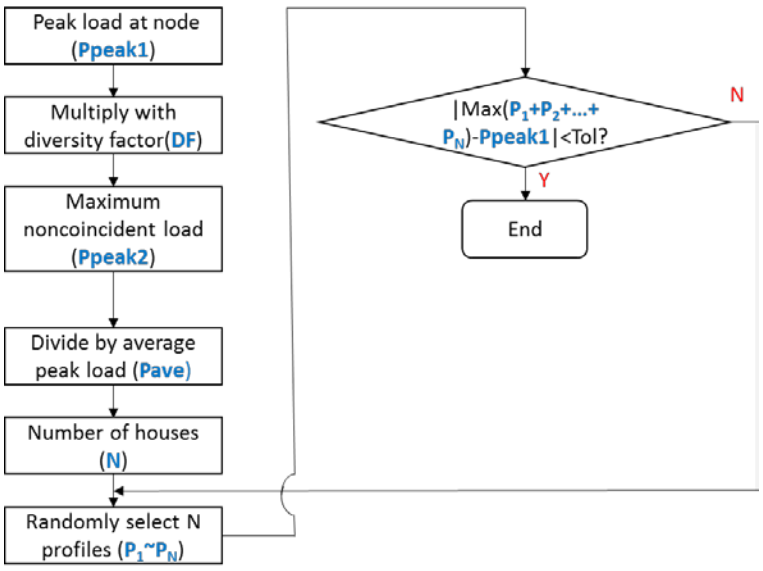

Fig.3. 5 Load disaggregation method

The load profiles at two load buses are shown in Fig. 3.4. As we can see, the variations are modeled in detail with sufficient load diversity reflected in both the magnitudes and the shape of the load profiles.

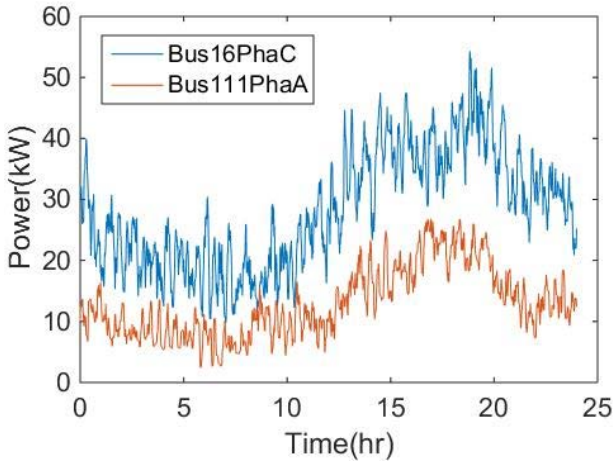

Fig.3. 6 Load profiles at the load bus on a distribution feeder

C. PV Integration

The capacity of the PV is calculated at each selected bus so that the overall penetration matches the targeted PV penetration level. By selecting load buses at different feeder locations, we can study the impact of PV locations. The PV power output profiles used in this work are collected in Duke Energy Carolina System [58]. This data set covers various weather types including sunny day, partial cloudy day, cloudy day and etc. Also, the time-shifting impact caused by cloud moving could also be reflected in this data set. Sample profiles are plotted in Fig. 3.7.

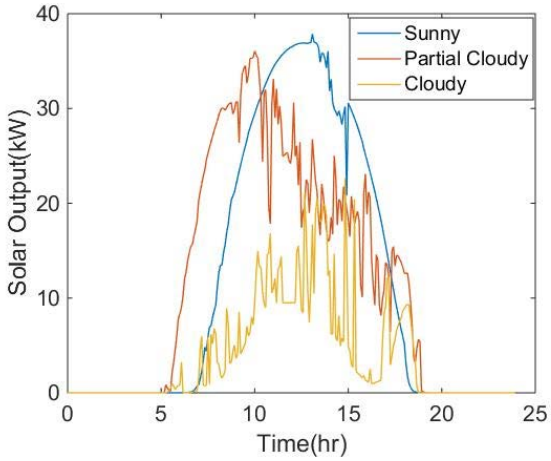

Fig.3. 7 Sample PV profiles

3.1.4 Feeder Analysis

With daily simulation, various case studies have been performed on this feeder, including different PV penetration levels, different PV installation cases, with and without voltage regulation devices, and etc. Two selected cases will be introduced in this section.

A. With and without PV installation

Cases with different PV penetration levels and installation locations have been conducted on this feeder. The PV penetration level is defined as the ratio of peak PV power output to the peak feeder load. Only residential roof-top PV is considered in this study, Fig. 3.8 shows the daily voltage profiles for Bus 68 Phase A from the case with 100% penetration level. It can be observed that the voltage will have significant rise if the PV penetration level is high.

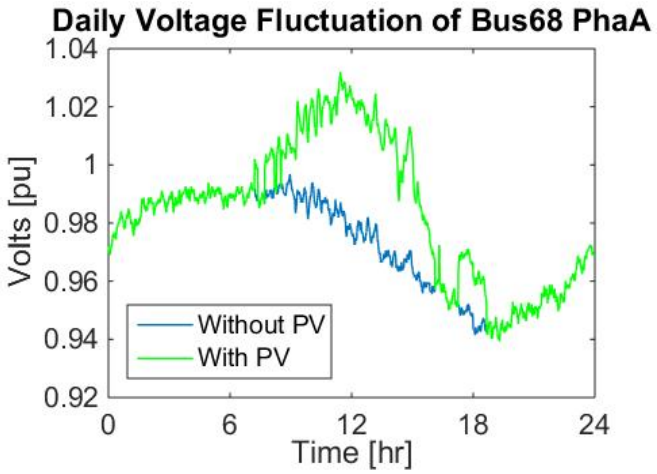

Fig.3. 8 Voltage profile comparison: with and without PV

B. With and without VR implementation

To investigate the impact of PV integration on the operation of the voltage regulation devices, we have studied two cases: with and without VRs. Fig. 3.9 (a) shows a boxplot of the daily voltage profiles for eight buses along the distribution feeder, for the case without VRs in the system. The blue lines represent the case with PV as 100% penetration level in the system and the red lines represent the without-PV case. The envelope of the box plot shows the maximum and minimum voltage excursions. Fig. 3.9 (b) is the with-VRs case. It can be observed that the voltage rises are smaller if there is VR in the system. For example, for bus 71, the maximum voltage rise is 0.0353 pu without VR in the system and is 0.0030 pu for the with-VR case.

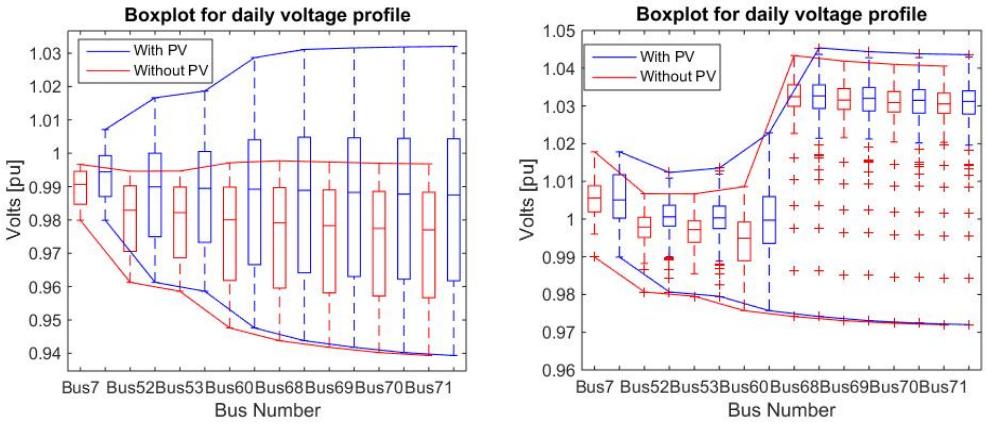

(a) (b)

Fig.3. 9 Profile boxplot comparison between without VR (a) and with VR (b)

Daily voltage difference at bus 68 between 100% PV and 0% PV cases are plotted in Fig.3.10, for both without-VR and with-VR situation. As expected, the voltage deviation is larger if there is no VR in the system.

Table 3.3 shows the total number of daily VR tap changes of the regulators in the system, between the case with PV integrated and the case without PV. It can be shown that 40 more tap changes happened for the system with PV installed. However, frequent VR tap adjustments will cause degradation of VR remaining life. Therefore, other approaches like load control and PV curtailment are needed to help regulate the voltage and reduce the number of VR moves.

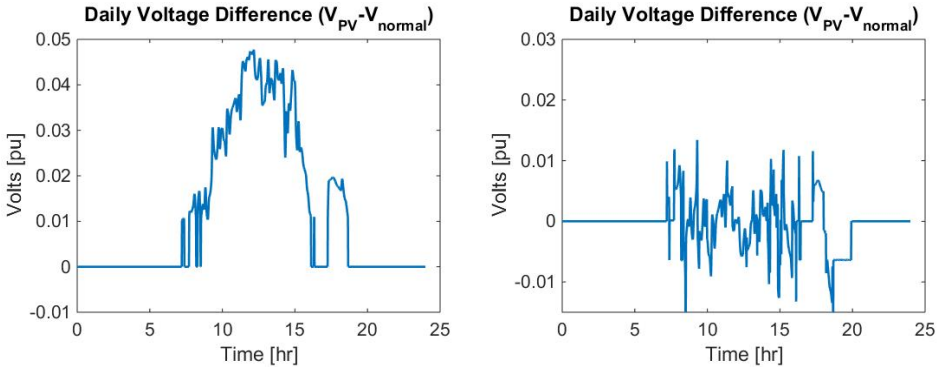

(a) (b)

Fig.3. 10 Voltage deviation comparison between without VR (a) and with VR (b)

Table 3. 3 VR Move Analysis

Cases	Number of VR tap changes (One day)
Without PV	110
With PV	150

3.1.5 Test Cases

A. Case 1: First-Stage Control Case

In case 1, the performance of the first-stage algorithm is tested. The DR dispatch results when $P_{DR}^{Total} = 200\text{kW}$ and $Q_{DR}^{Total} = 1400\text{kvar}$ are shown in Fig. 3.11.

The demand response requirements have been distributed to each node accordingly by the optimization control strategy. At each node, the controllable loads will be turned on to consume more energy and the PV will be curtailed to generate less in order to draw more power from the main grid; meanwhile, smart PV inverters will feed to the main grid reactive power.

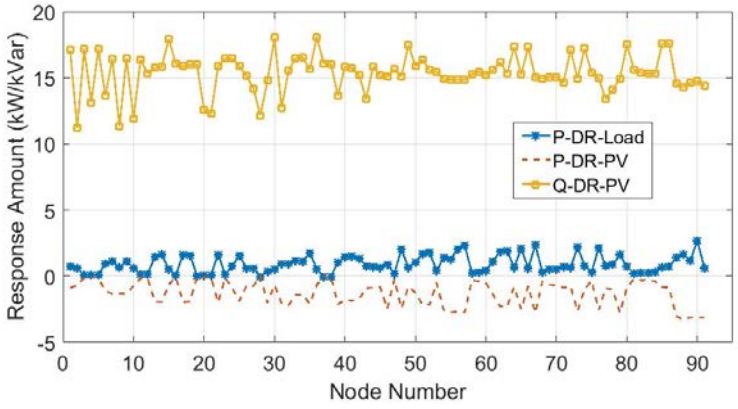

Fig.3. 11 DR response at each node

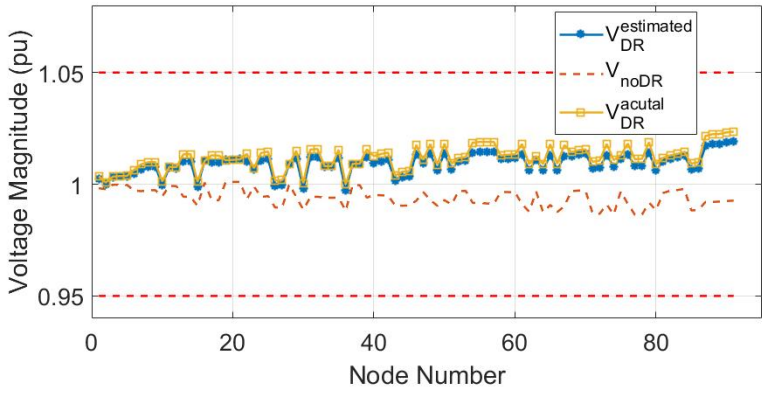

Fig.3. 12 Voltage magnitude at each node

The voltage magnitudes before and after the DR at nodes of the feeder are plotted in Fig.3.12. In this figure, V_{noDR} $V_{noDR}$is the voltage magnitude before implementing the demand response; $V_{DR}^{estimated}$ is the estimated voltage magnitude calculated according to VLSM and demand response optimization results; V_{DR}^{actual} V_{DR}^{actual} is the actual voltage after the DR deployment. As shown in this figure, the calculated voltage is very close to the actual voltage. The percentage error of the estimated voltage (See Table 3. 4) defined as $|V_{actual} - V_{estimated}|/V_{actual}$ is used to estimate the accuracy of the VLSM estimated voltage.

Table 3. 4 Error Percentage for First Stage Control Case

Mean	Min	Median	Max
0.16%	1.39×10^{-3}%	0.17%	0.35%

In this case, ϖ_1 and ϖ_2 are both set as 0.5. The ΔV is 0.017 and the total cost is 1589. If we adjust the weight coefficient to $\varpi_1 = 0.2$ and $\varpi_2 = 0.8$, the results will be ΔV=0.014 and total cost is 1619 because the optimization places heavier emphasis on minimizing the over voltage

deviation.

B. Case 2: Second-Stage Control Case

In this case, we demonstrate the performance of the second-stage algorithm designed for eliminating the voltage violations along the distribution feeder after DR requests are deployed.

The response amount distribution along the feeder are plotted in Fig. 3.13. The voltage results after the second layer control is plotted in Fig. 3.14. It could be observed that the voltage violations have been eliminated after the control strategy is implemented.

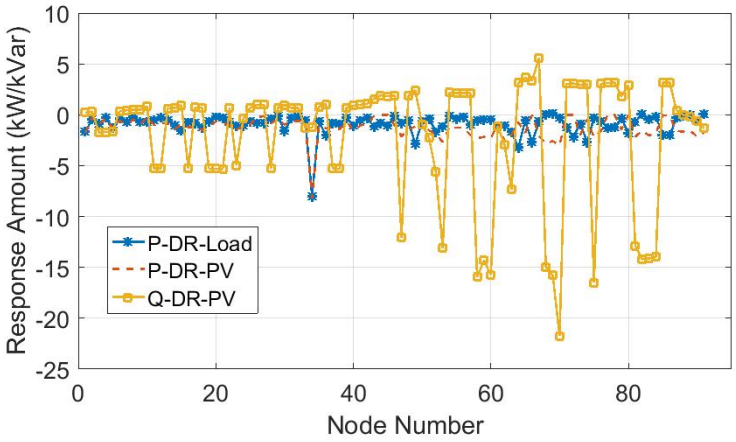

Fig.3. 13 DR response at each node

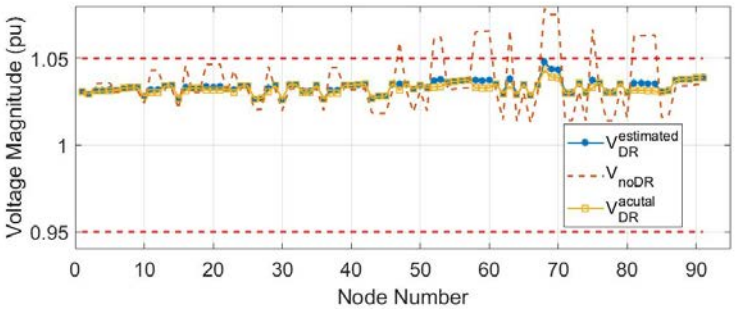

Fig.3. 14 Voltage magnitude at each node

The error rate statistics are shown in Table III. It could be seen that the estimated voltage calculated from VLSM is close to the actual voltage.

The optimization objective in second layer is to minimize the response cost and also the response amount so that the accomplish rate for transmission required response could be maintained at a high level. The total real power response amount of this second layer control case is 31.04kW (increase), the total reactive power response amount is 191.2582(absorption). The real and reactive power requirement from transmission system is 400kW (decrease) and 3000kVar (generation) respectively. The accomplish rate is 92.24% and 93.63%.

Table 3. 5 Error Percentage for First Stage Control Case

Mean	Min	Median	Max
0.066%	$3.99\times10^{-5}\%$	0.046%	0.16%

C. Case 3: Time-Series Study

A 24-hour time series study have been done to test the control strategy. The control will be performed every 5 mins. The response requirements from transmission system are shown in Fig. 3.15. The voltage profiles before and after the demand response at two sample nodes are shown in Fig. 3.16 and 3.17 respectively. It could be seen that the voltage profiles after demand response are within the limit and don't have large fluctuations. The voltage dip in the morning is caused by the large amount Q absorption requirement from transmission system.

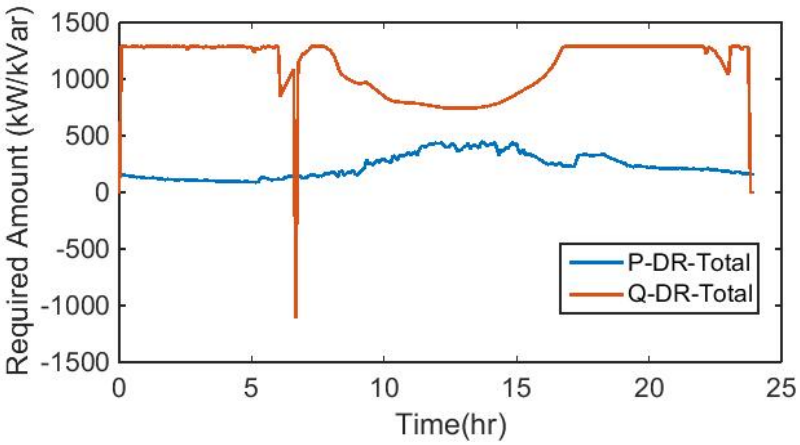

Fig.3. 15 Required response amount of P and Q from transmission system

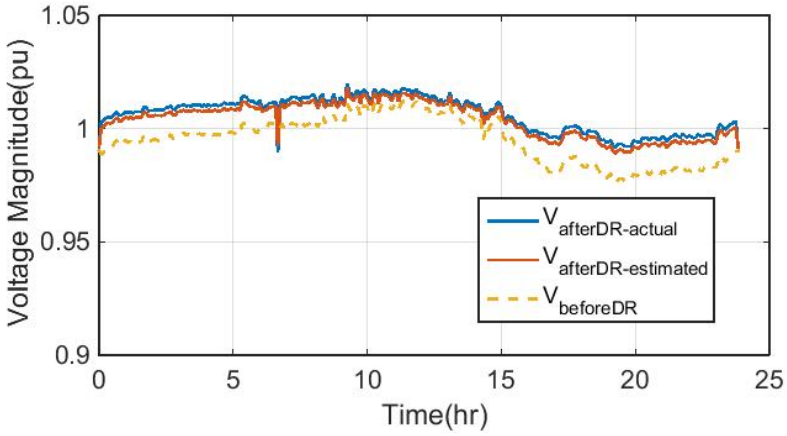

Fig.3. 16 Voltage profiles at bus 11 phase A

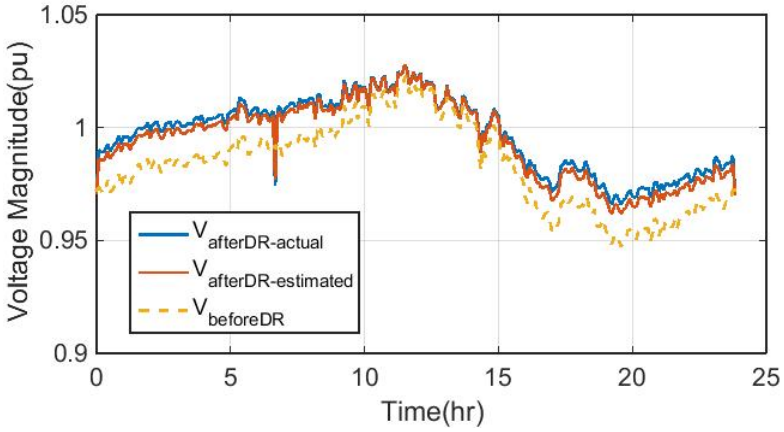

Fig.3. 17 Voltage profiles at bus 65 phase C

Considering all the nodes in the 123-feeder system, the maximum and minimum voltage magnitudes during this day are shown in Table 3.6. It could be seen that they are all within the limitation. The error rate statistics are shown in Table 3.7, it could be observed that the error rate is very small, the maximum is 1%.

Table 3. 6 Error Percentage for Second Stage Control Case

Maximum voltage (pu)	Minimum voltage (pu)
1.0328	0.9598

Table 3. 7 Error Percentage for Time Series Study

Mean	Min	Median	Max
0.25%	$8.34\times10^{-6}\%$	0.3%	1%

CHAPTER 4 SUMMARY

Motivated by addressing the problems brought by the increasing PV penetration in distribution feeder, the research work has been developed in four sub-areas: HEMS algorithm development which is aiming to help end users improve the solar power utilization rate, PV and ES sizing methodology and tool development which is targeting at selecting appropriate ES for end users and utilities from technical perspective, cost-benefit study for sizing PV and ES which could help users select the ES and PV systems in an economic way, VLSM-based voltage control scheme development which could help regulate the voltage profiles at distribution feeders. The work in each sub-area is abridged as follows:

A. HEMS Algorithm Development

A Matlab-based toolbox for HEM algorithm development is developed in this study. The design considerations and modeling approach are expected to help other researchers developing similar test systems. Based on our preliminary results on developing HEM algorithms for PV integration and for responding to time-of-use and critical-peak-prices, the platform not only saves the developers time for setting up different test cases, but also provide a consistent performance evaluation tool to quantify the benefits of each algorithms. The standardized modeling platform we have developed will not only shorten the time for developing algorithms but also provide a virtual environment for customers to experience the benefit of using HEM for energy efficiency and energy saving programs.

B. PV and ES Sizing Methodology and Tool Development

In this study, we developed a graphical, performance-based energy storage sizing method. Because ensembles of daily load profiles are generated based on both the historical data and the load models, the selection of ESD power and energy capacity can be based on the consumers' or utilities' expectation of meeting a specified sizing criterion (such as meeting the backfeeding power and energy limit) with and without DSM. EPLs on a CC-CDF plot provide users with a compact graphical tool to select ESDs based on the probability of meeting a specified performance criterion. The gradients of the EPLs indicate the marginal benefit of the energy storage size increase.

Using this tool, we compare the needs of ESDs at different locations for different seasons, and for various PV installed capacities. The conclusions of the study include:

1) In different seasons, the needs of using ESDs may vary greatly. Therefore, allowing some ESD capacity to be flexible (e.g. rented, mobile energy storage) may be more economical because the utilization rate of the overall energy storage system will increase.

2) There exists an optimal combination of PV+ESD capacity for a given residential load pattern. Therefore, it is recommended to use a combined approach for sizing the ESD and PV together considering the load characteristics.

3) Load diversity can significantly reduce the needs for storing excess PV power. Therefore, it is more economical for the utilities and load aggregators to provide energy storage services at the transformer- or community- levels than the home-level ESD deployment.

4) Demand-side energy management systems reduce the size of ESD. However, coordination among demand side resources is needed to achieve desired performance at the aggregated level.

C. Cost-Benefit Study for Sizing PV and ES

In this work, a cost-benefit study for sizing PV panels and ES at residential houses under TOU rates has been presented. TOU rates at Duke Energy (North Carolina, residential) are selected as the main criteria for calculating the electricity bill. TOU rates at PG&E are used for comparison. Four cases are designed: case 1 (Pure house loads, base case), case 2 (Installed with PV panel), case 3 (Installed with PV panel and ES), case 4(Installed with PV panel and ES, DSM also involved).

NPV and YR of each house have been calculated and compared. Marginal values of increasing one unit PV capacity or ES size are analyzed. Impacts of different TOU rates are investigated by comparing the electricity bill savings under Duke Energy and PG&E. Findings drawn from the study are as follows: First, marginal values of increasing PV and ES sizes are declining as the sizes increase. For a specific house, a critical size at which the cost and saving are equal can be found from the saving-cost curve. Second, for some loads, there is no need to install an ES with the residential PV system. Third, as shown by the NPV values of case 2-4, implementing DSM programs will greatly increase the NPV.

The comparison of electricity bills shows that rate structures will significantly influence the sizing of PV and ES system. Our future study will focus on addressing an optimal rate structure

design to reduce the adverse impact of integrating large amount of PV into the power distribution grid.

D. VLSM-Based Voltage Control

A two-stage hierarchical control strategy for deploying demand response on distribution system is developed in this work, with the control objective of implementing DR requirement from transmission system while regulating the voltage profiles at distribution system.

This control strategy enables the co-optimization of DR operation between the transmission and distribution systems. We developed a VLSM-based resource dispatch strategy. The VLSM and the price functions for different DR resources we developed have enabled us to consider the coordination among different DR resources including both customer-owned and utility-owned devices.

We have tested the control strategy on IEEE-123 feeder and the results have demonstrated the effectiveness and capability of this control scheme. Real household load profiles are used to build the load profile at each load bus, in this way the load diversity at home level could be accounted, therefore realistic residential feeder could be imitated. Various PV profile types have been used to simulate different weather conditions. Time-series study instead of snap shot simulation could be done by using OpenDSS, so that the voltage variation in a day could be simulated.

REFERENCES

[1] Payne, Adam, Richard Duke, and Robert H. Williams. "Accelerating residential PV expansion: supply analysis for competitive electricity markets." Energy Policy 29.10 (2001): 787-800.

[2] Thomson, M., and D. G. Infield. "Impact of widespread photovoltaics generation on distribution systems." Renewable Power Generation, IET 1.1 (2007): 33-40.

[3] Ueda, Yuzuru, et al. "Analysis results of output power loss due to the grid voltage rise in grid-connected photovoltaic power generation systems." Industrial Electronics, IEEE Transactions on 55.7 (2008): 2744-2751.

[4] Povlsen, Arne Faaborg. "Impacts of power penetration from photovoltaic power systems in distribution networks." Report IEA PVPS T5-10 2002 (2002).

[5] Scott, Nigel C., David J. Atkinson, and James E. Morrell. "Use of load control to regulate voltage on distribution networks with embedded generation." Power Systems, IEEE Transactions on 17.2 (2002): 510-515.

[6] DOE-EIA, “Energy efficiency and renewable energy. International energy outlook,”2011 [Online]. Available: http://205.254.135.24/forecasts/ieo/pdf/0484(2011).pdf

[7] Nourai, Ali, V. I. Kogan, and Chris M. Schafer. "Load leveling reduces T&D line losses." Power Delivery, IEEE Transactions on 23.4 (2008): 2168-2173.

[8] Albadi, Mohamed H., and E. F. El-Saadany. "Demand response in electricity markets: An overview." IEEE power engineering society general meeting. Vol. 2007. 2007.

[9] Lee, M., et al. "Assessment of demand response and advanced metering." Federal Energy Regulatory Commission, Tech. Rep (2013).

[10] Mohsenian-Rad, Amir-Hamed, and Alberto Leon-Garcia. "Optimal residential load control with price prediction in real-time electricity pricing environments." Smart Grid, IEEE Transactions on 1.2 (2010): 120-133.

[11] Du, Pengwei, and Ning Lu. "Appliance commitment for household load scheduling." Smart Grid, IEEE Transactions on 2.2 (2011): 411-419.

[12] Chen, Zhi, Lei Wu, and Yong Fu. "Real-time price-based demand response management for residential appliances via stochastic optimization and robust optimization." Smart grid, IEEE transactions on 3.4 (2012): 1822-1831.

[13] Pedrasa, Michael Angelo A., Ted D. Spooner, and Iain F. MacGill. "Coordinated scheduling of residential distributed energy resources to optimize smart home energy services." Smart Grid, IEEE Transactions on 1.2 (2010): 134-143.

[14] Li, Na, Lijun Chen, and Steven H. Low. "Optimal demand response based on utility maximization in power networks." Power and Energy Society General Meeting, 2011 IEEE. IEEE, 2011.

[15] Yi, Peizhong, et al. "Real-time opportunistic scheduling for residential demand response." Smart Grid, IEEE Transactions on 4.1 (2013): 227-234.

[16] Lu, Ning. "An evaluation of the HVAC load potential for providing load balancing service." Smart Grid, IEEE Transactions on 3.3 (2012): 1263-1270.

[17] Lew, Debra, et al. "Impact of high solar penetration in the western interconnection." Contract 303 (2010): 275-3000.

[18] Bank, J., B. Mather, J. Keller, and M. Coddington. "High Penetration Photovoltaic Case Study Report." Contract 303 (2013): 275-3000.

[19] N Lu, YV Makarov, MR Weimar, F Rudolph, S Murthy, J Arseneaux, C Loutan, and S Chowdhury. The Wide-area Energy Storage and Management System Phase II Final Report - Flywheel Field Tests, PNNL-19669, 2010, Pacific Northwest National Laboratory, Richland, WA.

[20] B. S. Borowy and Z. M. Salameh, "Methodology for Optimally Sizing the Combination of a Battery Bank and PV Array in a Wind/PV Hybrid System," IEEE Trans. On Energy Conversion, pp.367-375, 1996.

[21] Bruce Dunn, Haresh Kamath, and Jean-Marie Tarascon, "Electrical Energy Storage for the Grid: A Battery of Choices" Science 18 November 2011: 334 (6058), 928-935. [DOI:10.1126/science.1212741]

[22] J. P. Barton and D. G. Infield, “Energy storage and its use with inter- mittent renewable energy,” IEEE Trans. Energy Convers., vol. 19, no. 2, pp. 441–448, Jun. 2004.

[23] P. Denhol, E. Ela, B. Kirby, and M. Milligan, The Role of Energy Storage With Renewable Electricity Generation, vols. NREL/TP-6A2- 47187, Jan. 2010.

[24] T. K. A. Brekken, A. Yokochi, A. von Jouanne, Z. Z. Yen, H. Max Hapke, and D. A. Halamy, “Optimal energy storage sizing and control for wind power applications,” IEEE

Trans. Sustain. Energy, vol. 2, no. 1, pp. 69–77, Jan. 2011

[25] Yang, Hongxing, Lin Lu, and Wei Zhou. "A novel optimization sizing model for hybrid solar-wind power generation system." Solar energy 81.1 (2007): 76-84.

[26] Katiraei, Farid, and Julio Romero Agüero. "Solar PV integration challenges." Power and Energy Magazine, IEEE 9.3 (2011): 62-71.

[27] Thomson, M., and D. G. Infield. "Impact of widespread photovoltaics generation on distribution systems." Renewable Power Generation, IET 1.1 (2007): 33-40.

[28] Ru, Yu, Jan Kleissl, and Sonia Martinez. "Storage size determination for grid-connected photovoltaic systems." IEEE Transactions on Sustainable Energy 4.1 (2013): 68-81.

[29] Ellis, Abraham, et al. "PV output smoothing with energy storage." Photovoltaic Specialists Conference (PVSC), 2012 38th IEEE. IEEE, 2012.

[30] Zhu, Xiangqi, et al. "A Matlab-based home energy management algorithm development toolbox." Power and Energy Society General Meeting (PESGM), 2016. IEEE, 2016.

[31] Payne, Adam, Richard Duke, and Robert H. Williams. "Accelerating residential PV expansion: supply analysis for competitive electricity markets." Energy Policy 29.10 (2001): 787-800.

[32] Jiyu Wang, Xiangqi Zhu, David L. Lubkeman, Ning Lu, and Nader Samaan, “Continuation Power Flow Analysis for PV Integration Studies at Distribution Feeders.” Innovative Smart Grid Technologies (ISGT), 2016 IEEE PES. IEEE, 2016.

[33] Lu, Shuai, et al. Duke Energy Photovoltaic Integration Study: Carolinas Service Areas.

No. PNNL-23226. Pacific Northwest National Laboratory (PNNL), Richland, WA (US), 2014.

[34] Baran, Mesut E., et al. "Accommodating high PV penetration on distribution feeders." IEEE Transactions on smart grid 3.2 (2012): 1039-1046.

[35] Kundur, Prabha, Neal J. Balu, and Mark G. Lauby. Power system stability and control. Vol. 7. New York: McGraw-hill, 1994.

[36] Dietrich, Kristin, et al. "Demand response in an isolated system with high wind integration." IEEE Transactions on Power Systems 27.1 (2012): 20-29.

[37] Lu, Ning. "An evaluation of the HVAC load potential for providing load balancing service." IEEE Transactions on Smart Grid 3.3 (2012): 1263-1270.

[38] Samarakoon, Kamalanath, Janaka Ekanayake, and Nick Jenkins. "Investigation of domestic load control to provide primary frequency response using smart meters." IEEE Transactions on Smart Grid 3.1 (2012): 282-292.

[39] Spees, Kathleen, and Lester B. Lave. "Demand response and electricity market efficiency." The Electricity Journal 20.3 (2007): 69-85.

[40] Zakariazadeh, Alireza, et al. "A new approach for real time voltage control using demand response in an automated distribution system." Applied Energy 117 (2014): 157-166.

[41] Christakou, Konstantina, et al. "GECN: Primary voltage control for active distribution networks via real-time demand-response." IEEE Transactions on Smart Grid 5.2 (2014): 622-631.

[42] Lu, Ning, and Srinivas Katipamula. "Control strategies of thermostatically controlled appliances in a competitive electricity market." Power Engineering Society General Meeting, 2005. IEEE. IEEE, 2005.

[43] Ke, Xinda, Ning Lu, and Chunlian Jin. "Control and Size Energy Storage Systems for Managing Energy Imbalance of Variable Generation Resources." Sustainable Energy, IEEE Transactions on 6.1 (2015): 70-78.

[44] GridWise Demo. Available online: www.pnl.gov/news/2006/gridwise/gridwise- demo-flier-final.CDF

[45] Lin, Yu-Hsiu, and Men-Shen Tsai. "Development of an Improved Time–Frequency Analysis-Based Nonintrusive Load Monitor for Load Demand Identification." Instrumentation and Measurement, IEEE Transactions on 63.6 (2014): 1470-1483.

[46] Kong, Seongbae, et al. "Home appliance load disaggregation using cepstrum-smoothing-based method." Consumer Electronics, IEEE Transactions on 61.1 (2015): 24-30.

[47] N. Lu, P. Du, X. Guo, and F. Greitzer, “Smart meter data analysis,” Proc. of Transmission and Distribution Conference and Exposition (T&D), 2012 IEEE PES, May 2012, pp. 1–6.

[48] National Solar Radiation Data Base. Available Online: http://rredc.nrel.gov/solar/old_data/nsrdb/1991-2010/hourly/siteonthefly.cgi?id=727920

[49] Best Research-Cell Efficiencies. Available online: http://www.nrel.gov/ncpv/images/efficiency_chart.jpg

[50] N. Lu, "An evaluation of the HVAC load potential for providing load balancing service", IEEE Trans. Smart Grid, vol. 3, no. 3, pp.1263 -1270 2012.

[51] TOU price from Duke Energy Carolinas, LLC, available online: https://www.duke-energy.com/pdfs/NCScheduleRT.pdf

[52] Schoenung, Susan M., and William V. Hassenzahl. "Long-vs. short-term energy storage technologies analysis. a life-cycle cost study. a study for the doe energy storage systems program." Sandia National Laboratories (2003).

[53] Goodrich, Alan, Ted James, and Michael Woodhouse. "Residential, commercial, and utility scale photovoltaic (PV) system prices in the United States: current drivers and cost-reduction opportunities." Contract 303.2012 (2012): 275-3000.

[54] Masters, Gilbert M. Renewable and efficient electric power systems. John Wiley & Sons, 2013

[55] TOU price from PG&E, available online: https://www.pge.com/en_US/residential/rate-plans/rate-plan-options/time-of-use-base-plan/time-of-use-plan.page

[56] IEEE 123-bus Feeder, available online: https://ewh.ieee.org/soc/pes/dsacom/testfeeders/

[57] PecanStreet data report, available online: https://dataport.pecanstreet.org/

[58] Lu S, M Warwick, N Samaan, J Fuller, D Meng, R Diao, F Chassin, T Nguyen, Y Zhang, C Jin, and B Vyakaranam. 2014. “Duke Energy Photovoltaic Integration Study: Carolinas Service Areas.” PNNL-23226, Pacific Northwest National Laboratory, Richland, Washington. Available at http://www.pnnl.gov/main/publications/external/technical_reports/PNNL-23226.pdf

[59] Xiangqi Zhu, Jiyu Wang, David Lubkeman, Ning Lu, Nader Samaan, and Renke Huang.

“Voltage-Load Sensitivity Matrix Based Demand Response for Voltage Control in High Solar Penetration Distribution Feeders”， Power and Energy Society General Meeting (PESGM), 2017. IEEE, 2017

[60] Erickson, Robert W., and Dragan Maksimovic. Fundamentals of power electronics. Springer Science & Business Media, 2007.

[61] Xiangqi Zhu, Gonzague Henri, Jiahong Yan, and Ning Lu. “A Cost-Benefit Study of Sizing Residential PV and ES Systems based on Synthesized Load Profiles”, Power and Energy Society General Meeting (PESGM), 2017. IEEE, 2017

[62] Zhu, Xiangqi, Jiahong Yan, and Ning Lu. "A Graphical Performance-Based Energy Storage Capacity Sizing Method for High Solar Penetration Residential Feeders." IEEE Transactions on Smart Grid 8.1 (2017): 3-12.

[63] Xiangqi Zhu, Jiyu Wang, and Ning Lu, “A Hierarchical VLSM-Based Demand Response Strategy for Coordinative Voltage Control between Transmission and Distribution Systems”, in press

[64] H. Jiang, Y. Zhang, E. Muljadi, J. Zhang, and W. Gao, “A Short-Term and High-Resolution Distribution System Load Forecasting Approach Using Support Vector Regression with Hybrid Parameters Optimization” IEEE Transactions on Smart Grid, 2016.

[65] Qinmiao Li, David Lubkeman, Ning Lu, Xiangqi Zhu, “Control Strategies for Residential Microgrids during Islanded Situation”, Proc. of 2016 Power & Energy Society General Meeting, 2016 IEEE.

[66] C. Yuan, M. Illindala, M. Haj-ahmed, A. Khalsa, “Distributed energy resource planning for microgrids in the United States,” in Proc. of 2015 IEEE Industry Applications Society Annual Meeting, Addison, TX, 18-22 Oct. 2015.

[67] Xiangqi Zhu, Jiahong Yan, and Ning Lu. “A Probabilistic-based PV and Energy Storage Sizing Tool for Residential Loads,” Proc. of 2016 PES Transmission & Distribution Conference & Exposition, 2016 IEEE.

[68] Jiahong Yan, Xiangqi Zhu, and Ning Lu. “Smart hybrid house test systems in a solid-state transformer supplied microgrid.” Proc. of 2015 Power & Energy Society General Meeting, 2015 IEEE.